Simulating regional groundwater flow in layered, faulted sedimentary basins: implications for groundwater age and shale gas

Claire Gassiat

Department of Civil Engineering and Applied Mechanics

McGill University
Montreal, Quebec, Canada
June 2013

A thesis submitted to McGill University in partial fulfillment of the requirements of the degree of Master of Engineering

Acknowledgments

I would like to thank my supervisor, Prof. Tom Gleeson, for offering me the opportunity to work on this interesting project, and for his guidance and support throughout my thesis. Tom is such a pleasure to work with, he is enthusiast about everything he undertakes and ensures that his students have everything they need to succeed and be happy. I learned a lot during these two years, and I really enjoyed our discussions about hydrogeology, meditation, or life. Tom, merci pour tout !

I am also very thankful to Dr. René Lefebvre and Dr. Jeffrey McKenzie, who co-supervised this thesis, for their help and support. I have been warmly welcomed in Quebec City and René's comments and advice really improved my work on shale gas modeling. I would probably have gone mad without Jeff, who was always available to share his knowledge and tricks about SUTRA's mysteries.

My MEng would not have been the same without Dr. Elco Luijendijk. Elco is a guru of python, and his help for the numerical simulations as well as his advice on the interpretation of my results were very valuable. I am also grateful to Stéphan Séjourné for his valuable help and his explanations about his work on the St. Lawrence Lowlands. Thanks a lot as well to Marc Laurencelle for his welcome at the INRS, for sharing his data of the St. Lawrence Lowlands and for making me discover the best hot chocolate in Quebec City – and maybe in the world.

Finally, I want like to thank all my friends who helped me during my thesis, and high five everyone in our great group meetings, Juliette, Elizabeth, Priyanka, Laurent, Mikhail, Mark and Elco for their advice and their surprising would you rather dilemmas.

Contribution of Authors

This thesis is written as two manuscripts submitted or to be submitted for publication in peer-reviewed journals, in accordance to the guidelines established by McGill University's Graduate and Postdoctoral Studies Office.

The papers from Chapter 3 and Chapter 4 in this thesis are as follow:

Chapter 3: Gassiat, C., Gleeson, T., and E. Luijendijk, "The location of old groundwater in hydrogeologic basins and layered aquifer systems", accepted for publication in *Geophysical Research Letters*.

Chapter 4: Gassiat, C., Gleeson, T., Lefebvre, R. and J. McKenzie, "Hydraulic fracturing in faulted sedimentary basins: numerical simulation of potential long term contamination of shallow aquifers".

The author of this thesis is the primary author in all papers included in this thesis. Professor Tom Gleeson is supervisor of the author's Master of Engineering program and is included as co-author in both manuscripts. Prof. Jeffrey McKenzie and René Lefebvre are co-supervisors of the research program on potential contamination of shallow aquifers due to hydraulic fracturing and are included as co-authors of the second manuscript. Prof. Tom Gleeson, Jeffrey McKenzie and René Lefebvre contributed in developing the initial research proposal, guiding in the conceptualization of the project, and editing these papers. Dr. Elco Luijendijk is included as co-author of the first manuscript, in recognition of his valuable help for numerical modeling and editing the paper.

Table of contents

List of tables

List of figures

Abstract

Groundwater plays an important role in a wide range of geologic processes. Sedimentary basins are heterogeneous, layered and faulted which strongly impacts regional groundwater flow. An important concern is how anthropogenic alterations such as groundwater or shale gas development affect these complex systems. Heterogeneities are likely to impact groundwater age and affect geologic processes that depend on groundwater or solute fluxes. They may also enhance long term contamination of shallow aquifers from the fracturing of the target shale unit, as contaminants may migrate from the shale to shallow aquifers through preferential pathways such as faults. We use numerical modelling to study the effect of a layered system on distribution of groundwater age in a regional groundwater basin and the impact of hydraulic fracturing in a generic faulted sedimentary basin on potential contamination of a shallow aquifer. First, we show that high age zones with predictable locations occur in layered geologic systems across a wide range of hydraulic gradients, basin geometries and permeabilities. The zones of older groundwater result from two mechanisms: low groundwater velocities in the low permeability layer; and the rejuvenation of the groundwater through mixing of different flow paths near discharge zones. Second, we show that hydraulic fracturing leads to the transport of contaminants along the fault and long-term contamination of a shallow aquifer in some specific, realistic cases. The location of the hydro-fractured zone relative to the fault zone and the top of the shale is the most critical factor controlling contaminant transport potential.

Résumé

L'eau souterraine joue un rôle déterminant dans de nombreux processus géologiques. Les bassins sédimentaires comportent des hétérogénéités, des couches sédimentaires ainsi que des failles géologiques, qui ont un impact important sur l'écoulement régional de l'eau souterraine. Une question essentielle est de comprendre comment les altérations anthropiques, comme l'extraction d'eau souterraine ou de gaz de schiste, affectent ces systèmes complexes. Les hétérogénéités peuvent probablement avoir un impact sur l'âge de l'eau souterraine et affecter les processus géologiques qui dépendent des flux d'eau souterraine ou de solutés. Elles peuvent aussi favoriser la contamination à long terme des nappes phréatiques par la fracturation hydraulique d'une formation de schiste, en permettant aux contaminants de migrer du schiste vers les nappes phréatiques peu profondes le long de chemins préférentiels comme les failles géologiques. Nous modélisons l'écoulement régional d'eau souterraine afin d'étudier l'effet d'un système à couches multiples sur la distribution de l'âge de l'eau souterraine, ainsi que l'impact de la fracturation hydraulique sur la contamination potentielle d'une nappe phréatique superficielle par migration le long d'une faille géologique. Premièrement, nous montrons que des zones de grands âges, dont la localisation est prévisible, se forment dans des systèmes géologiques à couche multiples pour de nombreux gradients hydrauliques, géométries et perméabilités. La formation de zones comportant de l'eau souterraine est due aux faibles vitesses de l'eau souterraine dans la couche peu perméable, ainsi qu'au rajeunissement de l'eau souterraine par mixage d'eaux issues de différentes trajectoires à proximité des zones de décharge. Deuxièmement, nous montrons que la fracturation hydraulique entraine le transport de contaminants le long de la faille géologique et la contamination à long terme d'une nappe phréatique superficielle dans certains cas réalistes. La localisation de la zone de fracturation par rapport à la faille géologique et à l'interface supérieure de la formation de schiste sont des facteurs critiques qui contrôlent le potentiel de transport de contaminants.

Chapter 1 Introduction

1.1 Project overview

Groundwater plays an important role in a wide range of geologic processes. Sedimentary basins are heterogeneous, layered and faulted which strongly impacts regional groundwater flow. An important concern is how anthropogenic alterations such as groundwater or shale gas development affect these complex systems. Heterogeneities are likely to impact groundwater age and affect geologic processes that depend on groundwater or solute fluxes. They may also enhance long term contamination of shallow aquifers from the fracturing of the target shale unit, as contaminants may migrate from the shale to shallow aquifers through preferential pathways such as faults.

Most aquifer systems and sedimentary basins consist of layered sediments or rocks, in which small changes in material properties such as grain size [*Koltermann and Gorelick*, 1995] or clay content [*Revil and Cathles*, 1999] can generate orders of magnitudes of changes in permeability. The presence of low-permeability units adjacent to one or more aquifers, called "confining units", may highly impact groundwater flow, and thus affect distribution of groundwater age. Groundwater age is defined as the time that has passed since the water crossed the water table [*Alley et al.*, 2002; *Kazemi et al.*, 2006]. Groundwater age plays an important role in a wide range of geologic processes [*Alley et al.*, 2002; *Ingebritsen et al.*, 2006; *Tóth*, 1999]. It determines the timescales of subsurface processes and contaminant transport rates [*Cook and Bohlke*, 2000] and is a key indicator for the renewability of groundwater resources [*Bethke and Johnson*, 2008; *Cook and Herczeg*, 2000; *Kazemi et al.*, 2006]. A number of questions arise relative to groundwater age in sedimentary basins: How is groundwater age distributed in layered systems? What is the impact of a confining unit on regional groundwater flow?

Fault zones have complex hydrological structures, and they can strongly impact groundwater flow. Understanding the processes driving groundwater flow around fault

zones is particularly important for addressing environmental concerns relative to shale gas development. Shale gas, an unconventional natural gas resource, has emerged as a viable and important energy resource over the last 30 years. Shale gas has been exploited in the United States for over 30 years and is considered as a viable resource in numerous countries where the volume of shale gas reservoirs has recently been estimated. In 2010, natural gas provided 25% of residential and industrial use of energy in the United States [*EIA*, 2011] as advances in technology and new applications of existing techniques helped develop the shale gas industry [*EPA*, 2012].

Shale is both a source rock, from which gas has been generated or is capable of being generated, and a reservoir rock, where gas is trapped. Natural gas in shale is formed by biogenic and thermogenic processes [*Martini et al.*, 1996]. As the permeability of shale is extremely low, natural gas does not migrate but is trapped in pore space and/or sorbed onto organic material. The low permeability of the shale makes shale gas a more difficult resource to extract than conventional natural gas resources from more permeable reservoirs. In order to produce economically viable quantities of natural gas from unconventional reservoirs such as shale, the technique of hydraulic fracturing is commonly used. Hydraulic fracturing consists in injecting high volumes of fracking fluid under pressures great enough to fracture the formation, in order to increase its local permeability [*EPA*, 2012]. The fractures created by the injected fluids are held open by the injection of solid particles, such as fine grains of sand or ceramic beads, called proppants, and they allow gas to flow to the production well [*EPA*, 2012]. Horizontal wells are often used in order to fracture a larger volume of the shale formation. After the fracturing operation, the pressure is relieved and the flowback, composed of fracture fluid and formation fluids, returns to the surface [*Gregory et al.*, 2011]. The fracking fluid is commonly composed of ~99.5% water and sand, and ~0.5% chemical additives including proppants, acids, solvents and biocides [*BAPE*, 2011; *Gregory et al.*, 2011]. Additionally, the flowback contains saline formation fluids and natural gas but also contaminants present in the host shale rocks such as naturally occurring radioactive materials and heavy metals [*Gregory et al.*, 2011; *Groundwater Protection Council and All Consulting*, 2009].

Concerns about the potential environmental impact of hydraulic fracturing have increased, especially risks relating to drinking water resources [*EPA*, 2012; *Kargbo et al.*, 2010]. To this may be added concerns about soil contamination, blowout during drilling operations, seismic risks and greenhouse gas emissions [*Zoback et al.*, 2010]. Some potential drinking water issues can be addressed by better design of wells and hydraulic fracturing operations, and the application of stringent regulations. However, the long term (~ 100 to 1000 years) impact and potential of contamination of groundwater aquifers from the fracturing of the target shale unit is unclear. Although in a deep sedimentary system, fluid migration rates are usually extremely slow, heterogeneities such as faults can provide preferential pathways through which contaminants may migrate more rapidly.

A number of questions about the safety of shale gas development are examined. How does hydraulic fracturing impact regional groundwater flow in a faulted aquifer? What are the travel times of contaminant which would migrate from the fractured zone to shallow aquifers? What characteristics of the basin, the fault zone and the fracturing operation are driving the migration of contaminants?

The objective of this thesis is to better understand and quantify the impact of heterogeneities, such as low-permeability layers and fault zones, on regional groundwater flow. We develop numerical models of a generic, regional groundwater basin in order to study the effect of a layered system on regional groundwater flow and the impact of hydraulic fracturing on groundwater flow in a faulted sedimentary basin. Simulations were conducted with SUTRA, a US Geological Survey numerical groundwater simulator that uses the finite element method [*Voss and Provost*, 2002], and with SUTRA-MS, the multiple-solutes transport version of SUTRA [*Hughes and Sanford*, 2005].

1.2 Study objectives and organization of thesis

Although more complex and heterogeneous permeability patterns are common in many aquifer systems and sedimentary basins, we simulate simplified systems to develop a process-based and potentially transferable understanding of the impact of heterogeneities on regional groundwater flow. We focus on 1) the impact of a low-permeability layer on regional groundwater flow and groundwater age distribution, and 2) the potential contamination of shallow aquifers due to hydraulic fracturing in a faulted sedimentary basin. Specific objectives of this thesis are:

1. Construct a two-dimensional model of a generic, regional, layered sedimentary basin and simulate groundwater age distribution;
2. Perform sensitivity analysis to determine the conditions and processes that lead development of a zone of high groundwater ages;
3. Gather publically-available data of shale gas formations, fault zone hydrogeology and hydraulic fracturing operations;
4. Develop a model of a realistic, generic, regional, faulted groundwater basin with hydraulic fracturing in the shale formation;
5. Simulate migration of contaminants from the shale unit to shallow aquifers over long timescales; and
6. Conduct sensitivity analysis to determine the parameters that control contaminant transport potential.

Chapter 2 provides an overview of the relevant literature relative to groundwater flow in sedimentary basins, groundwater age distribution, groundwater flow around fault zones, and hydraulic fracturing. The first two objectives of the thesis are covered in Chapter 3, which focuses on the impact of a low-permeability layer on groundwater age distribution. Chapter 4 addresses objectives 3-6 and focuses on the impact of hydraulic fracturing on groundwater flow around fault zones and potential contamination of shallow aquifers. Chapter 5 summarize key findings and suggestions for future research.

Chapter 2 Literature review

Most sedimentary basins are heterogeneous, layered and faulted, and regional groundwater flow is highly impacted by these heterogeneities. To these complex systems may be added anthropogenic alterations and contamination. In this section, we first describe regional groundwater flow in sedimentary basins and properties of shale gas formations. Second, we describe groundwater age distribution in sedimentary basins. Finally, we describe groundwater flow in a faulted aquifer and the potential impact of hydraulic fracturing on nearby fault zones.

2.1 Regional groundwater flow

2.1.1 Regional groundwater flow in sedimentary basins

In topographically driven groundwater flow systems, fluid circulation occurs from high-elevation recharge areas to low-elevation discharge areas [*Freeze and Witherspoon*, 1966; *Tóth*, 1963]. Most of the subsurface flow is restricted to the top 100 m of the crust [*Gleeson et al.*, 2011a], and only 10% of groundwater flow circulates through the deeper subsurface.

Permeability is a crucial hydrologic variable yet is heterogeneous, anisotropic, scale-dependent and has a huge range [*Freeze and Cherry*, 1979]. The permeability of common geologic media ranges in an interval of 16 orders of magnitude. Permeability is a scale-dependent property at laboratory to field scales [*Brace*, 1980] but at larger regional scales may be scale independent [*Gleeson et al.*, 2011b]. In many geologic processes, permeability must also be regarded as a time-dependent parameter because of ongoing deformation, dissolution and precipitation of minerals. Some geologic processes, such as compaction of sediments, cause a gradual evolution of permeability; other, such as hydrofracturing, act very rapidly [*Ingebritsen et al.*, 2006]. Finally, permeability exhibits spatial variability, both between geologic units and within particular units. In sedimentary basins the most important cause of anisotropic permeability is sedimentary layering,

which results in horizontal permeabilities being typically much larger than vertical permeabilities. Permeability also decreases systematically with depth, due to loss of porosity through increasing confining pressure and effective stress, and to temperature- and pressure-dependent diagenetic and metamorphic processes [*Ingebritsen et al.*, 2006]. Permeability has a significant impact on heat and solute transport. At low permeabilities, heat or solute transfer occurs mainly by diffusion. For high flow rates, advective transport becomes significant. The approximate threshold permeability for significant advective solute transport is 10^{-20} m² [*Ingebritsen et al.*, 2006].

Heat transfer is an important process in the subsurface, as temperature in the Earth's crust varies from ~0°C (near the surface) to 1200°C (the approximate basalt solidus), and corresponding fluid pressure range from 0.1 MPa (atmospheric pressure) to 1000 MPa (approximate lithostatic pressure at 40-km depth). Typical continental temperature gradients are from 20 to 35°C per km [*Ingebritsen et al.*, 2006]. This gradient may be lower in recharge areas due to downward movement of infiltrating groundwater [*Stute and Schlosser*, 2000]. Heat transport occurs by conduction (the transfer of kinetic, rotational, and vibrational energy according to a temperature gradient), and advection (the transport of heat by fluid movement) [*Ingebritsen et al.*, 2006].

Solute transport occurs due to molecular diffusion, advection, and hydrodynamic dispersion. Diffusion is the movement of solute due to a concentration gradient, and is dominant at lower groundwater velocities. Advection is the transport of solutes by fluid movement, whereby the solutes move at the same mean velocity as the groundwater. The variations in the velocity field caused by heterogeneities create an indirect transport process called mechanical dispersion, which depends on advection to operate and dominates at higher velocities. The combined effects of mechanical dispersion and molecular diffusion are called hydrodynamic dispersion [*Ingebritsen et al.*, 2006].

The density and viscosity of groundwater is influenced by solute concentration and temperature, which can significantly impact groundwater flow. Hydraulic conductivity varies with fluid density and viscosity but the intrinsic permeability (herein called

permeability) does not. The porosity can be filled with different phases (liquid, gas) of water and hydrocarbons. Due to capillary effects, the presence of oil and gas might impede water movement and fluid-pressure gradents in water, oil and gas may be different. [*Ingebritsen et al.*, 2006].

In general, fluid pressures in topographically and density-driven systems are close to the hydrostatic gradient, the pressure gradient due to overlying water. However, fluid pressures sometimes depart substantially from hydrostatic, due to heterogeneous permeability, heterogeneous pore fluids, osmosis, or processes related to ongoing geologic processes such as sediment compaction, or hydrocarbon generation. Abnormal fluid pressures are often associated with economically significant hydrocarbon accumulation, and there is growing recognition that generation, migration, and entrapment of hydrocarbons may be largely responsible for the development and maintenance of abnormal fluid pressures at the sedimentary basin scale. Production of elevated fluid pressures is caused by processes such as rapid deposition and compaction of fine-grained sediments, thermal expansion of pore fluids, and chemical reactions with positive volume change. Underpressured systems are also fairly common, and the central parts of many sedimentary basins are occupied by underpressured, gas-saturated, low-permeability material. Most of these basins are currently inactive and have experienced considerable cooling. These systems likely evolved from originally overpressured systems through processes such as progressive gas loss and gas-volume contraction associated with uplift, erosion, and cooling [*Ingebritsen et al.*, 2006].

2.1.2 Shale gas formations

Experimentation of deep shale gas production started during the 1980s and 1990s in the Barnett Shale in North-Central Texas. In the 2000s, producers began pursuing other shale formations, including the Haynesville, Marcellus, Woodford, and Eagle Ford shales [*EIA*, 2011a]. Currently, the most advanced shale plays are in North America (Figure 1). The emergence of shale gas as a viable and important energy resource has led to the assessment of worldwide shale gas potential. The *EIA* [2011a] assessed 48 shale gas basins in 32 countries, containing almost 70 shale gas formations (Figure 2).

Our study aims at assessing the impact of hydraulic fracturing in a generic basin. Therefore, we investigate the common features of shale gas formations as well as differences that could impact the influence of hydraulic fracturing on groundwater flow. We describe in greater detail the St. Lawrence basin in Quebec, which acts as a reference for our base case model, as well as the formations of the Marcellus shale and Barnett shale, which are the most studied shale gas units in the United States.

Figure 1. Current shale gas plays in North America. From *EIA* [2011b].

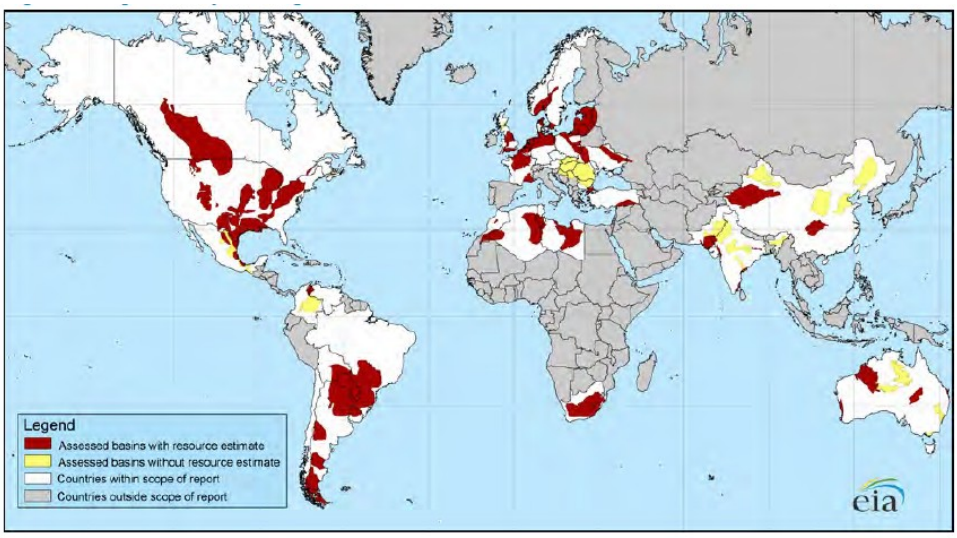

Figure 2. Major shale gas basins in the world, from *EIA* [2011a].

2.1.2.a Differences and common features of shale basins

Depth of shale formation

Shale formations are highly variable in depth and outcrop in some areas. However, the depth interval for prospective areas is commonly between 1 and 5 km [*EIA*, 2011a]. Formations deeper than 5 km have lower permeability and higher drilling and development costs. Formations shallower than 1km have lower pressure, a lower gas concentration, and have higher water content in their natural fracture systems.

In the 48 shale gas basins investigated in the EIA report [*EIA*, 2011a], shale units are between 1 and 4.5 km deep and 2.9 km deep in average (Figure 3). In the United States, shale gas formations are 500 to 4500 m deep [*EIA*, 2011b].

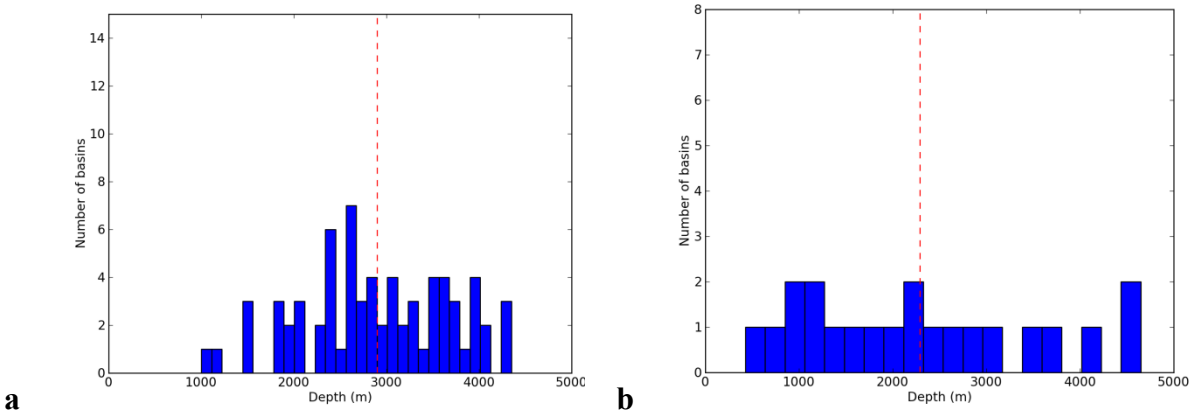

Figure 3. Depth of shale gas formations **(a)** in the world and **(b)** in the United States (data from EIA [*EIA*, 2011a; 2011b]). In red is the average value.

Thickness of shale formation

The thickness of shale units is relatively uniform, with a few extreme values. In the 48 shale gas basins investigated in the EIA report [*EIA*, 2011a], shale units are between 20 and 300 m thick, with only one unit above 150 m thick. Shale formations are 77 m thick in average (Figure 4). In the United States, 75% of shale formations are less than 150 thick, and formations are 190 m thick in average [*EIA*, 2011b].

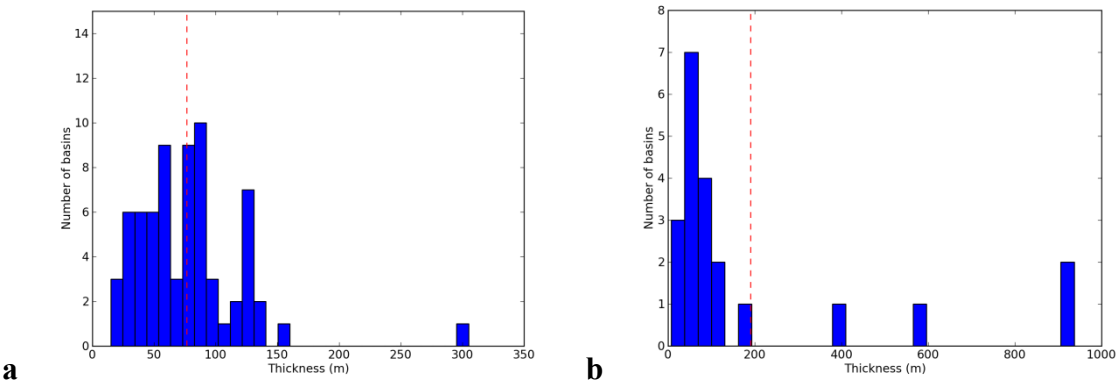

Figure 4. Average thickness of shale formations **(a)** in the world, **(b)** in the United States (data from EIA [*EIA*, 2011a; 2011b]). Red: average value.

Permeability and porosity

Permeability is a highly variable parameter, both between different basins and within a formation. According to *Freeze and Cherry* [1979], a reasonable estimate for shale permeability is in the range of 10^{-20} to 10^{-16} m², and *Gleeson et al.*[2011b] estimated the regional permeability of fine-grained sedimentary rocks between 10^{-18} and 2.10^{-15} m². The assessment of porosity in US shale gas plays shows that common porosity of shale formation is between 1 to 12% (Figure 5). Theoretical and experimental values of porosity and permeability with depth in sedimentary basins are presented in Figure 6.

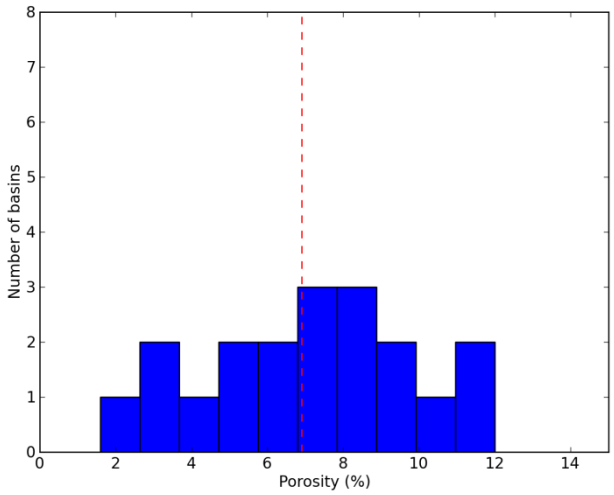

Figure 5. Average porosity in U.S. shale gas formations (data from *EIA* [2011b])

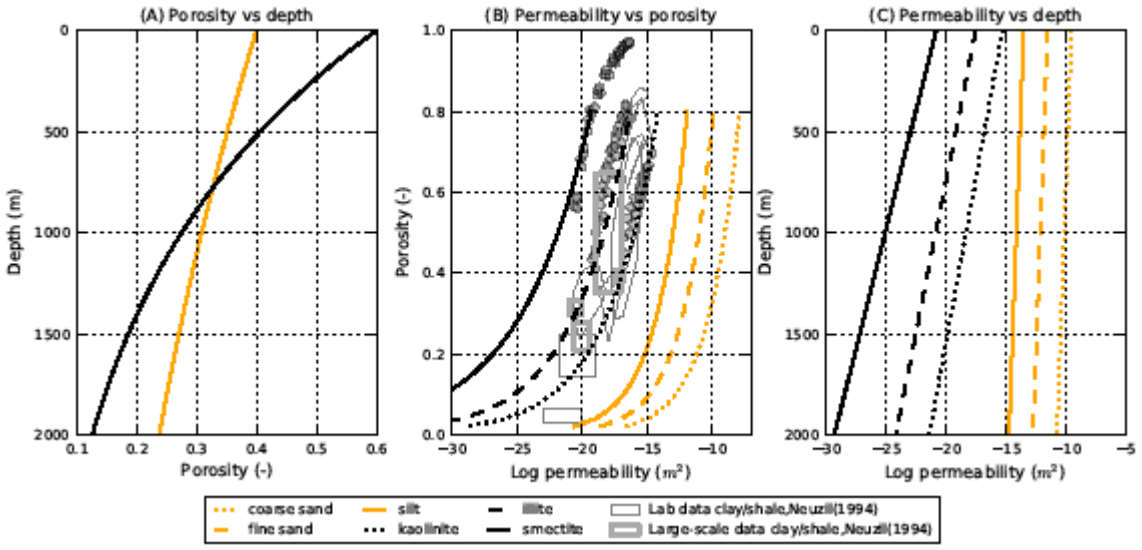

Figure 6. Theoretical and experimental values of permeability and porosity with depth.

Reservoir pressure

Shale gas reservoirs have pressure gradients either above (overpressured), under (underpressured) or close to the hydrostatic gradient. Almost 40% of worldwide shale gas formations studied by the *EIA* [2011a] are overpressured, 55% have a pressure gradient close to the hydrostatic gradient and less than 10% are underpressured (Figure 7).

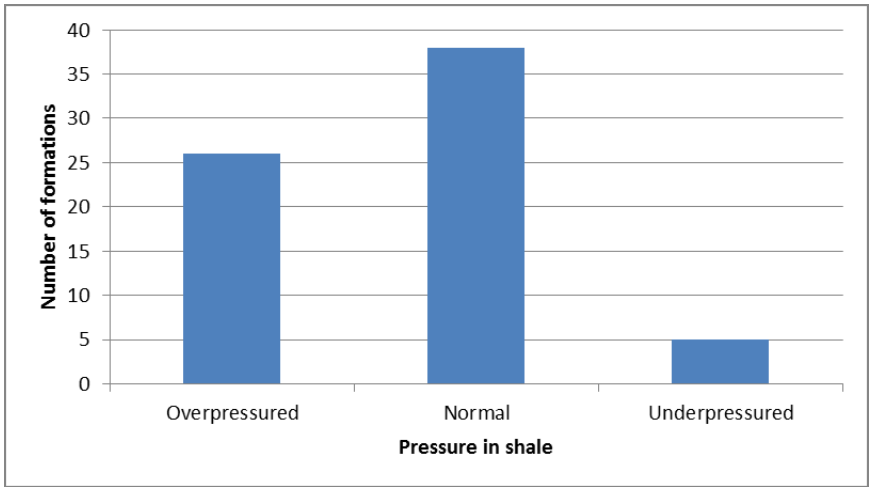

Figure 7. Pressure regime in shale units (data from *EIA* [2011a])

Formation above the shale unit

Target shale units are overlaid by highly variable formations. Some shale units, such as the Utica Shale (Quebec, Canada) and the Marcellus Shale (Pennsylvania, US) are overlaid by other shales and therefore the whole basin is dominated by low-permeability rocks [*EIA*, 2011a]; other target shale are overlaid by more permeable units, such as limestone and sandstone in the Liard Basin (Northeast British Columbia, Canada), limestone in some parts of the Maracaibo Basin (Venezuela), or alternating shale and limestone layers in the Bend Arch-Fort Worth Basin, over the Barnett Shale [*EIA*, 2011a].

Depth to saline fluids

In sedimentary basins, depth to saline fluids is commonly of a few hundred meters. In sedimentary basins in North America, salinities from 0 to 500 g/L have been reported between 0 and 4 km below the surface (Figure 8). As a comparison, Alberta defines water as non-salted when the concentration of salt is below 4 g/L [*BAPE*, 2011], and the concentration of sea water is 35 g/L.

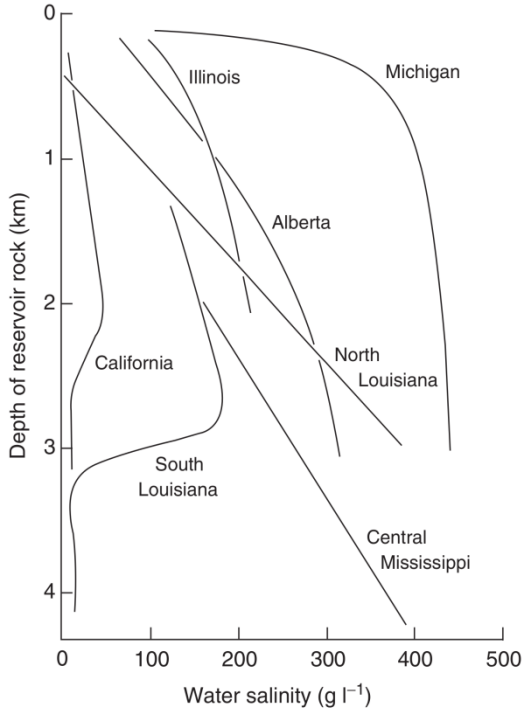

Figure 8. Salinity distribution with depth of reservoir rocks in North America, from *Clauer* [1992].

2.1.2.b The St. Lawrence Lowlands (Utica shale)

The St. Lawrence Lowlands are located in Quebec, Canada which is a ~3000m thick Paleozoic sedimentary basin, underlain by the Precambrian Canadian Shield and overlain by Quaternary glacial, glaciofluvial and lacustrian deposits. Most of the groundwater resource comes from the Quaternary deposits, and occasionally from the fractured rock formations [*BAPE*, 2011].Oil and gas drilling started in 1860 in the St. Lawrence Lowlands. These wells targeted shallow conventional hydrocarbon reservoirs. In October 2010, 121 licenses for oil, natural gas and underground reservoirs were given to 12 different companies and covered more than 20 000 km², extending beyond the area of the Utica shale. There are currently about 600 oil and gas drillings in the St. Lawrence Lowlands, with 150 completed in the Utica shale. Almost 300 exploration wells were drilled in 2010, with only 29 focused in the Utica shale. Eighteen of these twenty-nine wells are vertical and 11 are horizontal. Hydraulic fracturing has been performed in 9 vertical wells and 6 horizontal wells [*BAPE*, 2011].

Three regions were suggested by *Thiérault* [2012] for shale gas exploration in the southwest of Quebec (Figure 9). In the first corridor, local shale outcrops are frequent along the shore of the St. Lawrence River, and shale is 800 m deep on average. The second corridor lies between the Yamaska Fault and the Logan Line, and shale depth and thickness increase. The Utica shale is between 1200 and 2500 m deep. In the third corridor, starting at the Logan Line, the Utica shale is more than 2500 m deep, but the development of major faults have caused some slivers of Utica shale to be locally thrust to shallower depths. The current exploration work targets the Utica shale and focus in the second region. However, a potential for gas exploitation may also exist in the Lorraine shale and in the first region located along the shores of the St. Lawrence [*BAPE*, 2011].

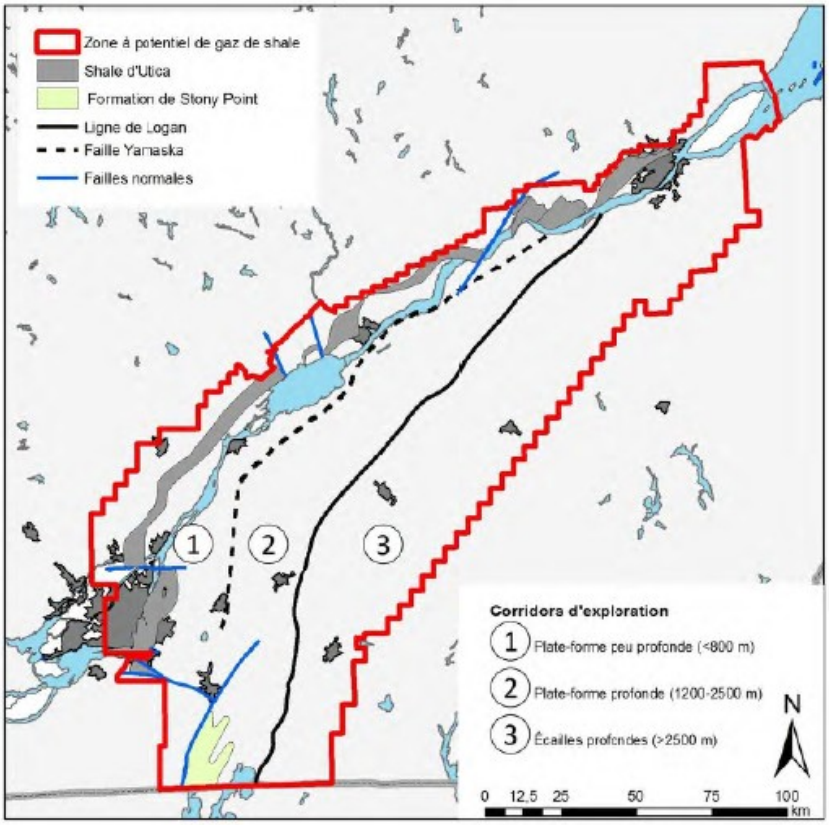

Figure 9. Shale gas play in the St.Lawrence Lowlands (from *Sejourné et al.*[2013])

Stratigraphy

The geological units of the St. Lawrence Lowlands are the Potsdam Group (Cambrian) and the Beekmantown, Chazy, Black River, Trenton, Utica, Lorraine and Queenston groups (Ordovician). They are covered with unconsolidated sediments of the Quaternary (Figure 10). These formations have been affected by geodynamic phenomena which have generated normal faults, overlapping structures and strike-slip deformations, forming interesting patterns for hydrocarbon exploration [*Hissein*, 2011].

Utica Shale

Unlike the Lorraine shale, the Utica shale is calcareous, which makes it suitable for hydraulic fracturing. Indeed, clay-rich materials such as the Lorraine shale lead to ductile deformation, without the creation of fractures, whereas calcareous materials such as the Utica shale are more likely to fracture under stress. In the second corridor, the Utica shale is between 1200 and 2500 m deep and 220 m wide on average [*BAPE*, 2011].

Lorraine group

The formation above the Utica shale is the Lorraine group, the thickest and most widespread group in the St. Lawrence Lowlands. It is composed of gray shale, sandstone, siltstone and limestone. Its carbonate content is increasing towards the top of the formation [*Globensky*, 1987].

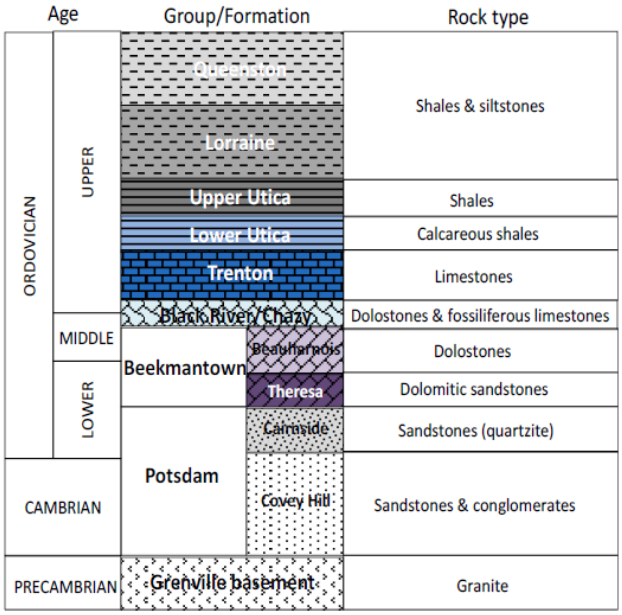

Figure 10. Stratigraphy of the St. Lawrence Lowlands, from *Tran Ngoc et al.*[2011]

Physical properties of the rock

Permeability and porosity

Values of permeability, porosity and saturation in the Utica Shale and Lorraine Group were reported by *Sejourné et al.*[2013] from drill stem tests, analyses of borehole samples, and publications (Figure 11, Table 1). These values show a great variability which can be attributed to the intrinsic heterogeneity of the shale but also to a difference in analytical methods. Permeability in the Utica shale is evaluated between 9 x 10^{-23} and 8 x 10^{-17} m², and porosity in the Utica shale is between 0.16 % and 6.6 % [*BAPE*, 2011; *Lavoie et al.*, 2008; *Rivard et al.*, 2012; *Séjourné et al.*, 2013]. Permeability of the Lorraine group is between 1x10^{-26} and 4x10^{-18} m² [*Séjourné et al.*, 2013], and the porosity is of a few percent, between 1.2 % and 3.2 % [*Rivard et al.*, 2012].

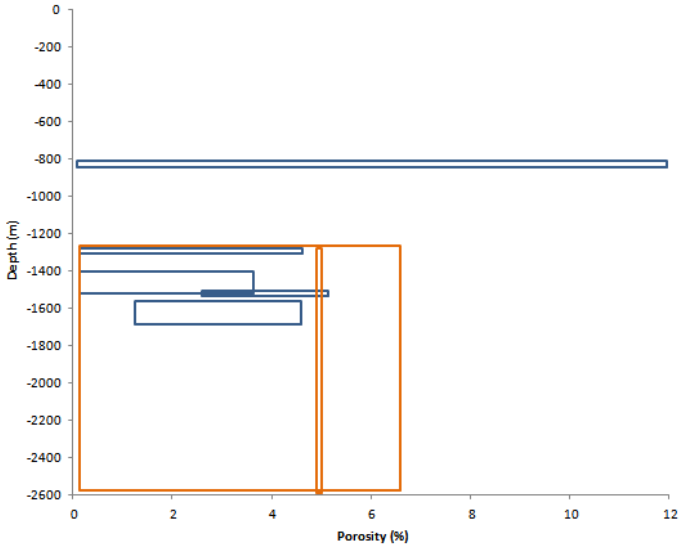

Figure 11. Porosity in the St Lawrence Lowlands (data from *Séjourné et al.*[2013]). In blue: DST values; in orange: values from *BAPE* [2011]

Table 1. Permeability in the St. Lawrence Lowlands, from *Séjourné et al.*[2013]

Stratigraphic unit	**Depth (m)**	**Permeability (m²)**	**Source**
Laurier	457 to 533	3E-19	DST
Terrebonne-Tétreauville	804 to 830	1E-17 to 4E-16	borehole sample
Laurier, Trenton, BR imbriqués	1045 to 1245	2,3E-17	DST
Laurier, Trenton, BR imbriqués	1052 to 1250	8,27E-18	DST
Lorraine	1325 to 1340	4E-27 to 7E-22	borehole sample
Utica	1419 to 1492	2E-27 to 2E-21	borehole sample
Lorraine	1491 to 1502	6E-22 to 5E-20	borehole sample
Lorraine	1554 to 1602	6,8E-16	DST
Utica	1574 to 1676	1E-22 to 2E-20	borehole sample
Utica	nd	1E-20 to 1E-19	Lavoie 2011
Utica	nd	1E-18 to 5E-18	Lavoie 2011
Utica	nd	1E-17 to 8E-17	Lavoie 2011
Lorraine	1280 to 2590	4E-19	BAPE 2010
Utica	1280 to 2590	3E-19	BAPE 2010

Pressure gradient

Sejourné et al.[2013] also reported values of the pressure gradient of the Utica Shale and Lorraine Group (Figure 12). The only reliable data to estimate the pressure gradients in the Utica Shale and overlying units are those from Drill Stem Tests and analyses of borehole samples. Analyses of borehole samples are the most reliable data and show the vertical variation of the pressure gradient. Other values are estimates of the surface pressure from old operations and are not reliable. Some values of pressure gradient in shale are also reported in reports of the Geological Survey of Canada [*Lavoie et al.*, 2008; *Rivard et al.*, 2012]. Accurate estimates of regional pressure gradients (maximum and minimum horizontal stress, vertical stress and contemporary tectonic regime) are reported by *Konstantinovskaya et al.*[2012]. These authors conclude that the current stress regime is a strike-slip stress regime between 250 and 4000 m depth, and some normal faults could be reactivated depending on their orientation relative to the horizontal principal stress and the fracturing pressure.

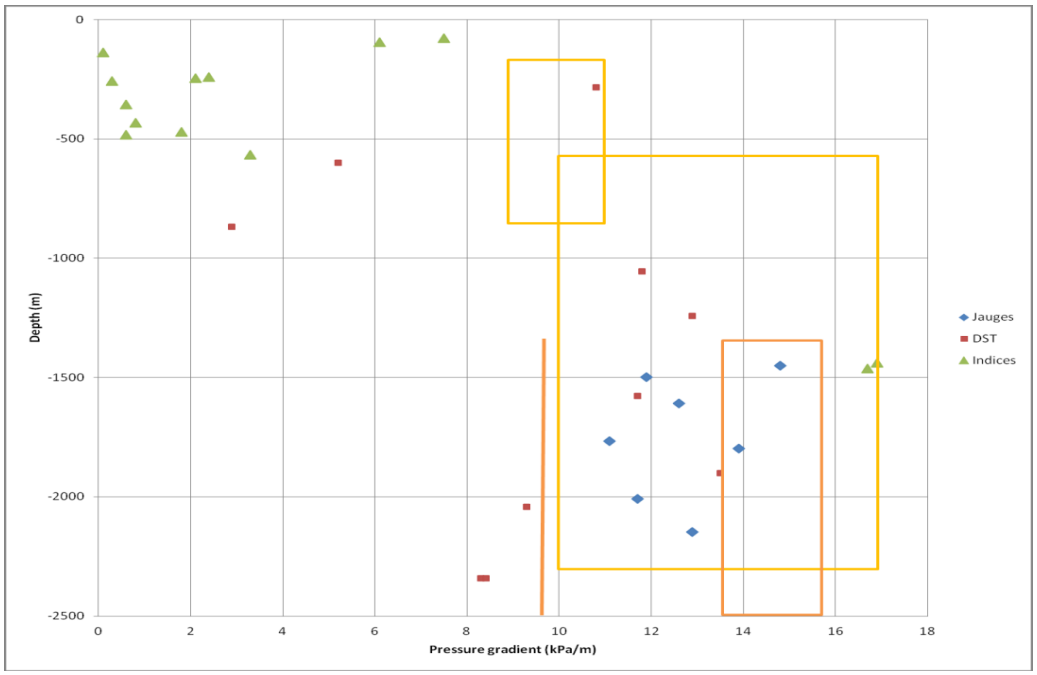

Figure 12. Pressure gradient in the St. Lawrence Lowlands (data from *Séjourné et al.*[2013]). In yellow: data from *Lavoie et al.* [2011]; in orange: data from *BAPE* [2010]

Depth and concentration of brines

Sejourné et al.[2013] reported values of depth of fresh water and saline water in the St. Lawrence Lowlands although the depth is difficult to resolve due to the lack of deep water wells (Figure 13). Concentrations in these domestic water wells were not reported. The results are heterogeneous, often with an interval of a few hundred meters between the fresh water and saline water index. In some cases however, the interval is less than ten meters which allows to accurately locate the transition between fresh water and brine. The sedimentary basin of the St. Lawrence Lowlands has high salinities [*Ngoc et al.*, 2011; *Séjourné et al.*, 2013; *Tran Ngoc et al.*, 2012]. Concentrations at shallow depth were reported by *Globensky* [1972] (Figure 14), and salinities in the units below the Utica shale were reported by *Tran Ngoc et al.*[2011] (Figure 15).

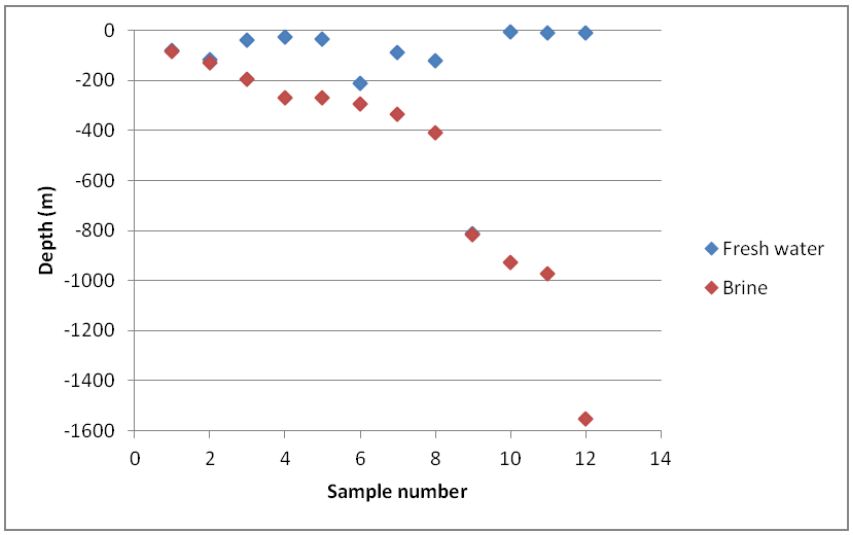

Figure 13. Fresh water and brine depth recorded in wells in the St. Lawrence Lowlands (data from *Séjourné et al.*[2013]).

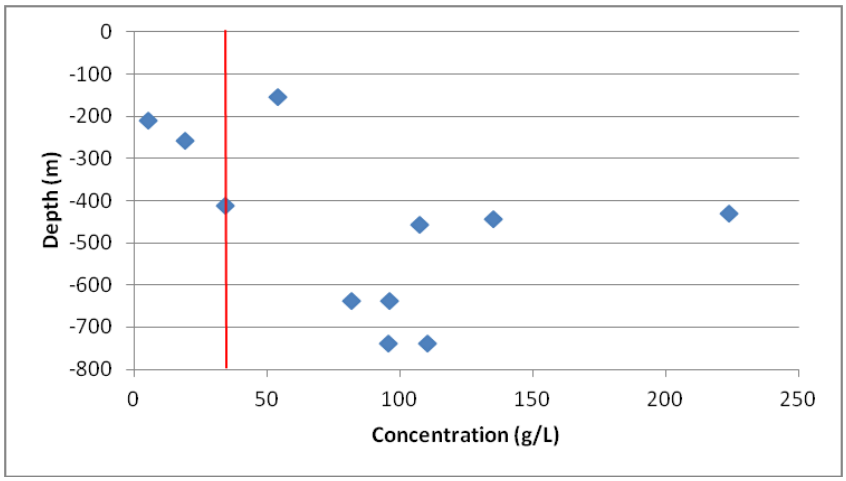

Figure 14. Salinity at shallow depth in the St. Lawrence Lowlands (data from *Globensky* [1972]). Red line: sea-water concentration

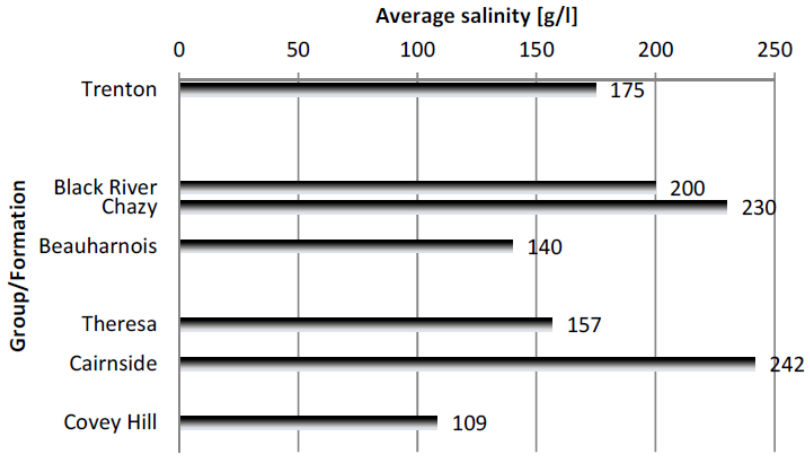

Figure 15. Salinity in the units below the Utica shale in the Becancour area (from *Tran Ngoc et al.*[2011])

Fault systems

The structural pattern in the St. Lawrence Lowlands consists of two major regional fault systems. The first system includes normal faults striking NE-SW in the Quebec City - Trois Rivieres areas and NNE-SSW in the Montreal area and dipping steeply to the SE–ESE (Figure 16). These faults affect the St. Lawrence Platform sedimentary formation up to the top of the Utica Shale (Figure 17) [*Castonguay et al.*, 2010]. The second regional fault system in composed of reverse and thrust faults trending NE–SW in Quebec City — Trois-Rivieres areas and NNE–SSW in the Montreal area with moderate to low dip. Additionally, field observations in the St. Lawrence Lowlands show the presence of

several fracture sets, which could have been formed during the multiple tectonic phases occurred in the region. Lineaments are present in four main strike directions [*Konstantinovskaya et al.*, 2009]. The short and individual lineaments may be related to vertical cleavage or joint systems, whereas the longer lineaments could correspond to regional fault systems. These lineaments are partly associated with the regional NE–SW normal and thrust faults and reflect the principal structural pattern of the area.

The St. Lawrence Lowlands area is currently characterized by a strike-slip stress regime [*Konstantinovskaya et al.*, 2012]. Therefore, the optimal fault or fracture subject to reactivation would be the near-vertical features. However, although the basement normal faults dipping at ~60° and the Appalachian thrusts faults dipping at ~30° strike slightly oblique to the maximum stress orientations, these zones may be associated with smaller faults or fractures that are near-vertical and optimally oriented for shear failure in the regional strike-slip stress regime (i.e. at 30° to the maximum horizontal stress) [*Konstantinovskaya et al.*, 2012].

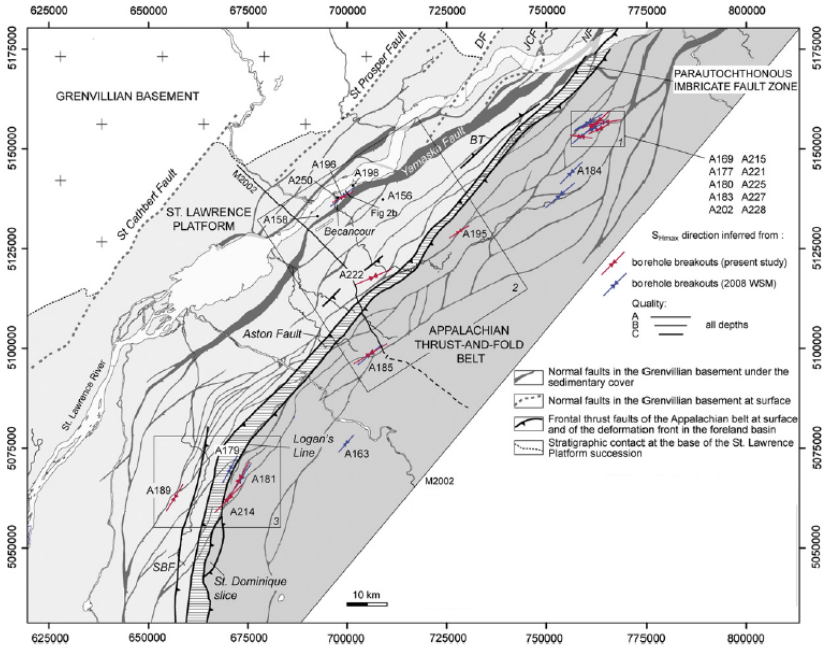

Figure 16. Stress orientation and regional fault pattern in the St. Lawrence Lowlands (modified from *Konstantinovskaya et al.* [2012])

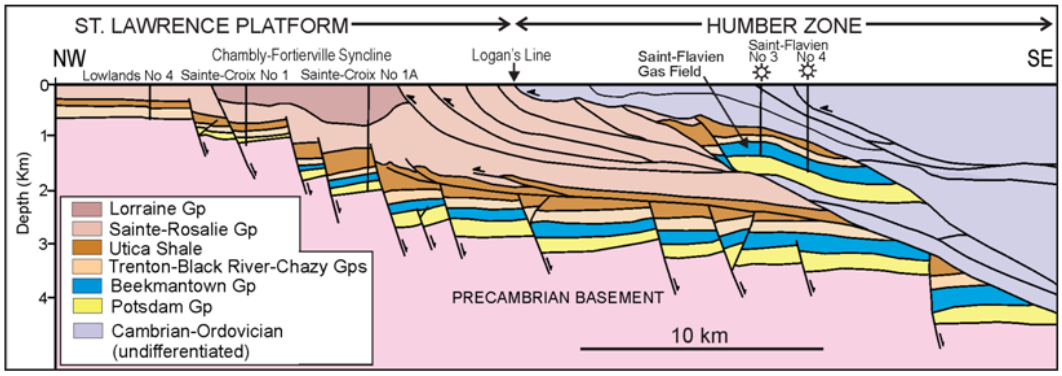

Figure 17. Cross-section of the St.Lawrence Lowlands (from *Castonguay et al.* [2010])

2.1.2.c The Appalachian basin (Marcellus shale)

The Marcellus Formation is a relatively well studied shale gas reservoir located in the Appalachian Basin in Pennsylvania, New York, and the northeastern US. The Marcellus Formation includes two distinct calcareous black shale units: the Union Springs (lower) and Mount Marion/Oatka Creek (upper), interrupted by the Cherry Valley limestone [*Warner et al.*]. Until recently, the Marcellus shale was not considered a viable resource because the depth of the formation makes it an expensive target [*Sumi*, 2008]. Since 2005, the development of Marcellus shale exploitation has increased in Pennsylvania and New York State. In 2008, the number of wells targeting the Marcellus shale had reached an estimated 450 wells in Pennsylvania [*Arthur et al.*, 2008].

The Appalachian basin sediments are underlain by Precambrian crystalline basement rocks of the Canadian Shield [*Warner et al.*]. Figure 18 shows the stratigraphic column of the southwestern portion of New York State and provides a general description of the composition of the overlying formations that were deposited after the Marcellus Shale [*Arthur et al.*, 2008]. The Hamilton Group units overlying the Marcellus are predominantly composed of siltstones and shales. The Upper Devonian is composed of sequences of grey shales, and sandstones [*Warner et al.*].

Period		Group	Unit	Lithology	
Penn		Pottsville	Olean		Quartz Pebble
Miss		Pocono	Knapp		Conglomerate and Sandstone Quartz Pebble, Conglomerate, Sandstone, and Minor Shale
Devonian	Upper	Conewango			Shale and Sandstone Scattered Conglomerates
		Conneaut	Chadakoin		Shale and Sandstone Scattered Conglomerates
		Candadaway	Undifferentiated	•"	Shale and Siltstone
			Perrysburg	•"	Minor Sandstone
		West Falls	Java Nunda Rhinestreet	•" •"	Shale and Siltstone Minor Sandstone
		Sonyea	Middlesex	"	Shale and Siltstone
		Genesee			Shale with Minor Siltstone and Limestone
	Middle		Tully	"	Limestone with minor Siltstone and Sandstone
		Hamilton	Moscow Ludlowville Skaneateles Marcellus	"	Shale with minor Sandstone and Conglomerate
			Onondaga	•"	Limestone
	Lower	Tristates	Oriskany	"	Sandstone
		Helderberg	Manlius Rondout		Limestone and Dolostone
	Upper		Akron	•"	Dolostone

Figure 18. General stratigraphic column of Southern New York State. From *Arthur et al.*[2008]

The Marcellus shale

The Marcellus formation is variable in depth, and outcrops in some areas of New York. However, the majority of the Marcellus shale is more than 1600 m deep [*Sumi*, 2008]. Marcellus shale units targeted for gas exploitation are 1220 to 2590 m deep and 15 to 60 m thick [*Arthur et al.*, 2008]. The Marcellus shale is considered having a "favorable mineralogy" as it is a low-density rock with relatively high porosity [*Sumi*, 2008]. A laboratory study of a core sample of the Marcellus shale reports a gas porosity of about 10% and a permeability of $2x10^{-16}$ m² at 2300 m depth [*Soeder*, 1988]. The northern part of the basin is slightly geopressured, whereas the southern part is underpressured [*Sumi*, 2008].

2.1.2.d The Bend Arch-Fort Worth basin (Barnett shale)

The Barnett Shale is an organic-rich black shale of middle–late Mississippian age [*Montgomery et al.*, 2005] located in the Bend Arch-Fort Basin, in Texas. Since 2008, the Barnett Shale Newark East field ranks first in the United States in terms of annual gas production [*EIA*, 2009]. The Barnett Shale is unusual in several aspects. First, the targeted units are at great depths and thus at higher pressures than other shale gas reservoirs. Second, Barnett shale gas is of thermogenic origin and often occurs with liquid petroleum [*Montgomery et al.*, 2005]. On average, the Barnett shale is 91 m thick

and occurs at a depth of 2300 m [*EIA*, 2011b]. Core analysis indicates that productive, organic rich parts of the formation have permeabilities of less than 10^{-17}m² [*Montgomery et al.*, 2005], and the average porosity of the Marcellus shale is 5% [*EIA*, 2011b]. At Newark East field, the formation is slightly overpressured (11.8 kPa/m) [*Montgomery et al.*, 2005].

Stratigraphy of the Fort Worth basin is shown in Figure 19. The Marble Falls Limestone, which immediately overlies the Barnett, grades from limestone at the Newark East field into shale in the southeastern part of the basin [*Pollastro et al.*, 2007]. Pennsylvanian strata above the Marble Falls Formation consist of Atokan conglomerates, sandstones, shales, and thin limestones [*Montgomery et al.*, 2005].

Structures in the Fort Worth basin include major and minor faulting, local folding. The Barnett Shale is also known to be naturally fractured. Local fault blocks are present in the northern basin. An important structural feature in this area is the Mineral Wells fault. In addition, minor high-angle normal faults are present in many parts of the basin. The changing orientation of these structures suggests that they are related to several major tectonic elements [*Montgomery et al.*, 2005; *Pollastro et al.*, 2007].

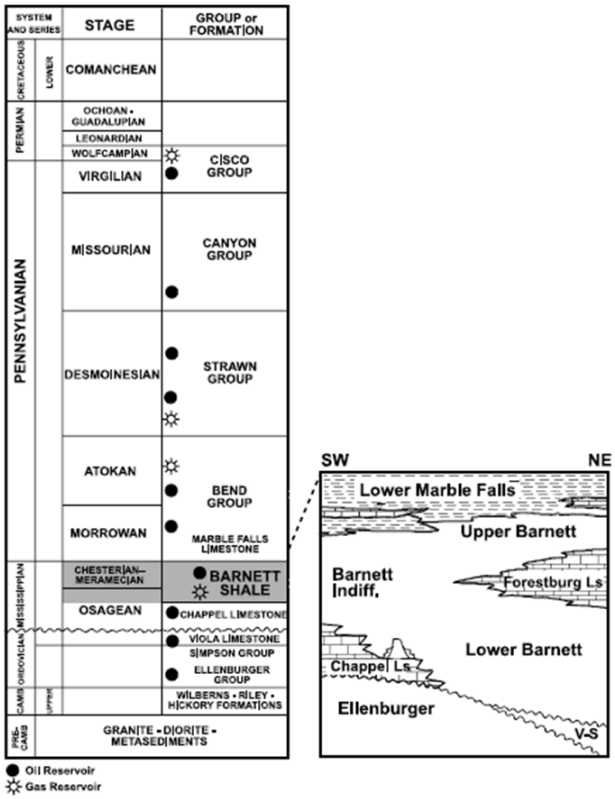

Figure 19. Stratigraphic column of the Fort Worth Basin (from *Montgomery et al.* [2005])

2.2 Groundwater age

Groundwater age and residence time are important in a lot of geologic processes [*Alley et al.*, 2002; *Ingebritsen et al.*, 2006; *Tóth*, 1999]. The age of groundwater, derived from radiogenic isotopes or other methods, determines the timescales of subsurface processes and contaminant transport rates [*Cook and Herczeg*, 2000]. Groundwater age is a key indicator for the renewability of groundwater resources [*Bethke and Johnson*, 2008; *Cook and Herczeg*, 2000; *Kazemi et al.*, 2006]. Groundwater age is defined as the time that has passed since the water crossed the water table [*Alley et al.*, 2002; *Kazemi et al.*, 2006], and residence time is defined as the time it takes for groundwater to flow from recharge to discharge areas. Groundwater age distributions have been studied in both saturated and unsaturated flow regime. Groundwater age might be sampled in a well which is open to the aquifer over a large vertical interval [*Cook and Bohlke*, 2000; *Haitjema*, 1995]. Sampled water is generally comprised of a mixture of water of different ages. The mean

age is then equal to the mean residence time $\tau = \frac{V}{Q}$, where τ is the mean residence time, V is the volume of mobile water in the aquifer and Q is the steady state outflow [*Cook and Bohlke*, 2000]. For homogeneous aquifers of constant thickness with a constant recharge rate, simple analytical solutions have been derived for groundwater age and velocity as function of depth and distance [*Vogel* 1967]. In this case, the age of the groundwater is given by $t = \frac{H\epsilon}{R} \ln\left(\frac{H}{H-z}\right)$, where H is the thickness and ϵ the porosity of the aquifer, R is the areal recharge rate and z the depth in the aquifer, and the age of groundwater is independent of the horizontal position in the aquifer. For a sample of groundwater from a well that is screened over the entire thickness of the aquifer, the relative cumulative frequency distribution of the age of groundwater is an exponential distribution $F(t) = 1 - e^{-t/\tau}$ and the mean groundwater age is equal to $\tau = \frac{H\epsilon}{R}$ [*Cook and Bohlke*, 2000].

Areas of stagnant groundwater form at the intersection of local, intermediate and regional flow systems [*Tóth*, 1963]. Such stagnant zones, with extremely high groundwater ages and low velocity, are important because they accumulate metallic ions, hydrocarbons and anthropogenic contaminants transported by groundwater [*Tóth*, 1999]. Distribution of groundwater age and formation of areas of stagnant water are closely related to groundwater flow pattern. Steady-state regional groundwater flow patterns within a non homogeneous, anisotropic basin are affected by parameters such as the depth:lateral extent ratio of the basin, the water-table configuration and the hydro-stratigraphy [*Freeze and Witherspoon*, 1967]. The location of stagnation points is sensitive to the basin geometry, the surface topography [*Tóth*, 1963] and to the decrease of permeability with depth [*Jiang et al.*, 2011]. Heterogeneities such as lenses or layers of high permeability have been shown to greatly modify regional groundwater flow and may change the pattern of discharge areas [*Freeze and Witherspoon*, 1967; *Tóth*, 1962]. In contrast, a low permeability layer beneath the aquifer has little or no effect on the flow pattern [*Freeze and Witherspoon*, 1967]. Previous modeling studies have simulated groundwater ages in basins with homogenous permeability [*Tóth*, 1963] or a gradual decrease of permeability with depth [*Jiang et al.*, 2011; *Jiang et al.*, 2010]. However, most aquifer systems and

sedimentary basins consist of layered sediments or rocks, in which small changes in material properties such as grain size [*Koltermann and Gorelick*, 1995] or clay content [*Revil and Cathles*, 1999] can generate orders of magnitudes of changes in permeability. Sanford [2011] showed that younger ages under older ages can exist where substantial vertically layered heterogeneity is present, regardless of the upper boundary condition. Field evidence indicates that these overturned ages exist in layered systems due to groundwater inflow from adjacent basins and mountains [*Sanford et al.*, 2004]. However, *Sanford* [2011] did not name or systematically study these 'high age zones', or examine the processes that control their formation.

2.3 Groundwater flow in a faulted aquifer

A fault is a fracture in a rock formation along which displacement has occurred. Discrete faults or fault zones have an important impact on geological processes, such as hydrothermal fluid circulation [*Berkowitz*, 2002; *Faulkner et al.*, 2010], hydrocarbon migration [*Berkowitz*, 2002; *Faulkner et al.*, 2010; *Sorkhabi and Tsuji*, 2005] and regional groundwater flow [*Bense et al.*, submitted; *Bense et al.*, 2008; *Mayer et al.*, 2007]. Faults affect the safe storage of nuclear waste [*Bredehoeft*, 1997], CO_2 sequestration [*Shipton et al.*, 2004] and the potential contamination of shallow aquifer due to hydraulic fracturing as they are the principal pathways through low permeability rocks [*Berkowitz*, 2002]**.**

2.3.1 Fault zone hydrogeology

Although the significance of understanding fluid flow around fault zones is widely recognized, the impact of faults on fluid flow is complex and often not well understood [*Bense et al.*, submitted]. The hydraulic properties of a fault zone depend on the geological setting, the host rock, the state of stress and the temporal evolution of the fault zone [*Lopez and Smith*, 1996; *Scholz and Anders*, 1994; *Smith et al.*, 1991].

Structure, mechanics and fluid flow properties of fault zones are inextricably coupled [*Faulkner et al.*, 2010]. Although brittle fault zones are lithologically heterogeneous,

anisotropic and discontinuous, the drag of sand- and clay-beds along the main fault plane in lithified sediments often results in rather consistent fault architectures [*Rawling et al.*, 2001], although, fault zones commonly show significant variation in complexity even over relatively short distances [*Lunn et al.*, 2008], and the fault zone structure and permeability can vary over time [*Faulkner et al.*, 2010].

Fault models are primarily inferred from outcrop descriptions and permeability measurements from the field and laboratory [*Bense et al.*, submitted]. A first order description of a fault zone structure is the distinction between a fault core and a damage zone [*Caine et al.*, 1996] (Figure 20). The fault core is defined as the central part of the fault where most of the displacement is accommodated and generally consists of gouge, cataclasite or ultracataclasite [*Faulkner et al.*, 2010]. The associated damage zone accommodates the remainder of strain along the fault. Damage zones contain fractures at a range of different scales from grain-scale microfractures to macrofractures. For low porosity rocks, macrofractures and microfractures commonly show an exponential decrease with distance from the fault core [*Faulkner et al.*, 2010]. The fault core and damaged zones are surrounded by relatively undeformed protolith. In this framework of fault zone description, total fault zone width can be described as being the combined thickness of the fault core and damage zone. Fault zone width is a crucial parameter which is directly controlling the rate of fluid mass- and associated solute- and heat fluxes [*Bense and Person*, 2006; *Haneberg*, 1995].

The fault core/damage zone conceptual hydrogeological model describes faults as effective barriers, hampering fluid migration [*Rawling et al.*, 2001], conduits propagating the movement of fluids, or as more complex conduit-barrier systems [*Aydin*, 2000 ; *Bense et al.*, 2008; *Caine et al.*, 1996]. The hydrogeological structure depends on the relative percentage of the fault core and the damage zone structures (Figure 21). The four end-members developed by *Caine et al.*[1996] are distributed conduit, localized conduit, localized barrier, or combined conduit-barrier systems.

The permeability of the fault core may be dominated by the grain-scale permeability of the fault rocks, whereas the damage zone permeability is dominated by the hydraulic properties of the fracture network. Subsidiary structures in damage zones cause heterogeneity and anisotropy in the permeability structure and elastic properties of the fault zone [*Bruhn et al.*, 1994]. The fracture network controls the damage zone permeability and the high density of fractures typically makes it more permeable than the adjacent protolith. For instance, the damage zone permeability in the Dixie Valley fault zone is two to three orders of magnitude higher than the permeability of fractured protolith, and four to six orders of magnitude higher than the fault core permeability [*Bruhn*, 1993]. Experiments indicate that permeability of initially low porosity rocks taken to failure increase by two to three orders of magnitude [*Faulkner et al.*, 2010].

Fault zones in siliciclastic sedimentary basins are typically sand-shale gouges acting as complex conduit-barrier systems in which along-fault flow is encouraged and across fault flow is impeded [*Faulkner et al.*, 2010]. Natural gouge can have permeability anisotropy of up to three orders of magnitude [*Faulkner and Rutter*, 2000]. Paleo-fluid flow patterns and inferences of its evolution through geological time as function of basin development in California [*Boles et al.*, 2004] and mineralogical analysis of cements along faults in New Mexico [*Caine and Minor*, 2009] show further evidence of the importance of along-fault flow in siliciclastic aquifers. *Bense et al.*[submitted] emphasize that the conceptual models proposed in the geological literature are in agreement with hydrogeological observations. Therefore, fault-parallel fluid flow and transport should be expected in a variety of structural and hydrogeological settings.

Hydrogeological models on a large scale (e.g. 10-100s km) [*Person et al.*, 1996] are usually grid based continuum models that represent the bulk permeability of a fault zone or fault zone component (e.g. fault core and damage zone) and the classical advection–dispersion equation is applied to quantify transport of conservative solutes. On the opposite, discrete fracture network models explicitly represent the shape, connectivity, orientation and aperture of discrete fractures. However, the scale of such models domains is typically restricted to a few tens of meters [*Bense et al.*, submitted]**.**

Measurement and quantitative analysis of solute transport in fractured systems remains one of the most challenging problems in subsurface hydrology. The inherent complexity of fractured formations severely limits the quality of data that can be obtained from field measurements and the level of certainty in model prediction. Ultimately, numerical modeling of flow and transport in fractured aquifer may at best provide conservative, ‘‘worst-case scenario’’ estimates of possible behaviors [*Berkowitz*, 2002]**.**

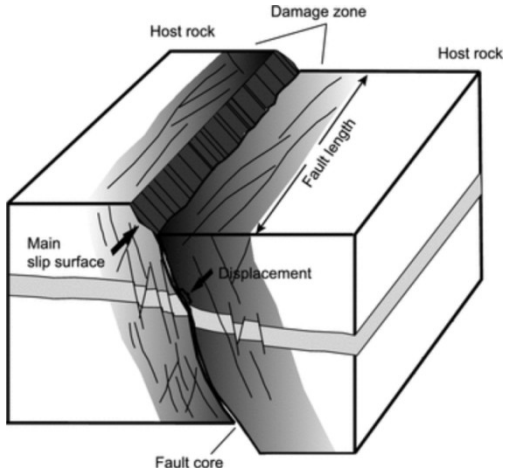

Figure 20. Conceptual model of a fault zone [*Kolyukhin and Torabi*, 2011]

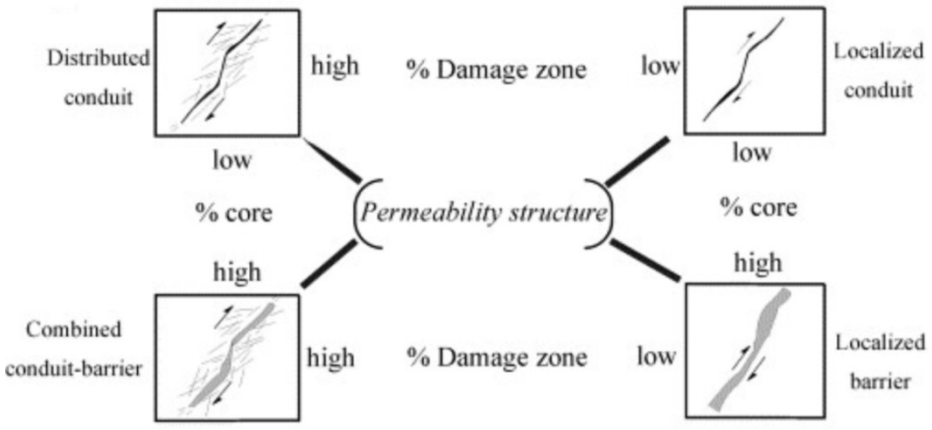

Figure 21. Conceptual scheme for fault-related fluid flow [*Caine et al.*, 1996]

2.3.2 Fault zones and hydraulic fracturing

Migration of contaminants from the shale unit to a shallow aquifer may be possible if hydraulic fracturing induces communication with other conductive paths, such as faults or wells. We can distinguish three scenarios where a fault zone would represent a potential pathway for leakage: 1) hydraulic fracturing reactivates (meaning causes additional offset and displacement) of a nearby fault zone due to the stress regime in the formation due to hydraulic fracturing; 2) hydraulic fractures may develop from the well to the fault zone, potentially increasing the size or permeability of the damage zone; and 3) the fault zone may act as a hydraulic conduit, even without interaction with hydraulic fractures.

Hydraulic fracturing operations and underground storage of CO_2 face common issues, such as groundwater contamination, which may occur by leakage through a preferential pathway such as faults. Impacts of injection and production on stress and risks of reactivation of a fault zone have thus been studied for in the context of hydraulic fracturing as well as underground storage of CO_2 [*Soltanzadeh and Hawkes*, 2008; 2009; *Streit and Hillis*, 2004; *Wessels et al.*, 2011].During hydraulic fracturing operations, faults are generally avoided when drilling as they give rise to a number of drilling problems [*Faulkner et al.*, 2010]. Diversion of fluid and proppant to a fault zone represent a significant cost for the operator. Moreover, the stimulation of a non-target formation may give rise to hydraulic connectivity with aquifers that ultimately increase water production. The negative effects of fracturing in the vicinity of a fault zone are thus a decreased stimulation of the target formation, a potential increase in water production, and a significant cost to the operator in terms of time and materials [*Wessels et al.*, 2011]. However, several reports underline the issues related to fault zone reactivation in hydraulic fracturing operations [*Cipolla et al.*, 2011; *Maxwell et al.*, 2009; *Soltanzadeh and Hawkes*, 2008; 2009; *Wessels et al.*, 2011], suggesting that fracturing at proximity of a zone is not an unusual practice.

Fault slippage and reactivation was first recognized as a possible cause of fluid flow in faulted areas by *Sibson* [1990]. This phenomenon is fundamentally controlled by the Mohr-Coulomb criterion, and has been extensively investigated [*Zoback*, 2007]. Faults can be classified [*Zoback*, 2007] as normal, strike-slip and reverse (or thrust) as a function of the vertical stress (σ_v) and the minimum and maximum horizontal stresses (σ_h and σ_H), as depicted in Figure 22. Fault zone reactivation is controlled by the shear and normal stress components on the fault plane [*Nacht et al.*, 2012].

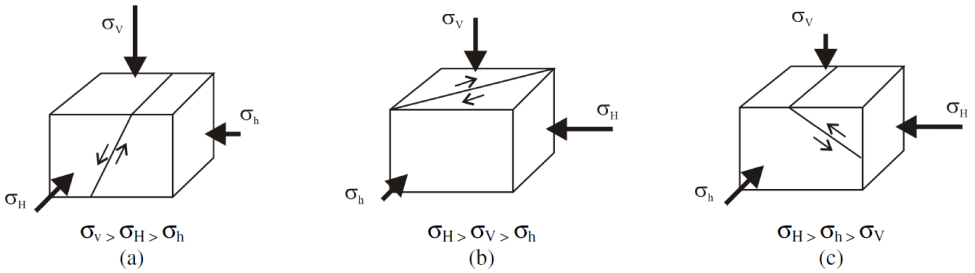

Figure 22. Classification of faults: **(a)** normal fault; **(b)** strike-slip fault; **(c)** reverse fault [*Nacht et al.*, 2012]

Increased formation pressures due to fluid or gas injection can potentially open fractures and cause displacement on fault zones that exist in a reservoir [*Soltanzadeh and Hawkes*, 2009; *Streit and Hillis*, 2004]. The phenomenon of fault zone reactivation is thus important for the achievement of fluid injection for enhanced hydrocarbon recovery, waste disposal or greenhouse gas sequestration, as it raises the same concerns regarding contamination of shallow aquifers due to leakage through potential pathways such as faults. In the case of hydraulic fracturing, fault zone activation may be caused by the hydraulic fracture propagating into the fault zone or by stress changes resulting from deformation caused by the hydraulic fracture [*Cipolla et al.*, 2011]. Alternatively, depletion of fluid pressures during production can lead to pore compaction in the reservoir rock, which can cause induced fault zone reactivation [*Streit and Hillis*, 2004].

Various risks are related to the reactivation of faults. After reactivation, these features are likely to serve as fluid leakage paths [*Wiprut and Zoback*, 2000]. Pressure depletion may also cause: ground subsidence [*Chan and Zoback*, 2007], which in turn might damage

surface structures; well bore casing failure; and the formation of new fractures [*Segall*, 1989; *Yudovich et al.*, 1989]. Such deformation can potentially compromise the integrity of fault and cap rock seals [*Streit and Hillis*, 2004]. In extreme cases, earthquakes may be induced, which may cause damage to operations equipment and civil structures [*Soltanzadeh and Hawkes*, 2008].

Analyses of fault zone stability require the determination of fault orientations, ambient pore fluid pressures and in situ stresses in a potential storage site [*Streit and Hillis*, 2004]. Risk of fault zone reactivation depends on fault orientation relative to the maximum tectonic stress. Extreme increases in pore fluid pressures in reservoir rock in the vicinity of faults with orientations unfavourable for reactivation would cause the formation of new fractures instead of fault zone reactivation. Such fault zones can be identified from failure plots if the differential stresses and the strength of rocks adjacent to faults are known [*Streit and Hillis*, 2004]. Maximum sustainable fluid pressures on faults are in most cases lower than pore pressures that induce new fractures [*Streit and Hillis*, 2004]. Therefore the risk of fault zone activation during hydraulic fracturing is important.

Rudnicki [2002] showed that for a thrust fault stress regime, the induced stress changes always favor fault stabilization during production and de-stabilization during injection. *Soltanzadeh and Hawkes* [2009] developed a methodology to find the range of fault dip angles that tend towards reactivation in either thrust or normal fault stress regimes. The results demonstrate that during production from a reservoir in a normal fault stress regime, fault zone reactivation is likely to occur within the reservoir and adjacent to its flanks. Depending on the amount of stress change within the reservoir, only moderate dip angles tend towards reactivation. For a thrust-fault stress regime, only faults located in rocks overlying and underlying the reservoir tend towards reactivation. The results for the analogous case of fluid injection are exactly the opposite. Sensitivity analyses show that the locations of the boundaries defining these regions of reactivation (or stabilization) tendency are not highly sensitive to the fault friction coefficient [*Soltanzadeh and Hawkes*, 2009]. It is also shown that fault reactivation potential is dependent on reservoir geometry and dip angle [*Soltanzadeh and Hawkes*, 2008], which demonstrates the

importance of accounting for the actual reservoir geometry when assessing fault reactivation location and potential.

Moreover, fault zone reactivation due to hydraulic fracturing has been reported by several microseismic studies. Microseismic imaging is a powerful method to map the hydraulic fracture stimulation of a well [*Maxwell et al.*, 2009]. This technique is genuinely used during hydraulic fracturing as being able to identify such features in real time allows the operator to not only identify fault zones but to stop treatment and avoid these features [*Kratz et al.*, 2012]. Fault zone activation is one of the most common anomalies identified using microseismic measurements. Fault zone activation can be identified by a significant, but localized, increase in event magnitudes [*Maxwell et al.*, 2009] and a marked change in the distribution of event magnitudes [*Cipolla et al.*, 2011]. Statistical analysis using frequency magnitude distribution histograms may be indicative of changes in the stress magnitude. Indeed, microseismicity generated by activation of natural fractures during hydraulic stimulation is mechanically dependent upon pumping whereas fault activity is not. Therefore natural fracture events will take place during pumping, and fault zone activation events will take place during a much longer period of time. This is due to the higher stress imposed on the fault that is slowly released with an overall lower *b* value, which means that for every unit decrease in magnitude, the increase in number of microseisms will be lower [*Wessels et al.*, 2011]. An interesting example lies in the events recorded in a gas well in Western Canada which intersected a reverse fault system with low angle thrust faults ranging in dip from 20-30°. The hydraulic fractures induced movement on a nearby fault [*Maxwell et al.*, 2009]. The activation is likely due to deformation effects and not pressure increase or lubrication due to fluid invasion since the fault events are disconnected from the main event pattern. The combination of the large number of localized high magnitude events, temporal behavior of these events, and the b-value of the events confirms that the events are associated with fault zone activation [*Cipolla et al.*, 2011]. Another case study in the Lower Barnett Shale of the Ft. Worth basin in the Mid-Continent USA shows how microseismic allows to identify events that are generated by motion along a fault plane and adapt the location of the subsequent

treatment stages in order to avoid diversion of pumped fluid and proppant into the fault zone [*Wessels et al.*, 2011].

The EPA acknowledges the risk for upward migration of hydrocarbons and other contaminants in hydraulic fracturing operation as their last report considers the scenario of sealed faults being activated by hydraulic fracturing and creating pathways [*EPA*, 2012]. The EPA concludes that the possibility of fault zone reactivation creating a pathway to shallow ground water resources is remote because preliminary simulation suggests that hydraulic fracturing may lead to fault rupture with lengths no greater than 40 to 50 meters [*EPA*, 2012]. However, as stated before, the hydrogeological properties of fault zones are poorly known, and a fault zone may act as a conduit for gas or contaminant. In this case, hydraulic fracturing could reactivate the fault zone near the reservoir and allow fluid migration through the upper part of the fault zone acting as a conduit.

Some studies [*Drilling and Completion Committee*, 2012] suggest that hydraulic fracturing might also induce communication with other conductive paths. The industry developed guidelines to assess the risk of interwellbore communication during hydraulic fracturing operations, suggesting that hydraulic fracturing can induce communication with other wells, either water wells or gas wells [*Drilling and Completion Committee*, 2012]. Interwellbore communication is defined as a fluid and/or pressure communication event at an offset well during a fracture stimulation operation on a wellbore that is receiving fracture stimulation. It can lead to well control event, blowout or production related problems. Interwellbore communication events may happen within or outside the target zone (the area being fracture stimulated in the well).
Hydraulic fracturing may thus induce communication with conductive paths. Communication might happen either with natural path, by reactivating a nearby fault zone or fracturing up to a fault zone, or with water or energy wells.

Chapter 3 The location of old groundwater in hydrogeologic basins and layered aquifer systems

3.1 Introduction

Groundwater age plays an important role in a wide range of geologic processes [*Alley et al.*, 2002; *Bethke and Johnson*, 2008; *Freeze and Cherry*, 1979; *Garven*, 1995; *Ingebritsen et al.*, 2006; *Tóth*, 1999]. Knowledge of the age of groundwater derived from radiogenic isotopes determines the timescales of subsurface processes and contaminant transport rates and is a key indicator for the renewability of groundwater resources [*Bethke and Johnson*, 2008; *Cook and Herczeg*, 2000; *Kazemi et al.*, 2006]. Groundwater age is defined as the time that has passed since the water crossed the water table [*Alley et al.*, 2002; *Kazemi et al.*, 2006]. *Tóth* [1963] demonstrated that areas of stagnant groundwater form at the intersection of local, intermediate and regional flow systems (Figure 23a). Such stagnant zones, with extremely high groundwater ages and low velocity, are important because they accumulate solutes and contaminants transported by groundwater [*Tóth*, 1999]. The location of stagnation points is sensitive to the basin geometry, the surface topography [*Tóth*, 1963] and to the decrease of permeability with depth [*Jiang et al.*, 2011]. Previous modeling studies have simulated groundwater ages in basins with homogenous permeability [*Tóth*, 1963] or a gradual decrease of permeability with depth [*Jiang et al.*, 2011; *Jiang et al.*, 2010]. *Jiang et al.* [2009] showed how decreasing permeability with depth limits regional groundwater flow while *Jiang et al.*[2010] importantly showed different groundwater flow both lead to simultaneous rejuvenation and aging of groundwater.

However, most aquifer systems and hydrogeologic basins consist of layered sediments or rocks, in which small changes in material properties such as grain size [*Koltermann and Gorelick*, 1995] or clay content [*Revil and Cathles*, 1999] can generate orders of magnitudes of changes in permeability. Lenses or layers of high or low permeability materials have been shown to greatly modify regional groundwater flow [*Freeze and*

Witherspoon, 1967] and groundwater age in specific basins has been simulated [*Sanford et al.*, 2004]. *Sanford* [2011] showed that overturned groundwater ages (younger ages under older ages) can exist where substantial vertically layered heterogeneity is present, regardless of the upper boundary condition. Field evidence indicates that these overturned ages exist in layered systems due to groundwater inflow from adjacent basins and mountains [*Sanford et al.*, 2004]. However, *Sanford* [2011] did not name these 'high age zones', document their occurrence in a wide variety of hydrogeological conditions, examine the processes that control their formation or discuss why they are important to a variety of Earth processes.

Hydrogeologic basins and aquifer systems commonly have laterally extensive low permeability layers. Laterally extensive low-permeability layers are particularly common in basins that form due to flexural or thermal subsidence, such as foreland and sag basins. In basins created by extensional or strike-slip tectonics faulting often limits the continuity of strata [*Ingersoll*, 1988]. In unconsolidated aquifer systems, laterally extensive, low permeability units such as glacial tills, lacustrine and marine clays and silts are common. In unconsolidated aquifer systems consisting of fluvial, glaciofluvial, alluvial and colluvial deposits [*LaBolle et al.*, 2006] units are less continuous. The heterogeneous permeability field in such discontinuous aquifer systems has been successful simulated with geostatistical methods [*Marsily et al.*, 2005]. Simulating the distribution of groundwater ages in such heterogeneous permeability field is computationally expensive and limited to small-scales (100s m) at sites with detailed hydrogeological data [*LaBolle et al.*, 2006].

Our objective is to scrutinise the processes and conditions that lead to the formation of high groundwater age zones at regional scales (Figure 23b). Therefore, we simulate a simplified layered and heterogeneous system in order to simulate the process of high age formation in a wide variety of hydrological and geological settings, while acknowledging that hydrogeologic basins and layered aquifer systems often have multiple low permeability zones and cross-cutting faults.

3.2 Numerical simulation

We numerically simulated groundwater age in steady-state, regional-scale (1-100s km) groundwater systems. We simulate mean groundwater age as a tracer subject to advection, diffusion and dispersion using a yearly production of one unit of conservative solute within the fluid [*Goode*, 1996; *Voss and Wood*, 1994]. Over 1000 simulations were conducted with SUTRA, a US Geological Survey numerical groundwater model that uses the finite element method [*Voss and Provost*, 2002]. The model domain consists of a rectangular cross-section of a generic basin with an imposed linear hydraulic gradient at the upper boundary and no flow boundaries on all other sides (Figure 23b). The basin contains three layers, an upper aquifer, a low permeability unit and a lower aquifer. Each unit is assumed to be homogeneous and isotropic. Parameters other than permeability such as diffusivity and porosity are kept constant within the whole domain. Values of dispersivity at the regional scale are uncertain [*Freeze and Cherry*, 1979]. We chose to assign the dispersivity at the minimum value that allows numerical stability, and we studied the effect of dispersivity on groundwater ages in a separate set of model simulations. Longitudinal dispersivity is set to one fourth of the local element dimension (α_L = 5m) and transversal dispersivity at one tenth of longitudinal dispersivity [*Voss and Provost*, 2002] (α_T = 0.5m). We explored the effects of a large range of values of the key parameters that control groundwater age, including the permeability of the low-permeability unit (k_2) and the high permeability unit (k_1), basin size and aspect ratio, hydraulic gradient and lateral continuity of the low-permeability layer. The parameter ranges (Table 2) are intended to capture the variability observed in natural hydrogeological systems.

We define 'high age zone' as a zone within the low permeability layer where the maximum groundwater age is at least twice that of surrounding water. The width of this high age zone was determined as the horizontal distance where the groundwater age is more than half the maximum age (Figure 24b). If groundwater age remained above 50% of the maximum on one side of the layer, we considered that the high age zone did not form (Figure 24a, c). The value of 50% of the maximum age is arbitrary; other cut offs such as 90% were also examined and result in similar patterns of high age zones.

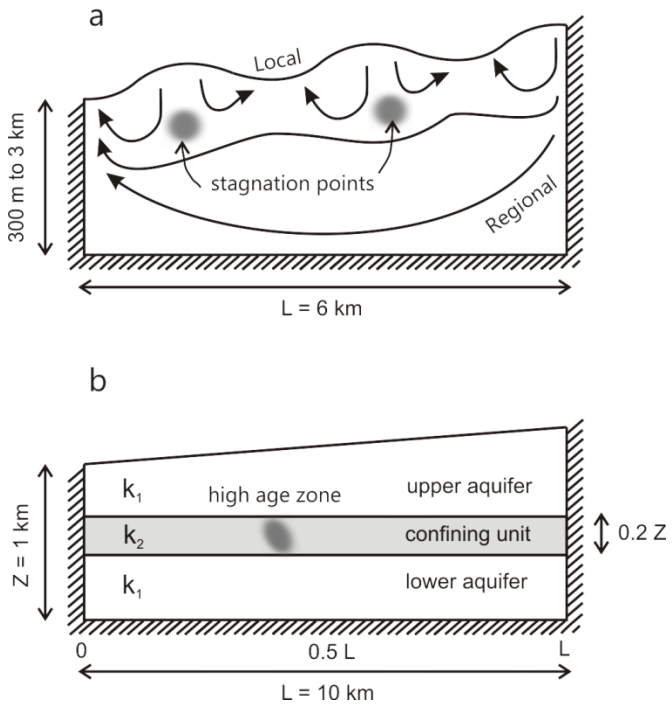

Figure 23. Stagnation points and zones of high groundwater age in regional-scale groundwater flow. **(a)** Theoretical model and results described in *Tóth* [1963]. Grey areas represent stagnation zones that form at the intersection of local, intermediate and regional flow systems. **(b)** Theoretical model used in this study with dark grey showing the high age zone. The hatched lines indicate a no-flow boundary.

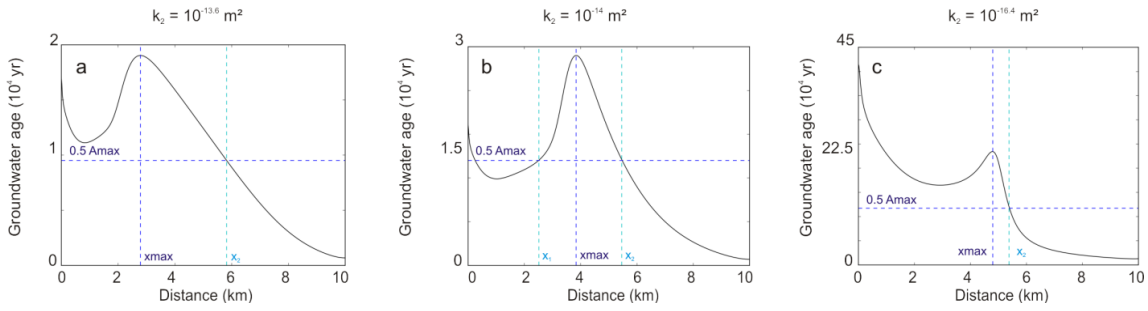

Figure 24: Determination of high age zone location. Cross-section of groundwater age and location of maximum age (x_{max}) and points where groundwater age is 50% of the maximum ($x_1 < x_{max} < x_2$) at the middle of the low-permeability unit under a 0.01 hydraulic gradient for sedimentary rocks ($k_1 = 10^{-13}$ m²) and a layer permeability of **(a)** $k_2 = 10^{-13.6}$ m², **(b)** $k_2 = 10^{-14}$ m² and **(c)** $k_2 = 10^{-16.4}$ m². High age zone forms in case b but not in cases a and c.

Table 2. Overview of parameter values

Parameter	Range of variation	Related figure
Permeability k_1 of the aquifer	$k_1 = 10^{-8}$ m² to 10^{-17} m²	Figure 2, Figure 3
Permeability k_2 of the low-permeability unit	$k_2 = 10^{-8.5}$ m² to 10^{-20} m²	Figure 2, Figure 3
Hydraulic gradient	0.001, 0.005, 0.01, 0.1	Figure 2
Depth of the low-k layer	0.1 to 0.9	Figure 4a
Thickness of the low-k layer	0.05 to 0.95	Figure 4b
Continuity of the low-k layer	0.05 to 1	Figure 4c
Length of the basin L	1 to 100 km	Figure 4d
Depth of the basin Z	100 m to 10km	Figure 4d
Aspect ratio of the basin	1:1 to 1:100	Figure 4e
Porosity	0.1, 0.3	All figures with n = 0.3 except for Figure S5.
Longitudinal dispersivity α_L	5, 50, 500 m	Figure S3
Transversal dispersivity α_T	0.005, 0.05, 0.5, 5, 50 m	Figure S3
Horizontal grid spacing	20 m	
Vertical grid spacing	5 m	

3.3 Where high age zones form

For a range of hydraulic gradients, and permeability values that represent typical value of sedimentary rocks ($k_1 = 10^{-13}$ m²) or unconsolidated sediments ($k_1 = 10^{-11}$ m²) [*Gleeson et al.*, 2011b], simulations show that distinct zones of high groundwater ages develop in the low-permeability unit (Figure 25). The location and width of this high age zone varies systematically with permeability contrast and hydraulic gradient. Three model simulations illustrate the location and width of the high age zone for different permeability contrasts between the low permeability layer and the surrounding medium

(Figure 25a-c). At low permeability contrast ($k_2 = 10^{-14}$ m²), the high age zone contains groundwater that is a little older than twice the age of the surrounding groundwater. The zone is spread out over a width of 0.3 of the total length of the basin (L) and the maximum age is located at 0.35 L (Figure 25a). At moderate permeability contrast ($k_2 = 10^{-15.4}$ m²), the ages in the high age zone are more than 30 times older than in the surrounding area. The maximum age within the low-permeability unit is located near the midline of the basin and the high age zone is relatively narrow (Figure 25b). At higher permeability contrast ($k_2 = 10^{-16}$ m²), the high age zone is wider and the age contrast less pronounced (Figure 25c). In all cases, the maximum groundwater age is located between 0.2 and 0.5L. When the permeability of the low-permeability unit (k_2) is lower than 10^{-16} m², the high age zone does not form (Figure 25e). In most simulations, high groundwater ages are also found near the down-gradient boundary condition as previous authors have shown [*Jiang et al.*, 2009; *Jiang et al.*, 2010].

The location of the high age zone depends on the depth, thickness and continuity of the low permeability layer and the aspect ratio of the basin. High age zones shift towards the down-gradient part of the low permeability layer for high values of layer depth or thicknesses (Figure 26). For both low and high values of continuity, the high age zone is located close to the midline of the aquifer. For moderate continuities, the high age zone is located further downgradient. This change in behavior is due to the transition from a single flow system (with one recharge area and one discharge area) to a more complex flow system with multiple recharge and discharge areas at a layer continuity of ~0.7. The aspect ratio of the basin also impacts the location of a high age zone. In shallow, wide basins the high age zone is located closer to the discharge zone with low to moderate permeability contrasts ($\log(k_1 - k_2) \leq 2$). For basins with high permeability contrasts the high age zone is independent of the aspect ratio. The location of high age zones is largely independent of the basin length (Figure 26d).

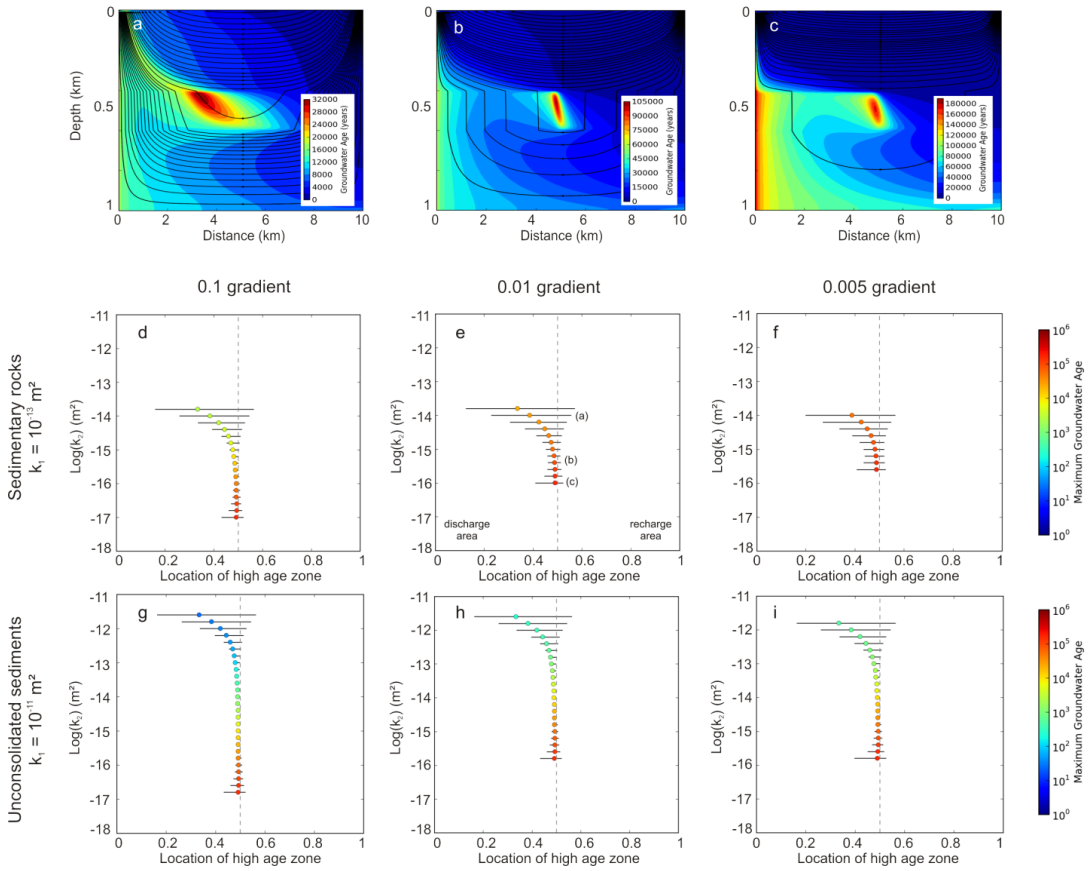

Figure 25. Zones of high groundwater age are common across a wide range of hydraulic gradients and permeability contrasts. **(a-c).** Distribution of groundwater age within the aquifer under a 0.01 hydraulic gradient for sedimentary rocks ($k_1 = 10^{-13}$ m²) and a layer permeability of **(a)** $k_2 = 10^{-14}$ m², **(b)** $k_2 = 10^{-15.4}$ m² and **(c)** $k_2 = 10^{-16}$ m². **(d-f).** Location of high age zone vs. k_2 for sedimentary rocks ($k_1 = 10^{-13}$ m²) under a gradient of **(d)** 0.1, **(e)** 0.01 and **(f)** 0.005. **(g-i).** Location of high age zone vs. k_2 for unconsolidated sediments ($k_1 = 10^{-11}$ m²) under a gradient of **(g)** 0.1, **(h)** 0.01 and **(i)** 0.005. Circles represent the location of the maximum groundwater age; lines represent the area where groundwater ages are higher than 50% of the maximum age. For each case, simulations have been run for values of k_2 from k_1 to 10^{-18} m². Values not specified mean that a high age zone does not form for this set of parameters.

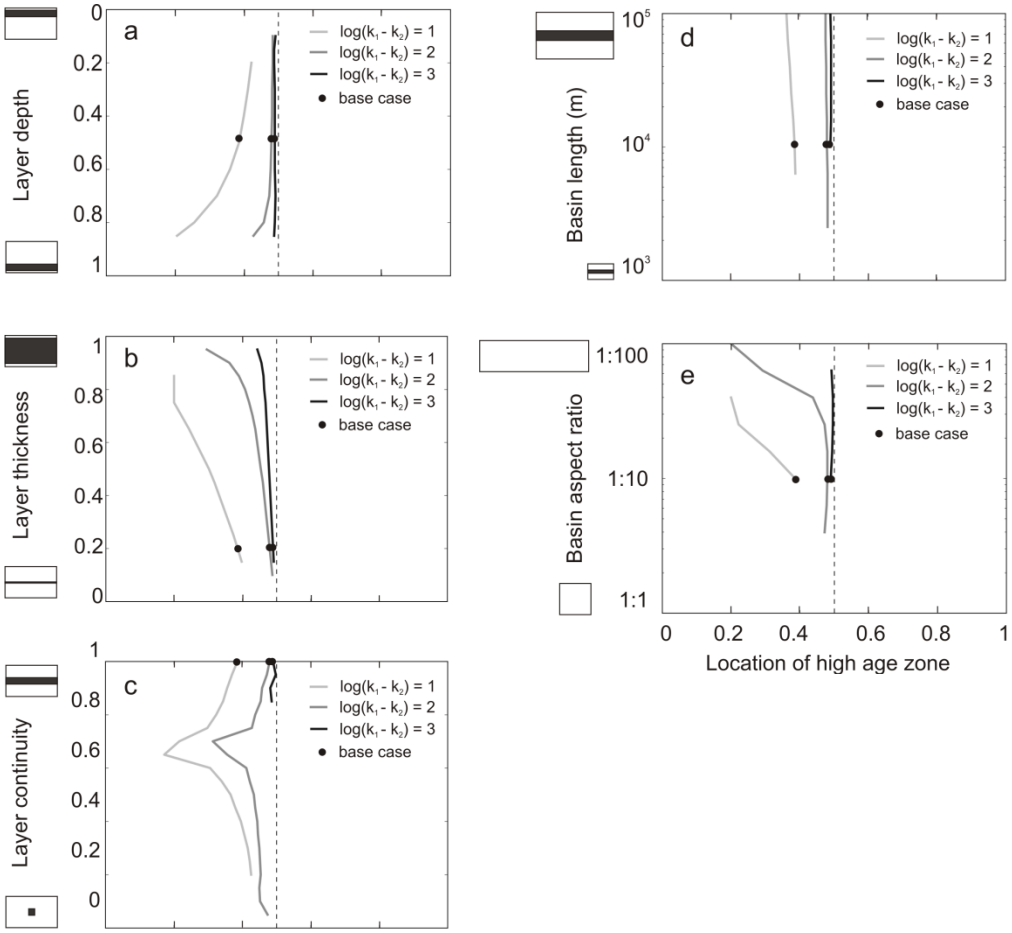

Figure 26. Zones of high groundwater age are common in diverse basin stratigraphies and geometries. Location of high age zone for sedimentary rocks ($k_1 = 10^{-13}$ m²) with permeability contrasts from 1 to 3 and under a 0.01 gradient, depending on **(a)** layer depth, **(b)** layer thickness, **(c)** layer continuity, **(d)** basin length and **(e)** basin aspect ratio. Black dots represent the basin geometry of the base case (Figure 1b). Values not specified mean that a high age zone does not form for this set of parameters. Layer depth and thickness are specified as fractions of the total depth and thickness of the basin. Layer continuity is specified as fraction of the total length of the basin and the layer is cut off both at the recharge and discharge ends.

3.4 Why high age zones form

Our results suggest that two mechanisms lead to the formation of a zone of high groundwater ages. First, high age zones are caused by mixing of groundwater from flow paths that travel through only the upper two layers and flow paths that travel through all three layers. For a wide range of permeabilities of the low permeability unit (k_2), the groundwater velocity in the lower aquifer is high enough for the groundwater to travel faster than the groundwater flowing only through the overlying low-permeability unit. Upward flow of the younger groundwater near the discharge zone leads to rejuvenation of groundwater age within the low-permeability unit. High age zones are formed upgradient of the intersection of flow paths going through the lower aquifer and the low-permeability unit, and through the low-permeability unit only. Second, the high age zones are controlled by the flow velocities in the low-permeability unit. The lowest velocities are found near the middle of the basin and coincide with the location of the high age zone.

Which of these two mechanisms is dominant controls the location of the high age zone and is predictable from the permeability contrast between the aquifer and the low-permeability unit. At low permeability contrasts the velocity is relatively constant over most of the low-permeability unit, and the high age zone is mainly controlled by the rejuvenation of groundwater below the discharge zone due to upward flow of groundwater from the lowest aquifer. At high permeability contrast the location of the high age zone follows the narrow zone of low flow velocities that is located in the middle of the basin. Model simulations confirm that high age zones are not necessarily stagnation points, zones where groundwater velocity is zero or/and flow is in opposite directions [*Jiang et al.*, 2011]. In our model simulation flow velocities maintain values of 10^{-4} m/yr or higher. However, high age zones develop in areas of low velocities.

3.5 High age zones form in a variety of basins

High age zones form in hydrogeologic basins and aquifer systems with a range of permeability contrasts (Figure 25). The permeability contrast (k_1-k_2) in which high age zones form in hydrogeologic basins and unconsolidated sediments is ~3-4 and ~5-6 orders of magnitude, respectively. At high permeability contrast, the whole low-permeability lens contains groundwater that is older than the surrounding area but no distinct high age zone forms within the unit. In fact, the permeability contrast (k_1-k_2) for which a high age zone develops is predictable (Figure 27). For example, for simulations with a 0.01 gradient, high age zones forms when the permeability of the low-permeability unit (k_2) is higher than 10^{-16} m² and one order of magnitude lower than the permeability of the rest of the aquifer k_1. The maximum groundwater age in the low-permeability unit depends on the layer permeability but not on the permeability of the aquifer, except when the permeability contrast is small. The formation of high age zones is thus primarily controlled by the permeability of the low-permeability layer. Moreover, in both hydrogeologic basins and aquifer systems, high age zones do not form when the permeability of the low permeability unit is less than approximately 10^{-16} m².

Model simulations show that high age zones develop for a wide range of depth, thickness and continuity of the low permeability unit and basin geometries (Figure 26). High age zones form in layer depths (normalized to total thickness) of 0.1 to 0.9 (Figure 26a). Similarly high age zones form in normalized layer thicknesses of 0.1 to 0.9 (Figure 26b). For low permeability contrasts ($\log(k_1 - k_2) < 3$) high age zones form in basins with a range of continuity values (Figure 26c). However, for higher permeability contrasts, high age zones form only in basins with nearly continuous low permeability layers (normalized continuity > 0.8). The size of the basin does not impact the location of the high age zone (Figure 26d). However, high age zones do not develop in relatively small basins ($<10^3$-10^4 m length). High age zones form in basins with a variety of aspect ratio from 1:10 to >1:50 (Figure 26e).

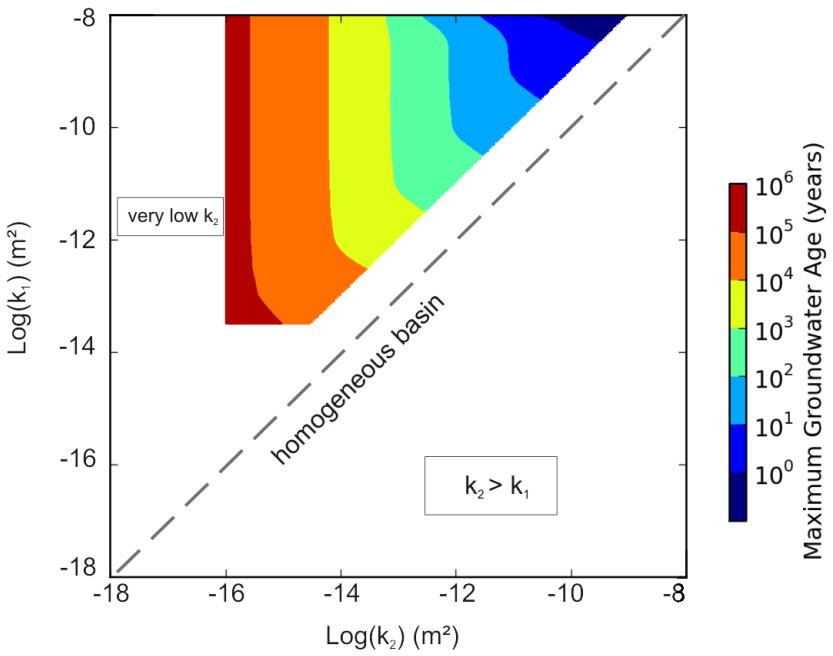

Figure 27. The permeability of the low-permeability unit controls the groundwater age. Values of k_1 and k_2 allowing the formation of high age zone under a 0.01 gradient. The colored area represents the couple (k_1, k_2) for which a high age zone forms. Color indicates the value of the maximum age within the low permeability layer. Simulations were run for $k_1 = 10^{-8}$ to 10^{-17} m² and $k_2 = 10^{-8.5}$ to 10^{-20} m².

3.6 Conclusions and implications

Numerical simulations clearly show that zones of high groundwater age should be expected in regional (>2 km length) layered hydrogeologic basins and aquifer systems over a wide range of natural-occurring permeability contrasts, hydraulic gradients and basin geometries. Narrow zones of groundwater with ages up to a million years form in low permeability units downgradient of midline of typical hydrogeologic basins and aquifers systems. These high age zones form due to low groundwater velocities in the low permeability layer and the rejuvenation of the groundwater through mixing of different flow paths near discharge zones. Simulations suggest these high age zones likely form if the permeability of the low permeability layer is at least one order of magnitude lower than the flanking units, but greater than ~10^{-16} m². The lower limit corresponds to the regional-scale permeability of fine-grained sedimentary rocks [*Gleeson et al.*, 2011b] or the highest permeability values for argillaceous material

[*Neuzil*, 1994]. Therefore, these high age zone are expected in many hydrogeologic basins and aquifer systems, although to our knowledge they have not been observed in the field. This is likely because groundwater age studies tend to focus on permeable units and low-permeability unit are rarely sampled in sufficient detail to reveal lateral age gradients. However, our model results are a testable hypothesis for a systematic sampling campaign of groundwater ages within a regional-scale low-permeability unit. The simplified layered system developed in this chapter leads to a relatively complex distribution of groundwater age and therefore we expect a more complex pattern in a field study. Additionally it is uncertain how three-dimensional flow in layered hydrogeologic basins and aquifer systems could affect the development and processes of high age zones.

The strong lateral variations in groundwater ages in low-permeability layers found in this study have implications for a range of geological processes and Earth science research fields. Water-rock interactions that depend on groundwater and solute fluxes, such as the precipitation or dissolution of carbonates, (de-)dolomitization and quartz cementation [*Bjørlykke*, 1994; *Ingebritsen et al.*, 2006; *Machel*, 1999], are likely to be limited in high-age zones. This may cause lateral variations in porosity, permeability and mechanical properties of low permeability materials, which to our knowledge have not previously been considered. High age zones may inhibit the subsurface transport of microbes by groundwater [*Walvoord et al.*, 1999] and the resulting biodegradation of oil and gas [*Head et al.*, 2003], which could have implications for the extraction of hydrocarbons from low-permeable strata. Similar to stagnation points [*Tóth*, 1999], high age zones can form favorable locations for the storage of radioactive waste, as the risk of the spreading of contaminants is relatively low. High age zones are likely to impact the interpretation of groundwater age tracers, which are key tools for characterizing natural flow systems and quantifying groundwater recharge and sustainable extraction rates [*Alley et al.*, 2002; *Cook and Bohlke*, 2000; *Kazemi et al.*, 2006; *Scanlon et al.*, 2002]. Finally, the observed lateral age variations in low-permeability units are also likely to have an impact on studies that use environmental tracers to reconstruct past hydrological [*Beyerle*, 1998] or climatological conditions [*Weyhenmeyer*, 2000], knowledge of their location allows targeted sampling of old groundwaters.

Chapter 4 Hydraulic fracturing in faulted sedimentary basins: numerical simulation of potential long term contamination of shallow aquifers

4.1 Introduction

Over the past 15 years, shale gas has emerged as a viable and important energy resource. In order to produce economically viable quantities of natural gas from unconventional reservoirs such as shale, the technique of hydraulic fracturing (or "fracking") generally has to be used [*BAPE*, 2011; *EPA*, 2012]. Hydraulic fracturing consists of injecting high volumes of 'fracture' fluid at pressures greater than lithospheric in order to fracture the formation and increase its local permeability [*EPA*, 2012]. After hydraulic fracturing, the pressure is relieved and the "flowback", composed of fracture fluid and formation fluids, returns to the surface [*Gregory et al.*, 2011]. The fracking fluid is commonly composed of ~99.5% water and proppants (generally sand), and ~0.5% chemical additives including acids, solvents and biocides [*BAPE*, 2011; *Gregory et al.*, 2011]. Additionally, the flowback not only contains saline formation fluids and natural gas but also naturally occurring contaminants present in the host shale rocks such as radioactive compounds and heavy metals [*Gregory et al.*, 2011; *Groundwater Protection Council and All Consulting*, 2009]**.** Concerns about the potential environmental impact of hydraulic fracturing have increased, especially risks relating to drinking water resources [*EPA*, 2012; *Kargbo et al.*, 2010]. Potential drinking water issues include: 1) water availability due to water withdrawal; 2) water pollution related to spills and leaks at above ground hydraulic fracturing operations; 3) unsuitable treatment of wastewater; 4) failures of wells in the shallow subsurface due to poor cementing or steel casing corrosion; and 5) geologic failures at depth as a result of the fracturing that could cause potential contamination of shallow groundwater aquifers via preferential pathways (Figure 28) [*EPA*, 2012].

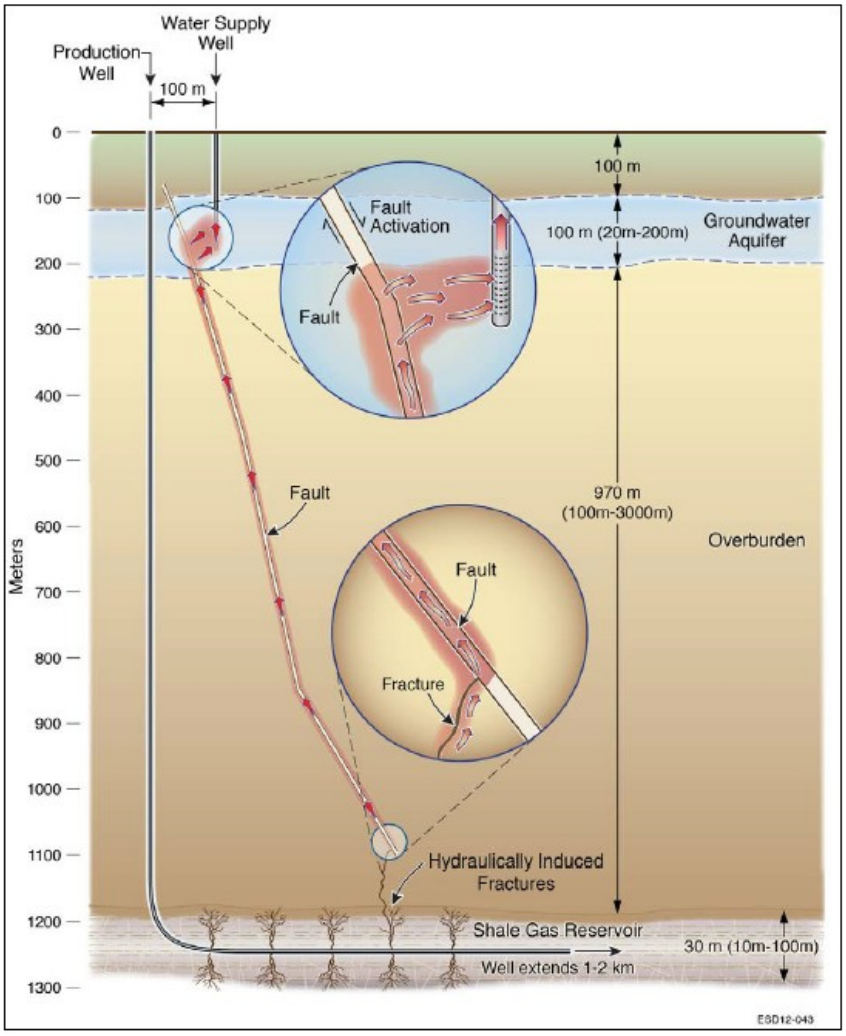

Figure 28. Potential upwards migration of contaminants through a fault zone from the shale unit to a shallow aquifer (from *EPA* [2012]).

Some of these issues can be addressed by better design and the application of stringent regulations. However, the long term impact and potential of contamination of groundwater aquifers related to the fracturing of the target shale unit is unclear. Although fluid migration rates are usually extremely slow in deep sedimentary systems, heterogeneities such as faults can provide preferential pathways through which fluids carrying contaminants may migrate more rapidly to reach shallow aquifers.

The potential contamination of shallow aquifers from fluids originating from gas shales through the migration of contaminants via preferential pathways such as faults has been acknowledged [*BAPE*, 2011; *EPA*, 2012], but is often consider negligible compared to

other potential drinking water issues related to shale gas exploitation. This type of contamination has been considered as highly unlikely because 1) no fracking fluid has yet been found in drinking water wells [*Osborn et al.*, 2011]; 2) the significant distance between the shale unit (at a few thousands meters depth) and the shallow aquifers (at less than a few hundred meters depth) would not lead to contaminant migration over short timescales [*Alpha Environmental Consultants*, 2009; *BAPE*, 2011; *Howarth et al.*, 2011; *Zoback et al.*, 2010]; 3) the formations above the shale unit often contains low-permeability lithologies that would decrease further the rate of transport [*Arthur et al.*, 2008; *BAPE*, 2011]; 4) it is very unlikely that hydraulic fractures would propagate over such long distances to directly connect the gas shale and shallow aquifers [*Zoback et al.*, 2010]; 5) fault reactivation due to hydraulic fracturing would likely occur on small distances of a few meters [*EPA*, 2012]; and 6) during gas production, downwards and horizontal flow to the horizontal shale gas well would be promoted, decreasing the risk of upwards migration [*Howarth et al.*, 2011]. Although fluid migration rates are usually extremely slow in deep sedimentary basins, migration of contaminants from the gas shale to a shallow aquifer may be possible if hydraulic fracturing induces communication with other fluid conductive paths, such as faults or wells. If conductive paths are present from the gas shale to shallower depths, the long distances and low-permeability units may not act as sufficient barriers for fluid flow to shallow aquifers. Furthermore, although fluid flow towards horizontal shale gas wells would be enhanced during gas production, it may not be the case once production has stopped as overpressure may still remain in the gas shale. Finally, the lack of observed contamination of drinking water wells, after less than 30 years of shale gas hydraulic fracturing does not preclude future groundwater contamination.

We discern three scenarios in which a hydraulically conductive fault zone could represent a potential pathway for contamination from a hydraulic fracture zone: 1) hydraulic fracturing reactivates a nearby fault zone due to the stress regime in the formation causing additional deformation and offset; 2) hydraulic fractures may develop from the well to the fault zone, potentially increasing the size or permeability of the damage zone associated with the fault; and 3) the fault zone may act as a hydraulic conduit, even

without interaction with hydraulic fractures. Fault zone reactivation and the loss of hydrofracturing fluids into fault zones suggest these scenarios are plausible. Fault slippage and reactivation [*Sibson*, 1990; *Zoback*, 2007] is caused by liquid or gas injection [*Soltanzadeh and Hawkes*, 2009; *Streit and Hillis*, 2004], or by depletion of fluid pressures during production [*Streit and Hillis*, 2004], and controlled by shear and normal stress components on the fault plane [*Nacht et al.*, 2012], fault orientation [*Rudnicki*, 2002; *Soltanzadeh and Hawkes*, 2009], and the reservoir geometry and dip angle [*Soltanzadeh and Hawkes*, 2008]. Fault zone reactivation due to hydraulic fracturing has been reported by several microseismic studies, and is is one of the most common anomalies identified using microseismic measurements [*Cipolla et al.*, 2011]. During hydraulic fracturing operations, faults are generally avoided when drilling as they give rise to a number of problems [*Wessels et al.*, 2011]. Diversion of fluid and proppant to a fault zone represents a significant cost for the operator. The negative effects of fracturing in the vicinity of a fault zone are a decreased hydraulic fracturing of the target formation, a potential increase in flowback water, and a significant cost to the operator in terms of time and materials [*Wessels et al.*, 2011]. Several reports underline the issues related to fault zone reactivation in hydraulic fracturing operations [*Cipolla et al.*, 2011; *Maxwell et al.*, 2009; *Soltanzadeh and Hawkes*, 2008; 2009; *Wessels et al.*, 2011], suggesting that fracturing at proximity of permeable fault zones at depth is not an unusual practice.

Although fault zones can clearly be permeable hydraulic features at the typical depth range of prospective shale gas formations (0.5 to 4.5 km [*EIA*, 2011b]), an important question is whether fault zones could be continuous permeable features from the depth of shale gas formations to near the surface. Fault zones have a complex hydraulic structure that can be barriers, conduits or conduit-barriers [*Aydin*, 2000; *Bense and Person*, 2006; *Caine et al.*, 1996; *Rawling et al.*, 2001]. Techniques for predicting low permeability fault zones in sedimentary basins, called “fault seals” have been described in the petroleum literature. For example, the shale gouge ratio [*Yielding et al.*, 1997] uses the estimated clay-content of faults to determine the fault’s sealing capacities, which lead to reduction in across-fault permeability. However, faults in sedimentary basins have also

been shown to be conduits of gas, petroleum and mineral deposits [*Pinti and Marty*, 2000]. Along-fault permeability can be estimated using clay-content as an indication of the potential presence of sand dragged along the fault zone and providing pathways for preferential flow [*Bense and Person*, 2006]. Fault zones in siliciclastic sedimentary basins are typically sand-shale gouges acting as complex conduit-barrier systems in which along-fault flow is encouraged and across fault flow is impeded [*Faulkner et al.*, 2010]. Transient fault permeability structures likely evolve on short to geological timescales [*Faulkner et al.*, 2010]. Multiple lines of evidence suggest that fault zones in sedimentary basins can be conductive features. Gas and mineral deposits located along strike clearly indicate that fault zones have transient permeability fields that are conductive from kilometers depth to shallow depths at least episodically over geologic time [*Garven*, 1995; *Pinti and Marty*, 2000]. Correlations between noble gas concentrations and geological features suggest the upwards migration of gas and deep fluids through fractures and faults [*Lombardi and Pinti*, 1992]. Given these observations and the evidence of fault zone reactivation and the loss of hydrofracturing fluids into fault zones, we hypothesize that some fault zones could in some sedimentary basins be conductive from the shale gas formation to shallow depths. For any given basin, actual sedimentary, stress, structural and hydraulic conditions will have to be assessed to identify the potential presence of hydraulically conductive faults.

The time frame of water resources management is typically 5 to 20 years [*Gleeson et al.*, 2012], which may be appropriate for surface water systems which have short residence times. However, groundwater can have very long residence times. The global average groundwater residence time is estimated to be 1400 years [*UNESCO*, 1978]. A multigenerational time horizon of 50 to 100 years for the management of groundwater has been proposed by *Gleeson et al.* [2012], so that the impacts of a broad range of hydrogeological conditions can be adequately built into effective management and policy plans. *Lenton* [2011] suggested an even longer time horizon of 1000 years as a full, ethical time horizon for which the human impact on biophysical systems should be evaluated. This timeframe would be especially appropriate for deep sedimentary basins, such as those where shale gas is found, where at least some part of the exploited

groundwater resources have a very long residence time and the impact of contamination at depth is likely irreversible.

The objective of this chapter is to assess whether hydraulic fracturing could lead to contamination of shallow aquifers via preferential fluid migration along faults, and what factors control the potential for significant contaminant transport into shallow aquifers. To achieve these objectives we: 1) compiled publically-available data on shale gas formations, fault parameters and hydraulic fracturing operations; 2) developed a model of a shale gas fracturing in a generic faulted sedimentary basin that is representative of the data from multiple basins; and 3) conducted a sensitivity analysis to examine the sensitivity of contaminant transport to basin, fault and hydraulic fracturing parameters that covers the range of parameters found in literature. The model is a two-dimensional, single-phase, multi-species, density-dependent, finite-element numerical groundwater model, and is used to assess the transport potential of conservative solutes along a fault zone, from a shale formation to a shallow aquifer, following hydraulic fracturing. Previously, a simple groundwater flow and transport model simulated the migration of contaminants from a shale formation to shallow depths through a fault zone [*Myers*, 2012]. However, the conclusions drawn from this model have been questioned because of the simplifications and assumptions of this model including unrealistic boundary conditions and using a constant density, finite-difference simulator [*Cohen et al.*, 2013; *Saiers and Barth*, 2012]. There is thus a need for more realistic modeling of these processes for a better understanding of the risks associated with long term contamination of shallow aquifers due to hydraulic fracturing.

4.2 Generic model

We systematically reviewed publically-available data to develop a generic model representative of shale gas basins (Table 1). Sedimentary basins are layered hydrogeologic systems that are often deformed by multiple cross-cutting fault zones. Prospective shale gas formations are generally at significant depths of 1 to 4 km [*EIA*, 2011a] and occur in regions of low to moderate topography. The distance between major

regional faults in rift or foreland basins is a few kilometers, at least in the St. Lawrence lowlands where the Utica shale is found [*Séjourné et al.*, 2013]. The permeability of shale gas formations is extremely low and these formations are often overpressured, partially due to the low permeability combined with the internal gas generation [*Gleeson et al.*, 2011b; *Soltanzadeh and Hawkes*, 2009]. The permeability of the sedimentary rocks overlying the shale gas formations can be low to moderate (10^{-20} to 10^{-13} m²) [*Gleeson et al.*, 2011b; *Séjourné et al.*, 2013]. In this section, we discuss the basin, fault and hydraulic fracturing parameters used to develop a generic model.

Although more complex and heterogeneous permeability patterns are common in many sedimentary basins, we simulate a simplified system in order to understand the mechanisms of transport of conservative contaminants present in fluid migrating along a fault due to hydraulic fracturing. We develop a model of a generic, regional groundwater basin based on hydrological and geological properties of multiple basins with shale gas formations. Primarily, we gathered information on the Utica shale gas development in the St. Lawrence Lowlands, QC, Canada, located between the Yamaska fault and the Logan's Line [*BAPE*, 2011; *Lavoie et al.*, 2008; *Rivard et al.*, 2012; *Séjourné et al.*, 2013] because this was the most readily available to the authors. In addition wherever possible, we gathered data on other active shale gas formations, primarily the Barnett shale in Texas and Marcellus shale in New York and Pennsylvania [*Arthur et al.*, 2008; *Davies et al.*; *EIA*, 2011b; *Lavoie et al.*, 2008; *Montgomery et al.*, 2005; *Sumi*, 2008]. In general, the data from the St. Lawrence Lowlands (such as the depth to shale) is consistent with other areas of shale gas development (Table 3). However, there are differences in the St. Lawrence Lowlands compared to other gas shales, such as the low permeability unit overlying the shale gas formation. We examine the sensitivity to basin model parameters below (Table 4).

Shale gas formations can be underpressured, at hydrostatic pressure, or overpressured. The Utica shale in the St. Lawrence Lowlands, the Barnett shale, and the northern part of the Marcellus formation are overpressured [*Lavoie et al.*, 2008; *Montgomery et al.*, 2005; *Rivard et al.*, 2012; *Sumi*, 2008]. Moreover, ~40% of the prospective areas for shale gas

extraction globally are overpressured [*EIA*, 2011a]. We simulate a scenario of an overpressured shale formation, under a pressure gradient of 13 kPa/m. If the pressure gradient is lower (either in a less overpressured or underpressured formation), the potential for contaminant migration would decrease. We examined the sensitivity to pressure gradient in shale.

High salinities are common in sedimentary basins and most sedimentary basins are saturated by brine. The depth at which shallow fresh groundwater transitions to saline fluids is commonly a few hundred meters [*Björlykke and Gran*, 1994; *Clauer et al.*, 1992; *Connolly et al.*, 1990; *Globensky*, 1972; *Hanor and McIntosh*, 2007]. In North America, salinities up to 500 g/L have been reported at depths of less than 4 km [*Clauer et al.*, 1992]. In the St Lawrence Lowlands, high salinities of 175 g/L have been reported in the Trenton group, below the Utica shale, which occurs at depths of 800 to 2000 m [*Ngoc et al.*, 2011]. Higher salinities reduce vertical groundwater flow from the shale gas formation to the shallow aquifer.

As discussed above, fault zones can be hydraulic barriers, conduits or conduit-barriers [*Aydin*, 2000; *Bense and Person*, 2006; *Caine et al.*, 1996; *Rawling et al.*, 2001]. We simulate a relatively simple scenario of fault zone that is a continuous, high permeability conduit from the shale gas formation to the shallow aquifer, as a potential worst-case scenario. If the fault zone is more of a barrier (either continuously or at specific depths), the potential for transport through the fault would be reduced or potentially negligible. We simulate the effect of reducing fault permeability as well as the case of conduit-barrier by changing the anisotropy (the ratio of permeability along fault to permeability perpendicular to fault) instead of simulating a discrete low permeability fault core flanked by a high permeability damage zone [*Caine et al.*, 1996].

In hydrofracturing operations, a horizontal well is drilled within the shale formations for a length of a few kilometers and hydraulic fracturing is performed in stages at intervals tens of meters apart [*Zoback et al.*, 2010]. Hydraulic fractures can extend up to a few hundred meters above and below the horizontal wellbore [*Davies et al.*, 2012; *King*,

2012; *Zoback et al.*, 2010] and can increase the permeability of the formation up to three orders of magnitude [*King*, 2012]. The shale gas formations are generally thin (less than 100 m in most major U.S. shale gas development [*EIA*, 2011b]) especially in comparison to the thickness typically hydro-fractured. The goal of hydraulic fracturing is to develop the maximum contact with the producing formation, while minimizing fracturing of formations above or below which can lead to additional costs in terms of fracking fluid, pressure loss and time [*King*, 2012]. Therefore, we assume that hydrofractured zones often extend to the top of the shale gas formation. We do not simulate the actual geomechanical deformation of hydraulic fracturing but rather the impact of increased permeability due to hydraulic fracturing. We focus on the period after hydraulic fracturing because the pressure pulse of hydraulic fracturing would rapidly decay and would not have a significant impact on long term migration of contaminants, which is the focus of the present study. For ductilely-deformed shale formations, permeability from hydrofracturing may be temporally reduced on decadal timescales which would reduce contamination potential.

Table 3. Compilation of parameter values reported in the literature from Quebec (QC), New York (NY), Texas (TX), Pennsylvania (PA) and other regions

Parameter	Range of values	References
Basin parameters		
Permeability above shale	Fine-grained sediments: 10^{-17} m²	[*Gleeson et al.*, 2011b]
	Coarse-grained sediments: 10^{-13} m²	
Permeability of shale	10^{-23} to 10^{-17} m²	[*Neuzil*, 1994]
	10^{-20} to 10^{-16} m²	[*Freeze and Cherry*, 1979]
	Utica (QC): $9x10^{-23}$ to $8x10^{-17}$ m²	[*Séjourné et al.*, 2013]
	Marcellus (NY, PA): $2x10^{-16}$ m²	[*Soeder*, 1988]
	Barnett (TX): < 10^{-17} m²	[*Montgomery et al.*, 2005]
Porosity above shale	Sandstone : 5 to 30 %	[*Freeze and Cherry*, 1979]
	Shale: < 10 %	
	Utica (QC): 1.2 to 3.2%	[*Rivard et al.*, 2012]
Porosity of shale	5 to 60% at 0.3 to 10 km depth	[*Neuzil*, 1994]
	< 10 %	[*Freeze and Cherry*, 1979]
	US: 1 to 12%, median: 7%	[*EIA*, 2011b]
	Utica (QC): 0.7 to 6.6%	[*BAPE*, 2011; *Lavoie et al.*, 2008; *Rivard et al.*, 2012; *Séjourné et al.*, 2013]
	Marcellus (NY, PA): 8%	[*EIA*, 2011b]
	Barnett (TX): 5%	[*EIA*, 2011b]
Topographic gradient	St. Lawrence Lowlands (Utica): 2.3 ± 2.7 %	[*GeoBase Canada*, 2012]
	Appalachian basin (Marcellus): 2.5 ± 2.9 %	
	Fort Worth basin (Barnett): 1.0 ± 0.7 %	
Matrix compressibility	Jointed rock: 10^{-10} to 10^{-8} Pa^{-1}	[*Freeze and Cherry*, 1979]
	Sound rock: 10^{-11} to 10^{-9} Pa^{-1}	
Pressure gradient in shale	Utica (QC): 10 to 17 kPa/m	[*BAPE*, 2011; *Lavoie et al.*, 2008; *Rivard et al.*, 2012; *Séjourné et al.*, 2013]
	Marcellus (NY, PA): northern basin overpressured	[*Sumi*, 2008]
	Barnett (TX): 10.4 to 11.8 kPa/m	[*Lavoie et al.*, 2008; *Montgomery et al.*,

		2005]
	World[1]: 40% overpressured	[*EIA*, 2011a]
Depth to saline formations	North America: 0 to 2 km	[*Clauer et al.*, 1992]
	Utica (QC)[2]: 86 to 1554 m	[*Séjourné et al.*, 2013]
	Utica (QC): 150 to 740 m	[*Globensky*, 1972]
Salinity	North America: 0 to 500 g/L	[*Clauer et al.*, 1992]
	Utica (QC), shallow depths: 5 to 225 g/L	[*Globensky*, 1972]
	Utica (QC), high depths[3]: 100 to 240 g/L	[*Ngoc et al.*, 2011]
Depth to shale gas formation	World: 1 to 4.5 km, average: 2.9 km	[*EIA*, 2011a]
	US: 0.5 to 4.5km, average: 2.3 km	[*EIA*, 2011b]
	Utica (QC) [4]: 1.2 to 2.5 km	[*BAPE*, 2011]
	Marcellus (NY, PA)[5]: 1.2 to 2.6 km	[*Arthur et al.*, 2008]
	Barnett (TX): 1.9 to 2.6 km, average: 2.3 km	[*Arthur et al.*, 2008; *EIA*, 2011b]
Thickness of shale gas formation	World: 20 to 300 m, average: 77 m	[*EIA*, 2011a]
	US: 7 to 940 m, average: 190 m	[*EIA*, 2011b]
	Utica (QC): 220 m on average	[*BAPE*, 2011]
	Marcellus (NY, PA): 15 to 60 m	[*Arthur et al.*, 2008]
	Barnett (TX): 30 to 280m, average: 91 m	[*Arthur et al.*, 2008; *EIA*, 2011b]
Fault parameters		
Distance between faults	Utica (QC): 0.6 to 27.7 km, average: 6.6 km	[*Séjourné et al.*, 2013]
Hydraulic fracturing (HF) parameters		
Length of hydrofracturing zone	1 to 3 km	[*Rivard et al.*, 2012]
	1.2 km	[*Zoback et al.*, 2010]
Vertical extent of hydraulic fractures	100 to 300 m	[*Rivard et al.*, 2012]
	Barnett (TX): 46 m above and 61 m below the wellbore	[*Zoback et al.*, 2010]
	Barnett (TX): < 588 m Marcellus (NY, PA) : < 536 m	[*Davies et al.*]
	Most < 90 m	[*King*, 2012]
Permeability of hydrofracturing zone	100 to 1000 times the permeability of the formation	[*King*, 2012]

[1] Potential shale gas development in 48 countries.
[2] Saline water index. The interval between the fresh water and saline water index is often of a few hundred meters, which does not allow to accurately locate the transition between fresh water and brine.
[3] Formations below the Utica shale (Postdam and Beekmantown groups).
[4] Only the area of interest for shale gas development, between the Yamaska fault and the Logan Line, has been considered.
[5] Marcellus shale targeted for exploitation.

4.3 Numerical methods and parameter values

Simulations were conducted with SUTRA-MS, a US Geological Survey numerical groundwater simulator that simulates multiple-solutes transport [*Hughes and Sanford*, 2005; *Voss and Provost*, 2002]. The base case value of each parameter and its range of variation in the sensitivity analysis are presented in Table 4 and other properties used for all simulations are presented in Table 5. The model domain consists of a vertical cross-section of a 50 km long, 2 km deep portion of a sedimentary basin (Figure 29) with a regular topographic gradient. To simulate the type of nested, active groundwater flow that occurs in undulating topography [*Tóth*, 1963], we imposed five recharge areas at the upper boundary, alternating with six specified pressure boundaries (P = 0) which represent discharge areas such as surface water bodies. The lateral sides and base of the model domain are no-flow boundaries. Permeability and thickness of the shallow aquifer were assigned based on field data from the St. Lawrence Lowlands and the recharge rate was adjusted in order to result in a realistic depth of the active flow zone (Table 2). A 3.5 mm/year value of recharge was chosen so that the active flow zone is approximately limited to the first 200 m below the surface for the permeability and geometry of the 100 m thick shallow aquifer. Although this is a lower recharge rate than expected in the St. Lawrence Lowlands, this study focuses on deep groundwater flow from the shale unit to shallow aquifers, and a modification of the recharge rate would not impact the results.

The basin contains three layers: 1) a 200 m thick, low permeability unit at the base of the model domain representing the gas shale unit; 2) a relatively permeable bedrock layer overlying the shale; and 3) a highly permeable, 100 m thick layer at the top of the basin representing a shallow unconsolidated aquifer. Depths and thicknesses of the different units were derived based on the St Lawrence Lowlands (structural corridor C of *Séjourné et al*. [2013]) and are representative of typical basins with shale gas extraction. Each unit is assumed to be homogeneous and anisotropic (k_x/k_z = 100). Permeabilities and porosities of the three units were derived from data of the St Lawrence Lowlands and literature values. We assigned the permeability of the shale unit at 10^{-20} m^2 by considering 1) the usual range of shale permeability (Table 3); 2) the relationship of permeability with

depth usually observed [*Ingebritsen et al.*, 2006] and 3) the capacity to maintain overpressure over geological times.

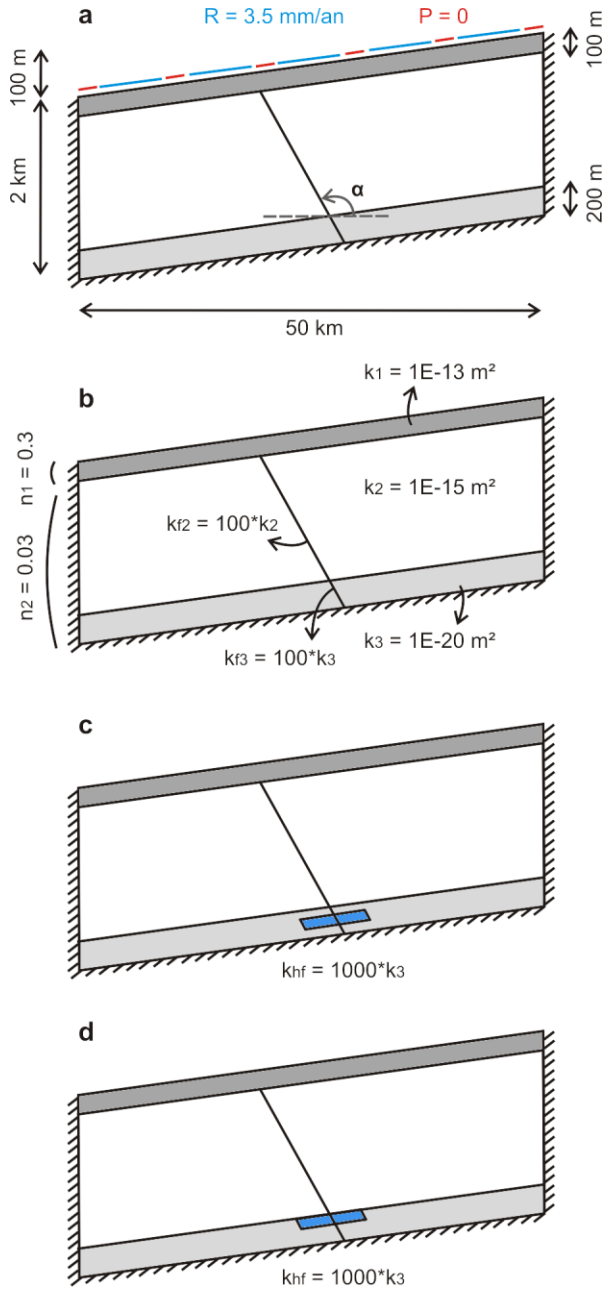

Figure 29. General set-up of the numerical model (not to scale). (a) Model domain and boundary conditions. R stands for recharge, P pressure relative to atmospheric conditions. The angle α measures the fault orientation relative to horizontal; **(b)** Permeability and porosity of the different units. k_1, k_2 and k_3 are the permeabilities of the upper, middle and lower layers respectively. k_{f2} and k_{f3} are the permeabilities of the fault in the middle and lower layers respectively; **(c)** Base case scenario with hydraulic fracturing in the middle of the shale. k_{hf} is the permeability of the target zone following hydraulic fracturing; **(d)** base case scenario with hydraulic fracturing at the top of the shale. Hydraulic fracturing is modeled by an increase of permeability in the hydraulic fracturing zone (in blue). In the base case, the hydraulic fracturing zone crosses the fault zone.

Table 4. Parameter values used in the base case model and range of variation for sensitivity analysis

Parameter	Base case value	Range of variation for sensitivity analysis
Basin parameters		
Permeability above shale (m²)	1×10^{-15}	1×10^{-18} to 1×10^{-13}
Porosity above shale (-)	0.03	0.01 to 0.1
Topographic gradient (-)	0.002	0.0004 to 0.01
Matrix compressibility (Pa^{-1})	1×10^{-8}	1×10^{-9} to 1×10^{-7}
Overpressure in shale (kPa/m)	13	9 to 25
Fault parameters		
Permeability of fault above shale (m²)	1×10^{-13}	1×10^{-15} to 1×10^{-11}
Permeability of fault in shale (m²)	1×10^{-18}	1×10^{-20} to 1×10^{-16}
Fault anisotropy above shale (-)	1	1 to 1000
Fault anisotropy fault in shale (-)	1	1 to 1000
Fault orientation relative to horizontal α (°)	135	30 to 150
Hydraulic fracturing (HF) parameters		
Permeability of HF zone (m²)	1×10^{-17}	1×10^{-19} to 1×10^{-15}
Distance from HF zone to fault zone (m)	0	0 to 1000
Thickness of shale above HF zone (m)	25	0 to 50
Length of HF zone (km)	2	1 to 3
Thickness of HF zone (m)	150	60 to 200

Table 5. Parameters used in all simulations

Parameter	Value
Liquid water	
Fluid compressibility [kg/(m.s²)]$^{-1}$	4.47×10^{-10}
Fluid viscosity [kg/(m.s²)]	1.0×10^{-3}
Solid matrix	
Solid matrix compressibility [kg/(m.s²)]$^{-1}$	1.0×10^{-8}
Density of solid grains (kg/m^3)	2,650
Porosity in the upper layer (-)	0.3
Porosity in the middle and shale layers (-)	0.03
Permeability in the upper layer (m²)	1×10^{-13}
Permeability in the middle layer (m²)	1×10^{-15}
Permeability in the shale layer	1×10^{-20}
Basin anisotropy k_x/k_z	100
Other	
Gravity (m/s²)	-9.81
Longitudinal dispersivity (m)	10
Transverse dispersivity (m)	1
Transport	
Molecular diffusivity of solutes in pure fluid (m²/s)	1.0×10^{-9}
Fluid base density (kg/m^3)	1000
Coefficient of fluid density change with concentration of salt [kg²/(m^3.kg)]	700
Coefficient of fluid density change with concentration of tracers [kg²/(m^3.kg)]	0
Upper boundary	
Fluid source rate at recharge nodes (mm/yr)	3.5

A 10 m wide, continuous normal fault zone is located in the middle of the model domain, and crosscuts the entire thickness of the bedrock but not the shallow, unconsolidated aquifer. An isotropic permeability of two orders of magnitude higher than the permeability of the surrounding material is assigned to the fault zone. Fault anisotropy, defined as the ratio of permeability along fault to permeability perpendicular to fault, is studied in the sensitivity analysis. Considering a single fault zone is consistent with the fault density in the St. Lawrence Lowlands and the purpose of the study. The spatial density of major faults in the St Lawrence Lowlands (Table 1) suggests that a single horizontal well would not likely cross more than one fault zone [*Séjourné et al.*, 2013]. The purpose of the simulations is a process-based understanding of contaminant transport potential, and not on the estimation of the total cumulative fluxes of contaminants that could migrate along faults due to regional-scale use of hydraulic fracturing of a gas shale unit.

The shale is considered overpressured, with a pressure gradient of 13 kPa/m [*Lavoie et al.*, 2008 ; *Rivard et al.*, 2012; *Séjourné et al.*, 2013], which corresponds to an overpressure of 6 MPa at 1.9 km depth (Figure 30). Brine has been observed at a few meters to a few hundred meters depth in the St Lawrence Lowlands [*Séjourné et al.*, 2013], and high salinities of 175 g/L have been reported in the Trenton group, below the Utica shale [*Ngoc et al.*, 2011]. The concentration of brine was thus assigned as 100 g/L below 200 m depth. As a comparison, water is often considered as non-saline when the concentration of salt is below 4 g/L [*BAPE*, 2011]. Hydraulic fracturing was simulated by increasing the permeability of a 2 km long, 150 m thick zone in the vicinity of the fault. We ran two base case scenarios, with the hydraulic fracturing zone located either in the middle of the shale unit (Figure 29c), or at the top of the shale unit (Figure 29d) since the width of the hydrofracturing zone relative to the thickness of shale gas formations suggests this is likely common. In both base case scenarios, the hydrofractured zone crosses the fault.

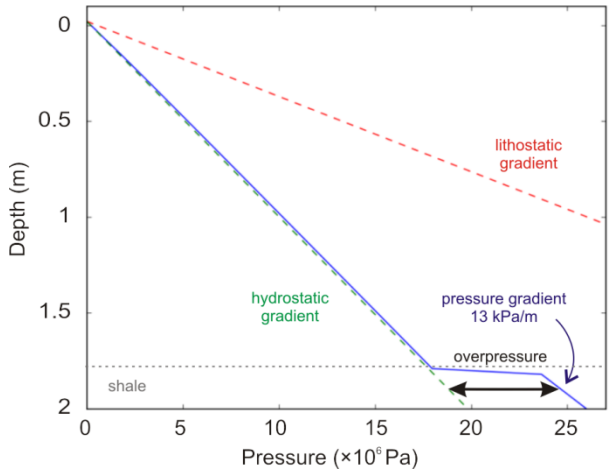

Figure 30. Initial pressure variation with depth at x = 10 km. A pressure gradient in the shale of 13 kPa/m corresponds to an overpressure of 6 MPa in the middle of the shale at 1900 m depth.

The 46060 elements mesh is shown in Figure 31. Grid spacing telescopes from 1 m × 10 m finite elements (vertical x horizontal extent) in the fault zone to 200 m × 30 m elements in areas located far from the fault. Horizontal discretization is 1 m for elements in the fault zone, 10 m for elements within 1 km of the fault zone and 200 m for elements at greater distances. Vertical discretization is 10 m in the upper (20-200 m depth) and lower (1700-2000 m depth) parts of the model domain and 30 m in between. Doubling the grid refinement showed that results were not sensitive to grid resolution. At each time step, the flow and transport equations were solved using Gaussian elimination.

Simulations were conducted in two consecutive runs. An initial 300,000 year run was used to reach steady-state conditions, with a specified pressure gradient in the shale and a specified concentration of brine below 200 m depth. The output of the first run was used as initial conditions of the second run, in which no pressure or concentration was specified since this can impact results [*Cohen et al.*, 2013; *Saiers and Barth*, 2012]. This second simulation was run over 100,000 years to assess whether the pressure field and the concentration field were stable. The pressure field was stable over 100,000 years when the permeability in the shale unit is 10^{-20} m^2. Five thousand years in the middle of the second simulation was thus selected as the time examined (t = 0 - 5000 years) to access potential long term contamination for scenarios with hydrofracturing (by modifiying permeability of the hydrofractured zone at t = 0 years) or without

hydrofracturing. The initial hydraulic head distribution and concentration field at t = 0 years are presented in Figure 32a and b. For each simulation, initial time step size was set at 1 year. Time step size was incremented by a factor of 1.5 every 10 time steps until the maximum time step size of 10 years is reached. Reducing the time step showed that results were not sensitive to the time steps used.

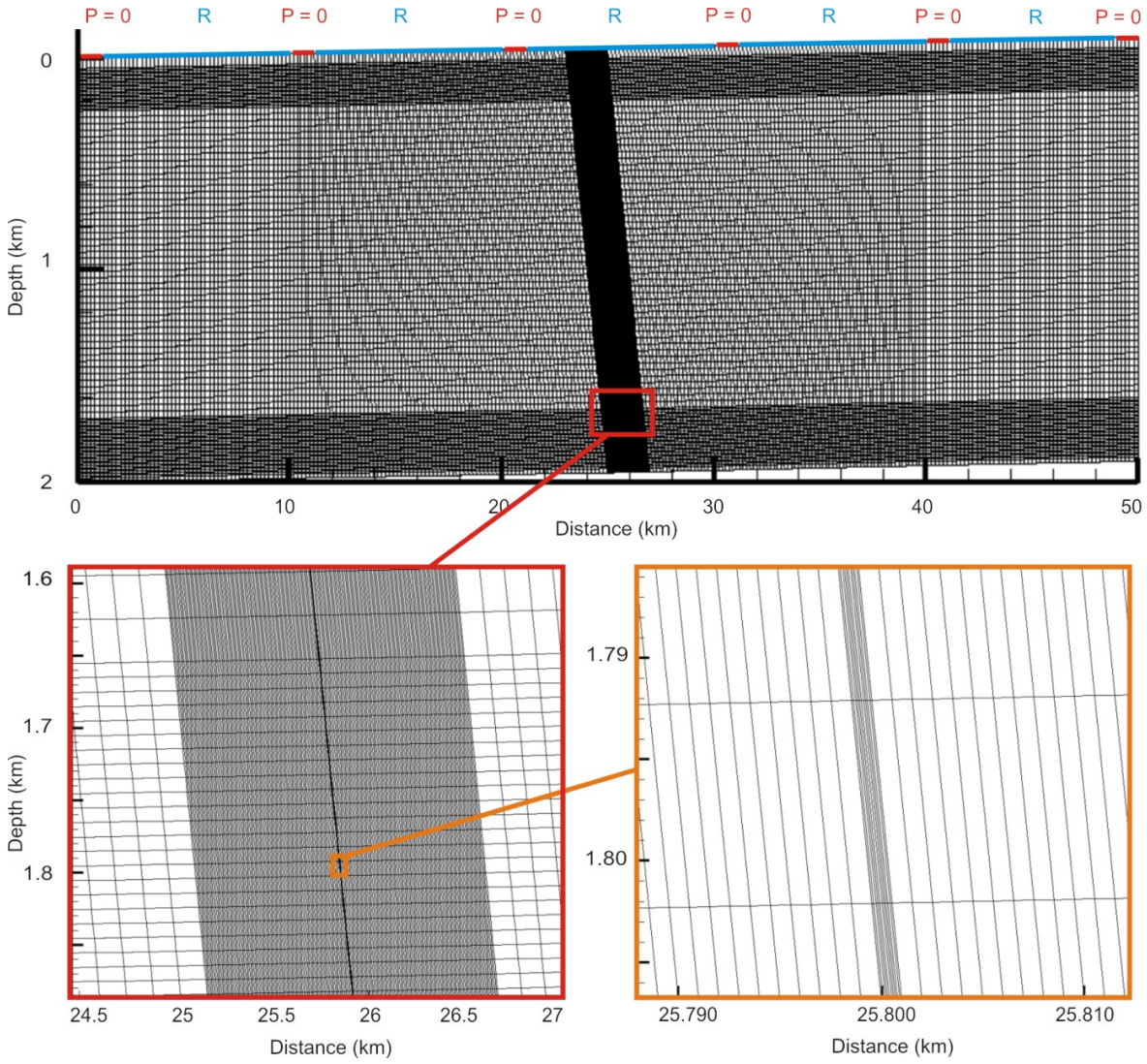

Figure 31. Finite-elements mesh used for the numerical simulation. Upper figure: five recharge areas (R, in blue) were imposed at the upper boundary, alternating with six specified pressure boundaries (P = 0, in red) which represent discharge areas. The lateral sides and base of the model domain are no-flow boundaries.

Simulations represent single-phase flow and thus examine the transport of dissolved constituents in a water phase that are not transported by gas-driven multiphase flow. To better describe the migration of the gas phase, one should consider gas carried in solution by oil, gas carried in solution by water, and gas movement as a separate phase. In multiphase flow under immiscible conditions, water, oil and gas would be subject to different buoyancy and capillary forces, which could potentially lead to migration patterns different from those predicted in single-phase flow [*Ingebritsen et al.*, 2006]. Buoyancy and capillary forces would have opposite, competing effects on the upwards migration of fluids in the fault zone. The buoyancy force exerted on gas would increase the potential for contaminant migration, whereas capillary forces would decrease it.

Three tracers were simulated in order to study the movement in regional groundwater flow due to hydraulic fracturing (Figure 32). At t = 0, the first tracer, herein called the 'shale tracer' is located in the shale layer ($-2000 < z < -1800$); the second tracer, herein called the 'lower basin tracer', is located in the lower part of the overlying unit ($-1800 < z < -1000$); and the third tracer, herein call the 'upper basin tracer', is located in the upper part of the overlying unit ($-1000 < z < -200$). We define the depth of potential contamination as the shallowest depth relative to the land surface where the concentration of the shale tracer is above 1% of its initial concentration in shale. The shale tracer represents any potential contaminant from the shale unit: chemicals in fracking fluid initially after fracturing, or naturally occurring contaminants in the shale such as radioactive materials or heavy metals for the entire duration of simulations. The value of 1% of initial concentration is arbitrary; other cut offs such as 10% of initial concentration were also examined, and show a similar behavior in sensitivity analysis as discussed below. We compiled the mass fluxes of the three tracers at the top of the fault (i.e. at the base of the shallow aquifer). We assumed that the initial concentration of TDS in the shale and lower basin was 100 kg/m^3 and calculated the sum of fluxes from the shale and the lower basin in order to estimate the total flux of potential dissolved contaminants in the shallow aquifer. The upper basin tracer was not considered as there is no clear influence of hydraulic fracturing on its migration (Figure 35).

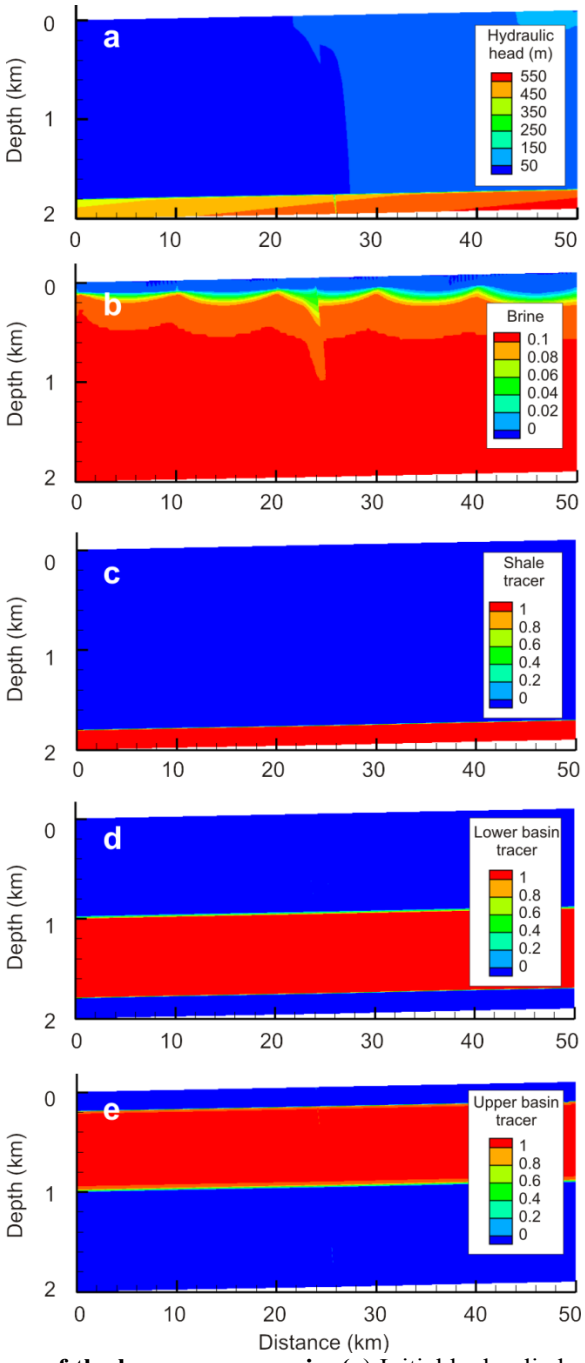

Figure 32. Initial conditions of the base case scenario. (a) Initial hydraulic head distribution. In the base case scenario, the shale is overpressured; **(b)** Initial concentration of brine; **(c)** Initial concentration of the shale tracer; **(d)** Initial concentration of the lower basin tracer; **(e)** Initial concentration of the upper basin tracer.

4.4 Results

Figure 33 compares the simulated spatial distribution of the shale tracer for the case without hydraulic fracturing (Figure 33a), for the base case scenario with hydraulic fracturing in the middle of the gas shale (Figure 33b) and for the base case scenario with hydraulic fracturing at the top of the gas shale (Figure 33c). No shale tracer migration occurs along the fault without hydraulic fracturing (Figure 33a). For the base case scenarios, shale gas moves up the fault after hydraulic fracturing (Figure 33b and Figure 33c). The base case with hydraulic fracturing in the middle of the shale formation leads to slow migration, which is indicated by the 1% concentration threshold reaching only 1500 m depth at simulation time of 5000 years (apparent on the lower graph of Figure 33b). With hydraulic fracturing at the top of the shale gas formation (Figure 33c), the 1% concentration threshold reaches 500 m depth after about 500 years and the upper part of the fault after about 1000 years. After 5000 years, a plume of shale tracer reaches the shallow aquifer with concentrations up to 5% of the initial tracer concentration in shale. Therefore, in this scenario, the shallow aquifer is significantly contaminated by the tracer from the shale formation.

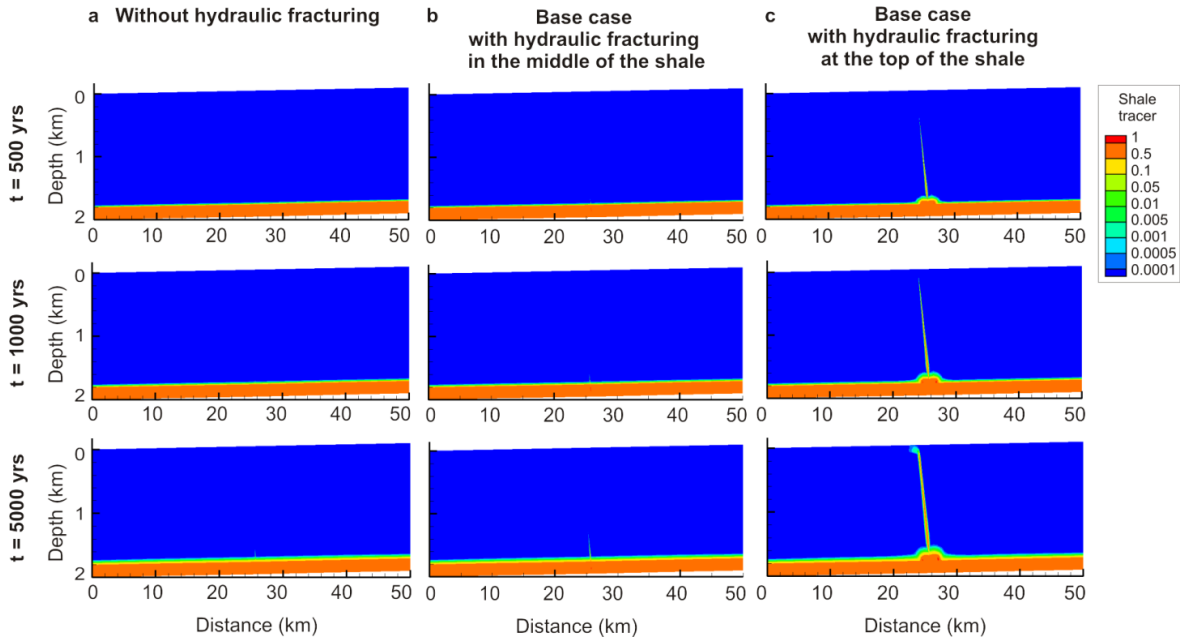

Figure 33. Migration of shale tracer through time (a) without hydraulic fracturing; **(b)** with hydraulic fracturing in the middle of the gas shale (base case scenario); **(c)** with hydraulic fracturing at the top of the gas shale.

Figure 34 shows the extent and relative concentration of the shale tracer (Figure 34a) and the lower basin tracer (Figure 34b) in the active flow zone at t = 5000 years in the base case scenario with hydraulic fracturing at the top of the shale (lower graph of Figure 33c). The lateral plume of concentrations of shale tracer higher than 0.01 (1%) in the active zone is 500 m, and the extent of concentrations higher than 0.001 (0.1%) is 1.2 km (Figure 34a). The plume withconcentrations of shale tracer higher than 0.01 (1%) in the active zone is 300 m, and the extent of concentrations higher than 0.001 (0.1%) is 1 km (Figure 34b). Maximum concentrations of the shale tracer and lower basin tracer in the shallow aquifer are ~5%.

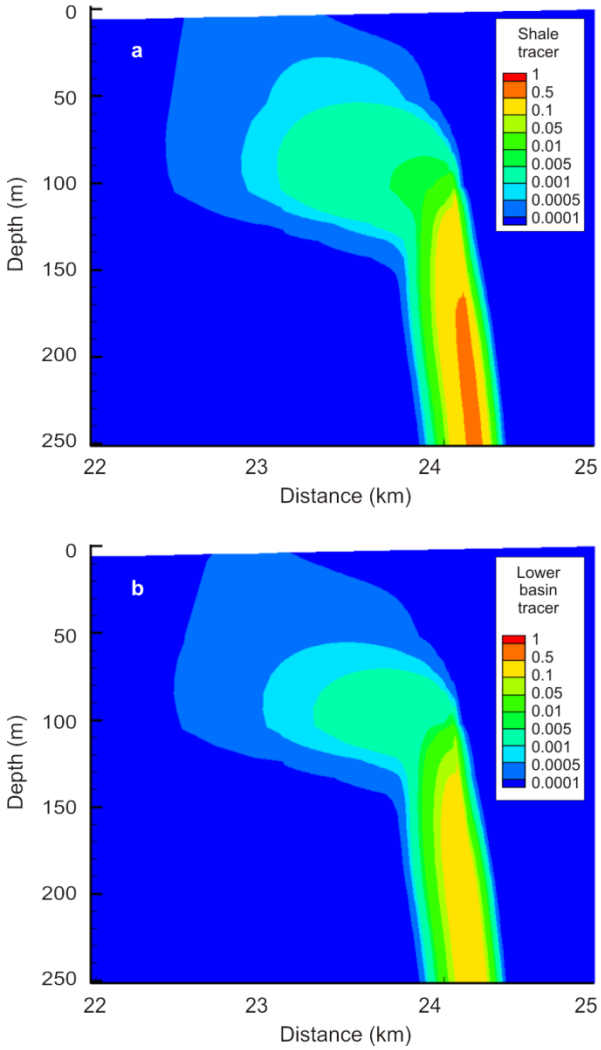

Figure 34. Extent of contamination in the shallow aquifer. Concentration of **(a)** shale tracer and **(b)** lower basin tracer in the shallow aquifer at t = 5000 years for the base case scenario with hydraulic fracturing at the top of the fault.

For the base case simulations, Figure 35 shows the migration through time of the three tracers (shale, lower basin and upper basin; Figure 32), without hydraulic fracturing or with hydraulic fracturing either in the middle of the shale (Figure 35a, c) or at the top of the shale (Figure 35b, d). Figure 35 compares tracers migration through time with or without hydraulic fracturing (Figure 35a, b), and for thresholds of 1 and 10% of initial concentration (Figure 35c, d). The shale tracer, which is initially in the shale, migrates higher upwards when there is hydraulic fracturing in the middle of the shale than without, 300 m compared to 100 m over 5000 years (Figure 35a). The lower basin tracer also moves up the fault, which is consistent with flow in the overlying unit being more significant than in the shale. However, the importance of this migration is quite similar with or without hydraulic fracturing; about 400 m upwards (Figure 35c). The difference in migration of the shale tracer between the case with hydraulic fracturing than without is a lot more significant when hydraulic fracturing occurs at the top of the fault, 1700 m compared to 50 m over 1500 years (Figure 35b). In this case, migration of the lower basin tracer is also more important with hydraulic fracturing than without, 900 m compared to 200 m over 1500 years. There is no clear influence of hydraulic fracturing on the migration of the upper basin tracer, which mimics the spatial distribution of solutes in the upper part of the overlying aquifer unit due to active groundwater flow (Figure 35a, b).

The depths of 1% and 10% concentration thresholds through time have the same pattern (Figure 35c, d) so we use a concentration of 1% as the cutoff for the remainder of the analysis. The lower elevation of the 10% concentration, compared to the 1% concentration, is indicative of dispersive effect on the transport of the tracer, either within the fault or due to the exchange of fluid with units adjacent to the fault. The following sections focus our analysis on the migration of the shale tracer, from the shale unit, as the potential impact of hydraulic fracturing on groundwater quality in the shallow aquifer is expected to be more related to fluids originating from the gas shale.

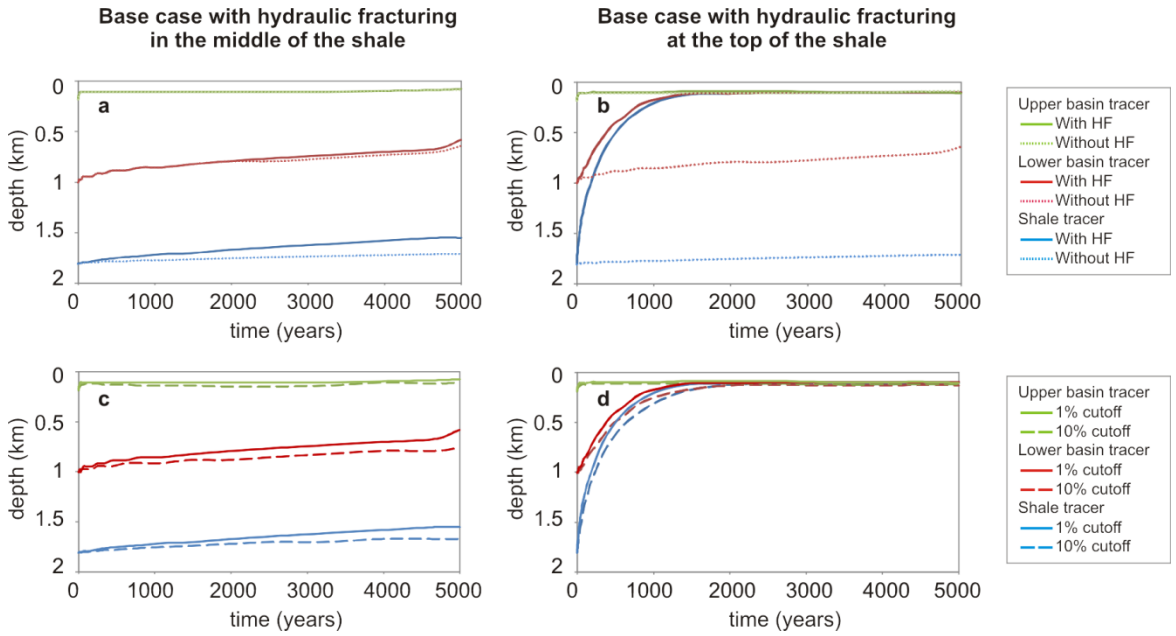

Figure 35. Depth relative from the land surface of potential contamination from the three tracers through time for the base case with hydraulic fracturing (HF) in the middle (a, c) or at the top (b, d) of the shale gas formations. (a, b) With and without hydraulic fracturing, with a 1% concentration threshold; **(a)** with hydraulic fracturing in the middle of the shale; **(b)** with hydraulic fracturing at the top of the shale; **(c, d)** with hydraulic fracturing with a 1% and 10% thresholds; **(c)** with hydraulic fracturing in the middle of the shale; **(d)** with hydraulic fracturing at the top of the shale.

Sensitivity analysis of a variety of basin, fault and hydraulic fracturing parameters shows that only a few parameters control contaminant migration potential from the gas shale to the shallow aquifer following hydraulic fracturing in the middle of the shale (Figure 36). First, we analyzed the impact of the following basin parameters (Figure 36a, d, g, j, m): pressure gradient in shale, permeability of the overlying unit, topographic gradient, matrix compressibility, and porosity of the overlying unit. The only sensitive basin parameter is the pressure gradient in the shale. Depth of potential contamination decreases systematically with an increase of the pressure gradient in the shale (Figure 36a). Pressure gradients above 13 kPa/m (overpressure in the middle of the shale above 6 MPa) lead to contamination above 1500m depth within 5000 years. The other basin parameters have a limited impact on potential contamination indicated by a shale tracer relative concentration of 1% for the model conditions of the base case.

Second, we examined fault parameters (Figure 36b, e, h, k, n): fault permeability in the overlying unit, fault permeability in shale, fault dip, fault anisotropy in the overlying unit,

and fault anisotropy in shale. Fault permeability in shale is the most important parameter, a higher permeability in the fault results in faster migration (Figure 36e). Fault permeability above 10^{-17} m² leads to contamination above 1000m depth within 5000 years. All other fault parameters studied have a limited impact on potential contamination for the base case model conditions.

Third, we studied the effect of hydraulic fracturing parameters (Figure 36c, f, i, l, o): hydrofracturing zone permeability, hydrofracturing zone distance to fault, thickness of shale above hydrofracturing zone, length of hydrofracturing zone, and thickness of hydrofracturing zone. The depth of potential contamination varies greatly depending on the thickness of shale above the hydrofracturing zone (Figure 36i). Migration of solutes is very slow if the thickness of shale above the hydrofracturing zone is more than 20m (contamination is restricted to 1500m depth within 5000 years), whereas it is fast when the thickness of shale above the fractured zone is less than 20 m (contamination occurs at 100m depth within 5000 years), because fluids from the shale travel to the fault through the overlying formation as well as through the hydrofractured zone of the shale formation. In our simulations, the thickness of shale above the hydrofracturing zone appears as the most important parameter controlling the migration along the fault. The other hydraulic fracturing parameters have a limited impact on potential contamination. In summary, when hydraulic fracturing occurs in the middle of the shale, the most important parameters controlling contaminant transport potential are thus parameters controlling migration to the fault in the overlying unit: pressure gradient in shale, fault permeability in shale, and thickness of shale above hydrofracturing zone.

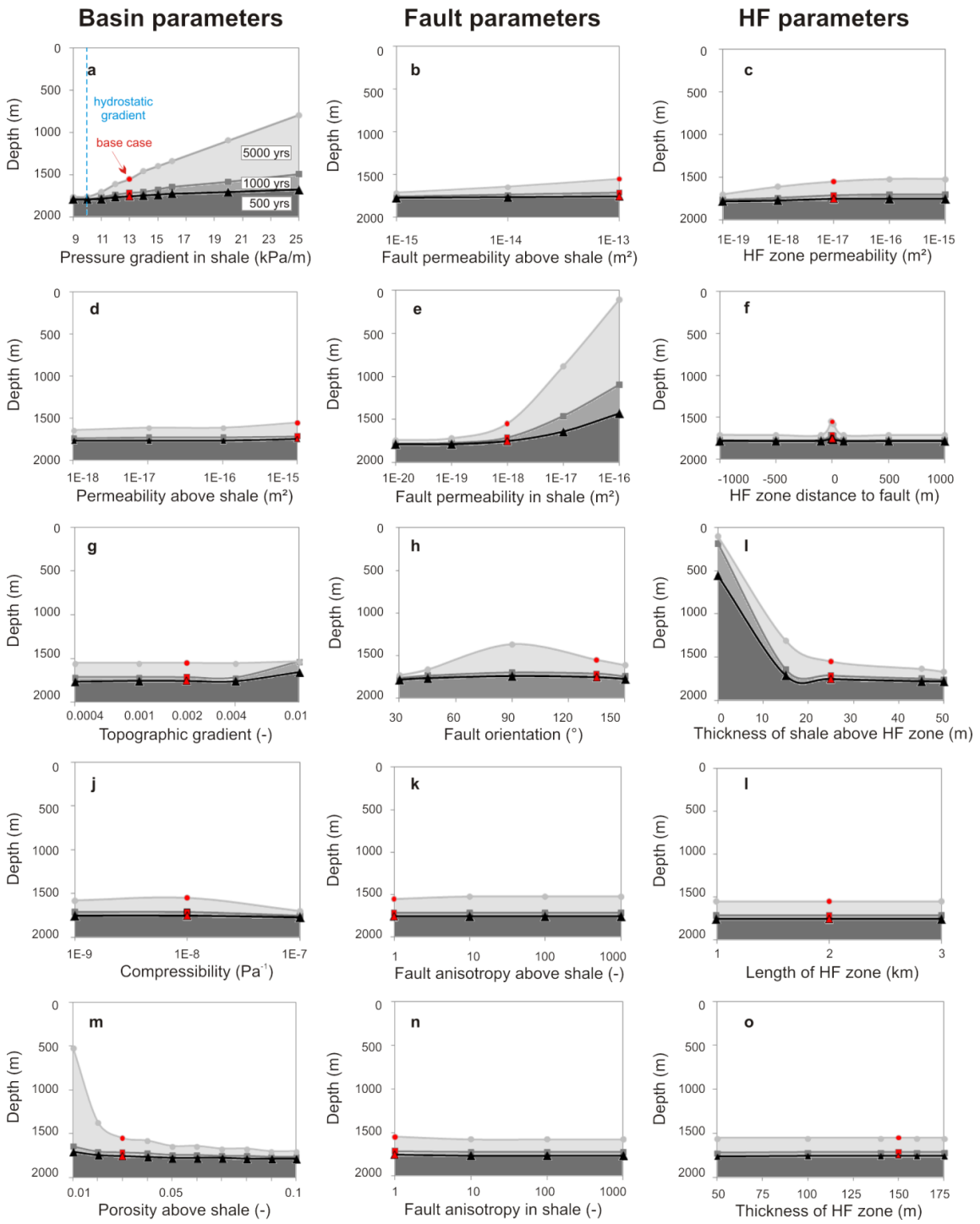

Figure 36. Sensitivity analysis with hydraulic fracturing in the middle of the shale. Depth relative to the land surface of potential contamination from the shale tracer depending on: **(a)** pressure gradient in shale; **(b)** fault permeability above shale; **(c)** HF zone permeability; **(d)** permeability above shale; **(e)** fault permeability in shale; **(f)** HF zone distance to fault; **(g)** topographic gradient; **(h)** fault orientation; **(i)** Thickness of shale above HF zone; **(j)** matrix compressibility; **(k)** fault anisotropy above shale. Fault anisotropy is defined as the ratio of permeability along fault to permeability perpendicular to fault; **(l)** Length of HF zone; **(m)** porosity above shale; **(n)** fault anisotropy in shale; **(o)** Thickness of HF zone. The lines and shading show the depth of potential contamination of a shale tracer relative concentration of 1% at t = 500 years (black), t = 1000 years (dark grey) and t = 5000 years (light grey). The base case scenario with hydraulic fracturing in the middle of the shale is shown in red circles.

Another set of sensitivity analysis with the same basin, fault and hydraulic fracturing parameters was conducted with the hydraulic fracturing zone at the top of the shale unit (Figure 37). Overall the contamination is faster and reaches shallower depths at greater concentrations, in part due to the short-circuit through the overlying formation. The most sensitive basin parameters (Figure 37a, d, g, j, m) are the pressure gradient in the shale and the permeability of the overlying unit. The speed on migration along the fault increases with the overpressure in shale, and contamination of shallow aquifers is likely to occur in overpressured shales only (pressure gradient in shale > 10 kPa/m) (Figure 37a). A decrease in permeability of the overlying unit leads to slower migration along the fault (Figure 37d). Conversely, potential contamination is largely insensitive to the topographic gradient. The most crucial fault parameter (Figure 37b, e, h, k, n) is fault permeability in the overlying unit (Figure 37e). The change in depth of contamination through time is negligible over the studied variations of fault permeability in shale, fault dip, fault anisotropy in the overlying unit and in shale (Figure 37e, h, k, n). Finally, some hydraulic fracturing parameters have an impact on potential contamination (Figure 37c, f, i, l, o). Speed of migration along the fault increases with increasing values of the hydraulic fracturing zone permeability (Figure 37c). Potential contamination occurs at shallower depth when the hydraulic fracturing zone is close to the fault zone (Figure 37f). Length and thickness of the hydraulic fracturing zone have a limited impact on potential contamination (Figure 37l and Figure 37o). In this case, the thickness of shale above the hydraulic fracturing zone appears as the most important parameter controlling the migration along the fault (Figure 37i).

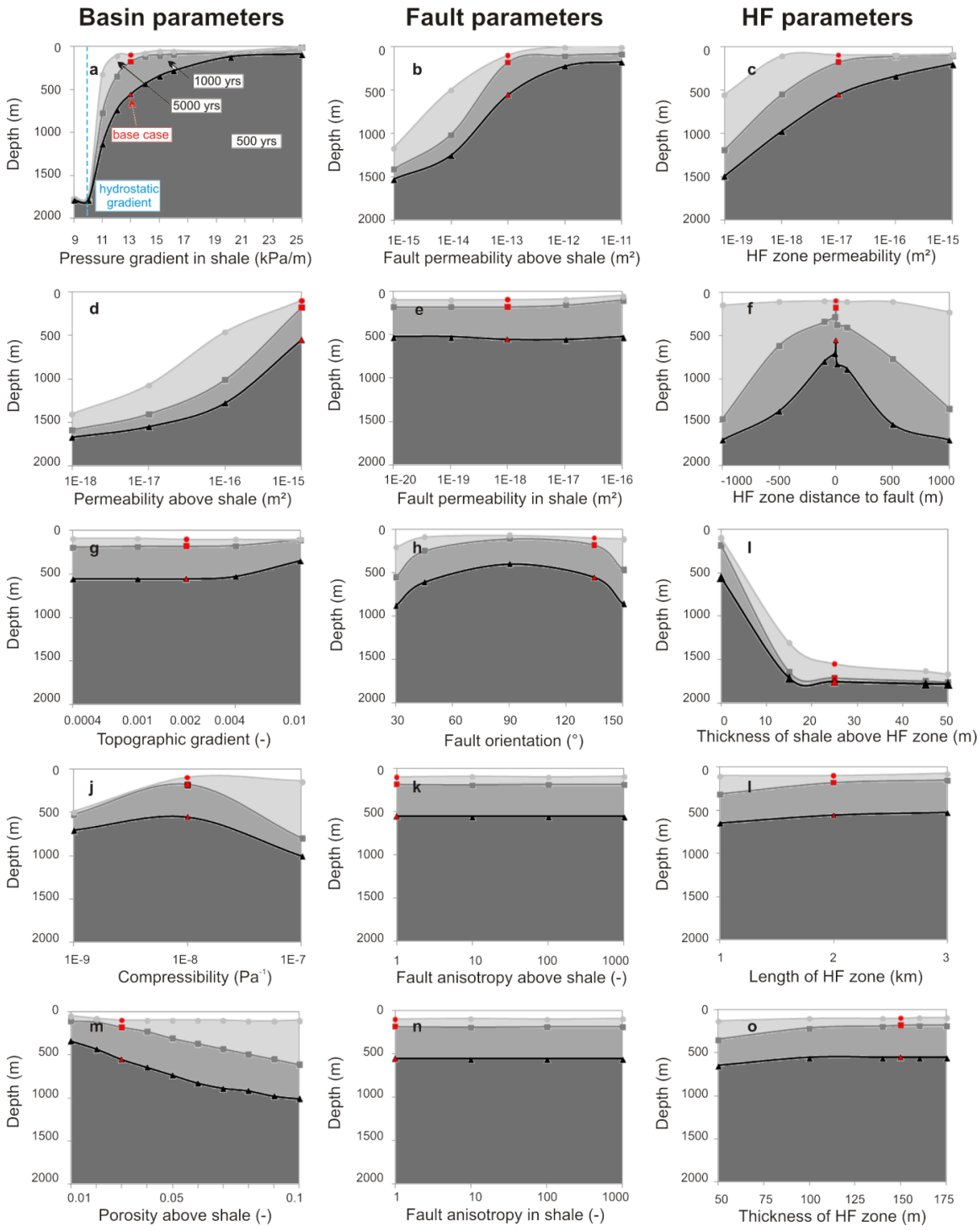

Figure 37. Sensitivity analysis with hydraulic fracturing at the top of the shale. Depth relative to the land surface of potential contamination from the shale tracer depending on: **(a)** pressure gradient in shale; **(b)** fault permeability above shale; **(c)** hydraulic fracturing (HF) zone permeability; **(d)** permeability above shale; **(e)** fault permeability in shale; **(f)** HF zone distance to fault; **(g)** topographic gradient; **(h)** fault orientation; **(i)** Thickness of shale above HF zone; **(j)** matrix compressibility; **(k)** fault anisotropy above shale. Fault anisotropy is defined as the ratio of permeability along fault to permeability perpendicular to fault; **(l)** Length of HF zone; **(m)** porosity above shale; **(n)** fault anisotropy in shale; **(o)** Thickness of HF zone. The lines and shading show the depth of potential contamination of a shale tracer relative concentration of 1% at t = 500 years (black), t = 1000 years (dark grey) and t = 5000 years (light grey). The base case scenario with hydraulic fracturing at the top of the shale is shown in red circles.

Figure 38 shows the concentration of shale tracer and lower basin tracer at the top of the fault and base of the shallow aquifer following hydraulic fracturing at the top of the fault for several values of pressure gradient in the shale, porosity above shale, fault permeability above shale, fault orientation; and hydrofractured zone permeability. Concentration of shale tracer at the top of the fault is 0.01 at 5000 years under a pressure gradient in shale of 13 kPa/m (overpressure of 6 MPa in the middle of the shale), and greatly increase under pressure gradients above 15 kPa/m (overpressure of 10 MPa in the middle of the shale) with concentrations up to 0.9 at 5000 years (Figure 38a). Concentrations of lower basin tracer are a bit lower (Figure 38c), with a maximum concentration of 0.1 at the top of the fault at 5000 years under a pressure gradient in the shale of 16 kPa/m (overpressure of 12 MPa in the middle of the shale). Concentrations of lower basin tracer decrease under pressure gradients above 16 kPa/m. This could be due to the fact that more fluid migrates along the fault as the pressure gradient in shale increases, which includes fluids from the shale and the lower basin up to a pressure gradient of 16 kPa/m. Above that value, the migration of fluids from the shale unit is so dominant that fluids from the overlying unit enter the fault to a lesser degree. Other parameters such as the fault permeability in the overlying unit and the fault orientation also have an impact on the concentrations of tracers at the base of the shallow aquifer following hydraulic fracturing at the top of the shale. If the fault zone has a very high permeability (~10^{-11} m²) concentrations of both the shale tracer and the lower basin tracer reach 0.3 at 5000 years (Figure 38e, f). A vertical fault zone leads to a concentration of shale tracer of 0.2 and a concentration of lower basin tracer of almost 0.1 at 5000 years (Figure 38g, h). Variations of other variables do not lead to high values of concentration (Figure 38).

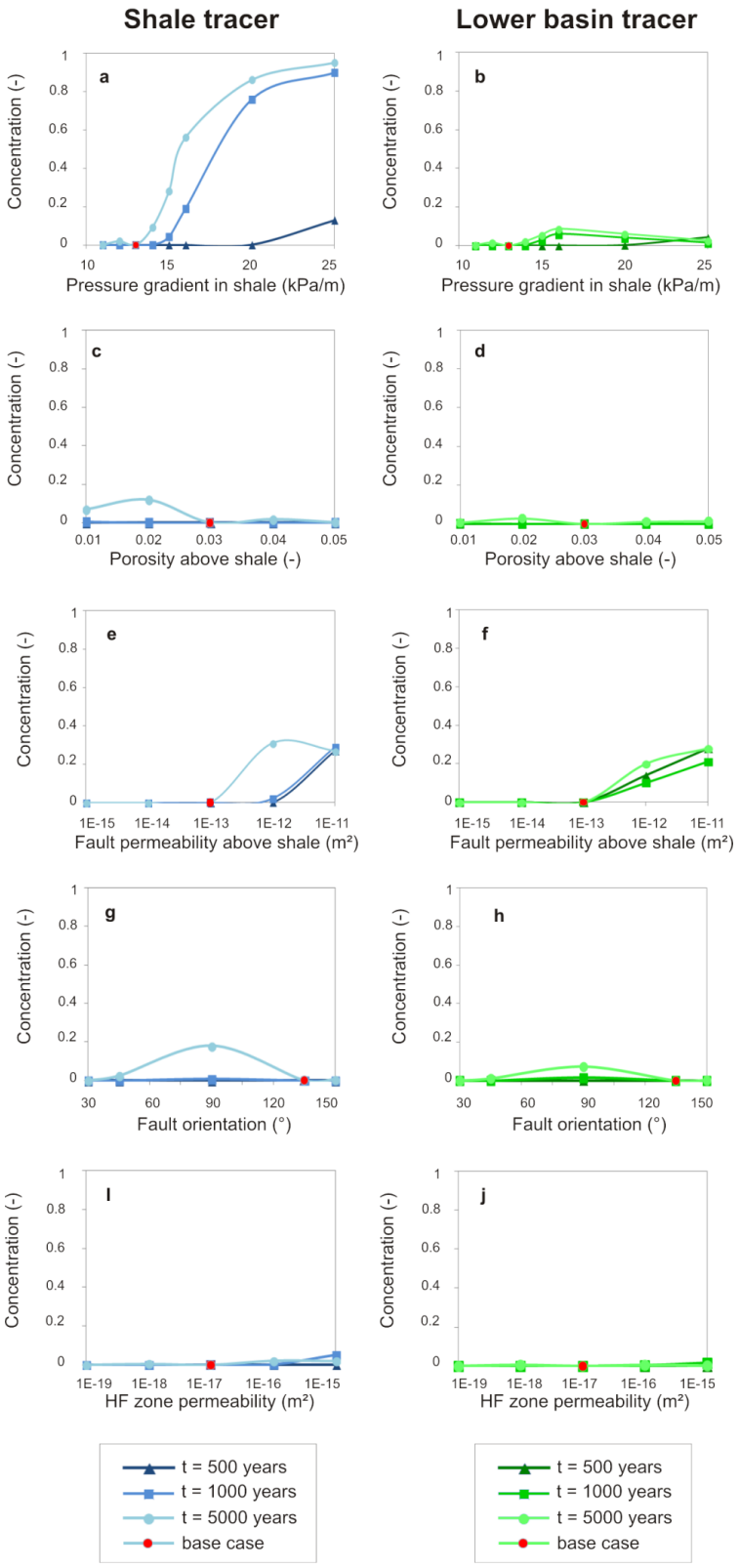

Figure 38. Concentrations at the base of the shallow aquifer. Concentration of **(a, c, e, g, i)** shale tracer and **(b, d, f, h, j)** lower basin tracer at the top of the fault following hydraulic fracturing at the top of the shale for several values of **(a, b)** pressure gradient in shale; **(c,d)** porosity above shale; **(e,f)** fault permeability above shale; **(g,h)** fault orientation; and **(i, j)** hydrofractured zone permeability. The lines show the depth of concentration of the shale (blue) or lower basin (green) tracer at the top of the fault at t = 500 years (dark blue, dark green), t = 1000 years (blue, green) and t = 5000 years (light blue, light green). The base case scenario with hydraulic fracturing at the top of the shale is shown in red circles.

We computed mass fluxes at the top of the fault by assuming that the initial concentration of TDS in the shale and lower basin was 100 kg/m^3. Figure 39a shows the potential sum of fluxes from the shale and the lower basin through time for the scenarios without hydraulic fracturing and for the base cases with hydraulic fracturing in the middle of the shale or at the top of the shale. Fluxes reach 180 g/yr following hydraulic fracturing at the top of the shale. Figure 39b shows the potential sum of fluxes from the shale and the lower basin under several pressure gradients in the shale following hydraulic fracturing at the top of the shale. Fluxes reach 3×10^4 g/yr under high pressure gradients.

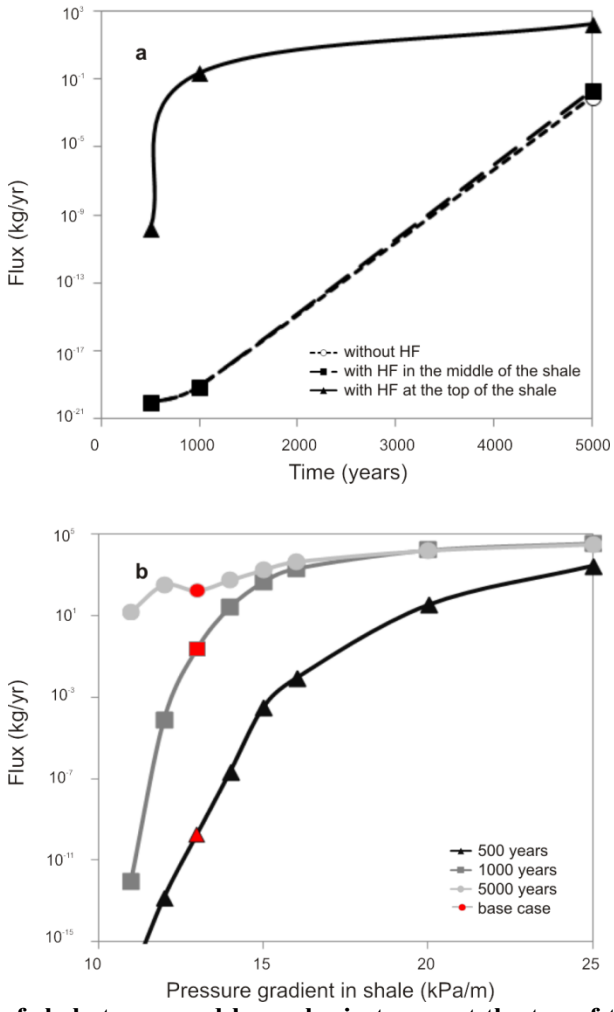

Figure 39. Mass fluxes of shale tracer and lower basin tracer at the top of the fault. (a) Sum of the fluxes of shale and lower basin tracers at the top of the fault through time for the three simulations shown in Figure 33 without hydraulic fracturing, with hydraulic fracturing in the middle of the shale or at the top of the shale; **(b)** Sum of the fluxes of shale and lower basin tracers at the top of the fault with hydraulic fracturing in the middle of the shale or at the top of the shale under several pressure gradients in shale. Fluxes were calculated by assuming an initial concentration of TDS of 100 kg/m^3 in the shale and the lower basin.

4.5 Discussion

While it is often considered that fluid migration via natural preferential pathways carrying contamination from a gas shale unit to a shallow aquifer due to hydraulic fracturing is very unlikely [*Arthur et al.*, 2008; *BAPE*, 2011; *EPA*, 2012; *Howarth et al.*, 2011; *Osborn et al.*, 2011; *Zoback et al.*, 2010], the simulation results presented in this paper show that long term migration of fluids and contaminants along a fault zone to shallow aquifers can occur under some specific conditions.

Numerical simulations show that fluid flow and contaminant transport potential is significantly enhanced when the hydrofractured zone is near the top of the shale unit (Figure 36i). Most shale formations are very thin; almost 30% of shale gas formations in the US are less than 50 m thick, and more than 60% of shale gas formations in the US are less than 100 m thick [*EIA*, 2011b]. It is thus technically and economically difficult to preserve intact shale over tens of meters above the hydraulically fractured zone. Hydraulic fracturing near the top of a gas shale unit is thus a realistic scenario. Similarly, fracturing of the overlying formations is generally avoided but has been reported [*Arkadakskiy and Rostron*, 2013]. Operators use micro-seismic monitoring to verify that hydraulic fracturing is restricted the shale gas unit. However, seismic monitoring was conducted in only about three percent of the hydraulic fracturing stages performed in the United States in 2009 [*Zoback et al.*, 2010]. It is thus difficult to evaluate how often the hydrofractured zone extends beyond the target formation. Fracturing of the overlying formation would highly increase the migration potential of contaminants according to the simulation results reported in this paper.

Another crucial parameter controlling contaminant transport potential is the distance of the hydrofractured zone relative to the fault. Results show that migration rates greatly decrease for hydrofractured zones located from 500 to 1000 m away from the fault zone (Figure 37f). The average distance between major faults is ~6.6 km in the St. Lawrence Lowlands [*Séjourné et al.*, 2013] and horizontal wells are usually 1 to 3 km long [*Rivard et al.*, 2012]. Regulations on well density and length as well as designing hydraulic

fracturing zones a safe distance away from potentially conductive faults could greatly reduce the risk of long term groundwater contamination due to migration via faults, although this assumes the three-dimensional distribution of faults zones is well defined and that the hydraulic properties of the fault zones is robustly characterized, and data is publicly-available for regulators and others to evaluate.

Finally, basin and fault properties impact the migration potential. Numerical simulations show that matrix permeability and fault permeability in the overlying sediments highly affect the risk of contamination at shallow depths (Figure 37b, d). Additionally, pressure gradients within the shale are critical, as overpressured shales cause the upwards migration of contaminants, whereas migration rates are greatly reduced in hydrostatic and underpressured shales (Figure 37a). These basin and fault properties greatly vary between shale gas formations, and even potentially between faults within a basin, so knowledge of regional geologic, structural and hydraulic properties would allow an initial assessment of contamination potential for a specific shale gas development. Depth to shale formation is also variable (500 m to 4.5 km in the United States [*EIA*, 2011b]). Although we conducted simulations for one value of depth to shale formation only (1.8 km), we expect that contamination would be more likely and rapid for shallower shale formations.

Simulation results show that for the base case scenario with hydraulic fracturing at the top of the shale, the extent of concentrations of shale tracer or lower basin tracer higher than 0.01 (1%) in the active zone is a few hundred meters, the extent of concentrations higher than 0.001 (0.1%) is ~1 km, and maximum concentrations of the shale tracer and lower basin tracer in the shallow aquifer are 5% (Figure 34). However, values of relative concentrations and extent of plume in the shallow aquifer should be used with caution, as they depend on the density of contaminants and the lateral groundwater velocities in the active zone which are not the focus of this study. Values of concentration at the base of the shallow aquifer (at the top of the fault) are more reliable. Simulations show that almost full concentration of the shale tracer and mass fluxes up to 10 kg/yr of TDS could reach the shallow aquifer under high pressure gradients in the shale, indicating that the impact on groundwater quality could be quite significant (Figure 38a, Figure 39).

We acknowledge that there are limitations to the numerical model used in this chapter. First, we simulate single-phase flow, whereas shale formations contain gas, water, and oil. In multiphase flow, buoyancy and capillary forces would impact fluid flow by their opposite, competing effects. The buoyancy force would increase the potential for contaminant migration, whereas capillary forces would decrease it. Further work is needed to assess the impact of multi-phase flow on this migration pattern. Second, we simulate the impact of hydraulic fracturing by a change in permeability, without considering the pressure regime in the well during and after hydraulic fracturing operations. This is justified by a long-term simulation of several thousand years, long after gas well closure. However, we acknowledge that it could impact migration of contaminants in the first decades of shale gas extraction.

This chapter considers the scenario of long-term contamination of shallow aquifers due to migration of contaminants from the shale formation along a fault zone. This scenario is one of many that may lead to groundwater contamination due to shale gas development. Other scenarios, such as groundwater pollution due to spills and leaks at above ground hydraulic fracturing operations, or failures of wells at shallow depth due to poor cementing or steel casing corrosion, would cause contamination of groundwater resources on shorter timescales.

Long-term risk of groundwater contamination due to migration via faults addresses the question of the appropriate time frame of water management. Although it is usually set to 5 to 20 years [*Gleeson et al.*, 2012], this timeframe is not appropriate for groundwater management, as groundwater processes and human impacts on groundwater resources occur on longer timescales. This scenario of irreversible contamination at depth illustrates how an ethical time horizon of 50 to 100 years as proposed by *Gleeson et al.* [2012], or 1000 years suggested by *Lenton* [2011] could lead to different policy plans to prevent groundwater contamination.

4.6 Conclusion

Publically-available data of shale gas basins and hydraulic fracturing operations were systematically compiled to serve as a basis for the development of a two-dimensional model of a generic, regional, faulted sedimentary basin having an active groundwater flow zone at its upper limit. Hydraulic fracturing was represented in the model by a change in permeability and simulations investigated its potential impact on fluid flow and contaminant transport from the shale formation to a shallow aquifer along a fault zone. A sensitivity analysis was carried out to identify which parameters control the contaminant transport potential.

Contamination from the target shale unit to shallow aquifers due to hydraulic fracturing is often neglected [*Arthur et al.*, 2008; *BAPE*, 2011; *EPA*, 2012; *Howarth et al.*, 2011; *Osborn et al.*, 2011; *Zoback et al.*, 2010]. However, numerical simulation results from this chapter show that migration of contaminants along a fault zone to shallow depths could occur under some specific, realistic conditions. Although simulation results show that contamination occurs on long timescales (~1000 years), this scenario of contamination should not be ignored, but should rather be further investigated. This study raises the question of the time frame of water resources management and the ethical time frame to be considered when actions are taken to prevent groundwater contamination. Results show that the most important parameter controlling contaminant transport potential is the location of the hydro-fractured zone relative to the fault zone and fracturing of the top of the shale. Basin and fault parameters, such as matrix and fault permeability in the overlying sediments, and overpressure in shale, also impact migration potential.

Further work is needed to assess potential upwards migration along a fault zone following gas shale hydraulic fracturing. Numerical simulations including multi-phase flow would allow a better description of hydrological processes in the shale, fault and overlying formations. Additional data from hydraulic fracturing operations, such as pressure regime and variation in permeability during hydraulic fracturing, should be

recorded and made publically available as they would be highly valuable in order to develop numerical models that are as realistic as possible. Before hydraulic fracturing operations, hydrogeological properties of the subsurface and faults location, density and hydraulic properties should be analyzed in order to evaluate the risk of shallow groundwater contamination by migration via fault zones. Regulations concerning the design of hydraulic fracturing zones and the proximity of wells from permeable faults should consider the long term contamination potential due to migration via faults.

Chapter 5 Summary

This research contributes to a better understanding and quantification of the impact of heterogeneities, such as low-permeability layers and fault zones, on regional groundwater flow. In this study, numerical modeling of regional groundwater flow in layered, faulted systems was conducted in order to assess the effect of a confining unit on groundwater age distribution and the potential contamination of shallow aquifers due to hydraulic fracturing a faulted sedimentary basin. Although the models developed represent a generic basin rather than a specific basin, and more complex and heterogeneous permeability patterns are common in many aquifer systems and sedimentary basins, these models can provide a good understanding of the processes involved and guide future research to focus on controlling parameters. Results presented in this thesis has implications for a range of geological processes and Earth science research fields, and provides relevant highlights for stakeholders interested in shale gas development.

The first two objectives of this thesis were to construct a two-dimensional model of a generic, regional, layered sedimentary basin and simulate groundwater age distribution and perform sensitivity analysis to determine in which conditions a zone of high groundwater ages form (presented in Chapter 3). Numerical simulations show that zones of high groundwater age form in regional (>2 km length) layered hydrogeologic basins and aquifer systems over a wide range of natural-occurring permeability contrasts, hydraulic gradients and basin geometries. Formation of these high age zones is due to low groundwater velocities in the low permeability layer and the rejuvenation of the groundwater through mixing of different flow paths near discharge zones. The strong lateral variations in groundwater ages in low-permeability layers have implications for a range of geological processes. Water-rock interactions that depend on groundwater and solute fluxes are likely to be limited in high-age zones, which may cause lateral variations in porosity, permeability and mechanical properties of low permeability materials. High age zones may also have implications for the extraction of hydrocarbons from low-permeable strata as they may inhibit the subsurface transport of microbes by

groundwater and the resulting biodegradation of oil and gas. Finally, high age zones are likely to impact the interpretation of groundwater age tracers, which are key tools for characterizing natural flow systems and quantifying groundwater recharge and sustainable extraction rates. Knowledge of location of high age zone provides valuable progress in Earth science research fields by allowing targeted sampling of old groundwaters and correction of interpretation of groundwater age tracers.

The third objective was to gather publically-available data relative to shale gas formations, hydrogeology of fault zones and hydraulic fracturing operations (presented in Chapters 2 and 4). Compiled data on shale gas formations, fault parameters and hydraulic fracturing operations . We gathered data from the St. Lawrence Lowlands (Quebec, Canada) and wherever possible from other active shale gas plays, primarily the Barnett and Marcellus shales. In general, the data from the St. Lawrence Lowlands, such as the depth to shale, is consistent with other shale gas plays. However, some parameters are highly variable between shale gas plays, such as the permeability of the unit overlying the shale gas formation or the overpressure in shale.

The fourth, fifth and sixth objectives were to develop a model of a realistic, generic, regional, faulted groundwater basin with hydraulic fracturing in the shale formation, simulate migration of contaminants from the shale unit to shallow aquifers over long timescales, and conduct sensitivity analysis to determine the controlling parameters of contaminant transport potential (presented in Chapter 4). A two-dimensional, single-phase, multi-species, density dependent, finite-element numerical groundwater model is used to assess the solute transport potential along a fault zone, from a shale formation to a shallow aquifer, after hydraulic fracturing. Although contamination from the shale unit to shallow aquifers due to hydraulic fracturing is often neglected, numerical simulations show that migration of contaminants along a fault zone to shallow depths occurs in some specific, realistic cases. Results show that the most important parameter controlling contaminant transport potential is the location of the hydro-fractured zone relative to the fault zone and the top of the shale. Basin and fault parameters, such as matrix and fault permeability in the overburden, and overpressure in shale, also impact migration

potential. This scenario of contamination considers very long timescales (~1000-5000 years) and raises the question of the time frame of water resources management and the ethical time frame to be considered when preventing groundwater contamination.

Future research should consider further numerical simulations as well as field studies. Our model results of groundwater age distribution in a layered aquifer system are a testable hypothesis for a systematic sampling campaign of groundwater ages within a regional-scale low-permeability unit. We would expect a complex pattern of age distribution in a field study as the simplified system developed in this thesis results in a relatively complex distribution of groundwater age. Furthermore, three-dimensional modeling of groundwater age distribution in a layered system would assess how three-dimensional flow could affect the development and processes of high age zones. The study of the impact of a fault zone on regional groundwater flow in the context of hydraulic fracturing operation also needs additional work. Numerical simulations including multi-phase flow would allow a better description of hydrological processes in the shale, fault and overlying formations, allowing a better assessment of upwards migration of contaminants along a fault zone. Additional data from hydraulic fracturing operations, such as pressure regime, variation in permeability during hydraulic fracturing, hydrogeological properties of the subsurface, and faults location, density and hydrogeological properties should be recorded and made publically available as they would be highly valuable in order to develop numerical model as realistic as possible.

References

Alley, W. M., R. W. Healy, J. W. LaBaugh, and T. E. Reilly (2002), Flow and storage in groundwater systems, *Science*, *296*(5575), 1985-1990.

Alpha Environmental Consultants, I. (2009), Technical consulting reports prepared in support of the draft supplemental generic environmenal impact statement for natural gas production in New York state*Rep.*, New York State Energy Research and Development Authority.

Arkadakskiy, S., and B. Rostron (2013), Tracking out-of-zone hydraulic fracturing in the Bakken with naturally occuring tracers, in *GeoConvention*, edited.

Arthur, J., B. Bohm, and M. Layne (2008), Hydraulic Fracturing Considerations for Natural Gas Wells of the Marcellus Shale, in *The Ground Water Protection Council Annual Meeting*, edited, Cincinnati, Ohio.

Aydin, A. (2000), Fractures, faults, and hydrocarbon entrapment, migration and flow, *Marine and Petroleum Geology*, *17*(7), 797-814.

BAPE (2011), Développement durable de l'industrie des gaz de schiste au Québec*Rep.*, 336 pp, Bureau d'audiences publiques sur l'environnement, Québec.

Bense, V., and M. Person (2006), Faults as conduit-barrier systems to fluid flow in siliciclastic sedimentary aquifers, *Water Resour. Res.*, *42*, doi:10.1029/2005WR004480

Bense, V., T. Gleeson, and S. Loveless (submitted), Fault zone hydrogeology, *Earth Sciences Review*.

Bense, V., M. Person, K. Chaudhary, Y. You, N. Cremer, and S. Simon (2008), Thermal anomalies indicate preferential flow along faults in unconsolidated sedimentary aquifers, *Geophys. Res. Lett.*, *35*(24), L24406.

Berkowitz, B. (2002), Characterizing flow and transport in fractured geological media: a review, *Advances in Water Resources*, *25*, 861-884.

Bethke, and Johnson (2008), Groundwater age and groundwater age dating, *Annual Review of Earth and Planetary Sciences*, *36*, 121-152.

Beyerle, U. (1998), Climate and groundwater recharge during the last glaciation in an ice-covered region, *Science*, *282*(5389), 731-734.

Björlykke, K., and K. Gran (1994), Salinity variations in North Sea formation waters: implications for large-scale fluid movements, *Marine and petroleum geology*, *11*(1), 5-9.

Bjørlykke, K. (1994), Fluid-flow processes and diagenesis in sedimentary basins, *Geological Society, London, Special Publications*, *78*, 127-140.

Boles, J., P. Eichhubl, G. Garven, and J. Chen (2004), Evolution of a hydrocarbon migration pathway along basin-bounding faults: Evidence from fault cement, *AAPG Bull.*, *88*(7), 947-970.

Brace, W. (1980), Permeability of crystalline and argillaceous rocks, *International Journal of Rock Mechanics and Mining Sciences & Geomechanics Abstracts*, *17*(5), 241-251.

Bredehoeft, J. (1997), Fault permeability near Yucca Mountain, *Water Resour. Res.*, *33*(11), 2459-2463.

Bruhn, R. (1993), Crack 2D: An unpublished MatLab computer program for deriving permeability tensors in two dimensions using the methods of Oda, 1986 and Oda et al., 1987, edited.

Bruhn, R., W. Parry, W. Yonkee, and T. Thompson (1994), Fracturing and hydrothermal alteration in normal fault zones, *Pure and Applied Geophysics*, *142*(3), 609-644.

Caine, J., and S. Minor (2009), Structural and geochemical characteristics of faulted sediments and inferences on the role of water in deformation, Rio Grande Rift, New Mexico, *Geological Society of America Bulletin*, *121*(9-10), 1325-1340.

Caine, J., J. Evans, and C. Forster (1996), Fault zone architecture and permeability structure, *Geology*, *24*(11), 1025-1028.

Castonguay, S., D. Lavoie, J. Dietrich, and J.-Y. Laliberté (2010), Structure and petroleum plays of the St. Lawrence Platform and Appalachians in southern Quebec: insights from interpretation of MRNQ seismic reflection data, *Bulletin of Canadian Petroleum Geology*, *58*(3), 219-234.

Chan, A., and M. Zoback (2007), The role of hydrocarbon production on land subsidence and fault reactivation in the Louisiana coastal zone, *Journal of Coastal Research*, *23*(3), 771-+.

Cipolla, C., S. Maxwell, M. Mack, and R. Downie (2011), A Practical Guide to Interpreting Microseismic Measurements, in *North American Unconventional Gas Conference and Exhibition*, edited, Society of Petroleum Engineers The Woodlands, Texas, USA.

Clauer, N., S. Chaudhuri, Y. Kharaka, and J. Thordsen (1992), Stable isotope geochemistry and origin of waters in sedimentary basins, in *Isotopic Signatures and Sedimentary Records*, edited, pp. 411-466, Springer Berlin Heidelberg.

Cohen, H., T. Parratt, and C. Andrews (2013), Potential Contaminant Pathways from Hydraulically Fractured Shale to Aquifers, *Ground Water*.

Connolly, C., L. Walter, H. Baadsgaard, and F. Longstaffe (1990), Origin and evolution of formation waters, Alberta basin, western Canada sedimentary basin. I. chemistry, *Applied Geochemistry*, *5*(4), 375-395.

Cook, P., and A. Herczeg (2000), *Environmental tracers in subsurface hydrology*, 529 pp., Kluwer.

Cook, P., and J. Bohlke (2000), Determining timescales for groundwater flow and solute transport, in *Environmental tracers in subsurface hydrology*, edited by P. G. Cook and A. L. Herczeg, pp. 1-30, Kluwer.

Davies, R., S. Mathias, J. Moss, S. Hustoft, and L. Newport (2012), Hydraulic fractures: How far can they go?, *Marine and petroleum geology*.

Drilling and Completion Committee (2012), Interim IRP 24: Fracture simulation: Interwellbore communication*Rep.*, Drilling and Completion Committee.

EIA (2009), Top 100 Oil and Gas Fields of 2009*Rep.*, 10 pp.

EIA (2011), Annual Energy Review 2010*Rep.*, 407 pp, U.S. Energy Information Administration, Office of Energy Statistics, U.S. Department of Energy, Washington, DC 20585.

EIA (2011a), World Shale Gas Resources: An Initial Assessment of 14 Regions Outside the United States*Rep.*, 365 pp, U.S. Department of Energy, Washington, DC 20585.

EIA (2011b), Review of Emerging Resources: U.S. Shale Gas and Shale Oil Plays*Rep.*, 105 pp, U.S. Department of Energy, Washington, DC 20585.

EPA (2012), Study of the Potential Impacts of Hydraulic Fracturing on Drinking Water Resources: Progress Report*Rep.*

Faulkner, D., and E. Rutter (2000), Comparisons of water and argon permeability in natural clay-bearing fault gouge under high pressure at 20 degrees C., *Journal of Geophysical Research - Solid Earth*, *105*(B7), 16415-16426.

Faulkner , D., C. Jackson, R. Lunn, R. Schlische, Z. Shipton, C. Wibberley, and M. Withjack (2010), A review of recent developments concerning the structure, mechanics and fluid flow properties of fault zones, *Journal of Structural Geology*, *32*(11), 1557-1575.

Freeze, and Witherspoon (1967), Theoretical analysis of regional groundwater flow, 2. Effect of water-table configuration and subsurface permeability variation, *Water Resour. Res.*, *3*(2), 623-634.

Freeze, R., and P. Witherspoon (1966), Theoretical analysis of regional groundwater flow, 1. Analytical and numerical solutions to a mathematical model, *Water Resour. Res.*, *2*, 641-656.

Freeze, R., and J. Cherry (1979), *Groundwater*, 604 pp., Prentice-Hall Inc., Eaglewood Cliffs, NJ.

Garven, G. (1995), Continental-scale groundwater flow and geologic processes, *Annual Review of Earth and Planetary Sciences*, *23*, 89-117.

GeoBase Canada (2012), Canadian Digital Elevation Data, edited, Canadian Council on Geomatics.

Gleeson, T., L. Marklund, L. Smith, and A. Manning (2011a), Classifying the water table at regional to continental scales, *Geophys. Res. Lett.*, *38*(5), L05401.

Gleeson, T., W. Alley, D. Allen, M. Sophocleous, Y. Zhou, M. Taniguchi, and J. VanderSteen (2012), Towards sustainable groundwater use: setting long-term goals, backcasting, and managing adaptively, *Ground Water*, *50*(1), 19-26.

Gleeson, T., L. Smith, N. Moosdorf, J. Hartmann, H. Dürr, A. Manning, L. van Beek, and A. Jellinek (2011b), Mapping permeability over the surface of the Earth, *Geophys. Res. Lett.*, *38*(2), L02401.

Globensky (1987), Geologie des Basses-Terres du Saint-Laurent.

Globensky, Y. (1972), Gaz - Pétrole - Eau salée dans les puits forés au Québec entre 1860 et 1970.

Goode, D. (1996), Direct simulation of groundwater age, *Water Resour. Res.*, *32*(2), 289-296.

Gregory, K., R. Vidic, and D. Dzombak (2011), Water Management Challenges Associated with the Production of Shale Gas by Hydraulic Fracturing, *Elements*, *7*(3), 181-186.

Groundwater Protection Council, G., and All Consulting (2009), Modern Shale Gas Development in the United States: A Primer*Rep.*, 116 pp, U.S. Department of Energy.

Haitjema, H. (1995), On the residence time distribution in idealized groundwatersheds, *J. Hydrol.*, *172*(1-4), 127-146.

Haneberg, W. (1995), Steady state groundwater flow across idealized faults, *Water Resour. Res.*, *31*(7), 1815-1820.

Hanor, J., and J. McIntosh (2007), Diverse origins and timing of formation of basinal brines in the Gulf of Mexico sedimentary basin, *Geofluids*, *7*(2), 227-237.

Head, I. M., D. M. Jones, and S. R. Larter (2003), Biological activity in the deep subsurface and the origin of heavy oil, *Nature*, *426*, 344-352.

Hissein, A. (2011), Basses-Terres du Saint-Laurent et leur potentiel en hydrocarbure, Universite Laval.

Howarth, R., A. Ingraffea, and T. Engelder (2011), Natural gas: Should fracking stop?, *Nature*, *477*(7364), 271-275.

Hughes, J., and W. Sanford (2005), SUTRA-MS a Version of SUTRA Modified to Simulate Heat and Multiple-Solute Transport*Rep.*, 141 pp, U.S. Geological Survey.

Ingebritsen, S., W. Sanford, and C. Neuzil (2006), *Groundwater in geological processes*, 562 pp., Cambridge University Press.

Ingersoll, R. V. (1988), Tectonics of sedimentary basins, *Geological Society Of America Bulletin*, *100*(11), 1704-1719.

Jiang, X., X. Wang, L. Wan, and S. Ge (2011), An analytical study on stagnation points in nested flow systems in basins with depth-decaying hydraulic conductivity, *Water Resour. Res.*, *47*.

Jiang, X., L. Wan, X. Wang, S. Ge, and J. Liu (2009), Effect of exponential decay in hydraulic conductivity with depth on regional groundwater flow, *Geophys. Res. Lett.*, *36*.

Jiang, X., L. Wan, M. Cardenas, S. Ge, and X. Wang (2010), Simultaneous rejuvenation and aging of groundwater in basins due to depth-decaying hydraulic conductivity and porosity, *Geophys. Res. Lett.*, *37*(5), L05403.

Kargbo, D., R. Wilhelm, and D. Campbell (2010), Natural Gas Plays in the Marcellus Shale: Challenges and Potential Opportunities, *Environmental Science & Technology*, *44*(15), 5679-5684.

Kazemi, G., J. Lehr, and P. Perrochet (2006), *Groundwater age*, 325 pp., Wiley-Interscience.

King, G. (2012), Hydraulic Fracturing 101: What Every Representative, Environmentalist, Regulator, Reporter, Investor, University Researcher, Neighbor and Engineer Should Know About Estimating Frac Risk and Improving Frac Performance in Unconventional Gas and Oil Wells, paper presented at SPE Hydraulic Fracturing Technology Conference.

Koltermann, C. E., and S. M. Gorelick (1995), Fractional packing model for hydraulic conductivity derived from sediment mixtures, *Water Resources Research*, *31*, 3283-3297.

Konstantinovskaya, E., M. Malo, and D. Castillo (2012), Present-day stress analysis of the St. Lawrence Lowlands sedimentary basin (Canada) and implications for caprock integrity during CO2 injection operations, *Tectonophysics*, *518–521*(0), 119-137.

Konstantinovskaya, E., D. Rodriguez, D. Kirkwood, L. B. Harris, and R. Thériault (2009), Effects of Basement Structure, Sedimentation and Erosion on Thrust Wedge Geometry: An Example from the Quebec Appalachians and Analogue Models, *Bulletin of Canadian Petroleum Geology*, *57*(1), 34-62.

Kratz, M., A. Hill, and S. Wessels (2012), Identifying Fault Activation in Unconventional Reservoirs in Real Time Using Microseismic Monitoring, in *SPE/EAGE European Unconventional Resources Conference and Exhibition*, edited, Society of Petroleum Engineers Vienna, Austria.

LaBolle, E. M., G. E. Fogg, and J. B. Eweis (2006), Diffusive fractionation of 3 H and 3 He in groundwater and its impact on groundwater age estimates, *Water Resour. Res.*, *42*, W07202.

Lavoie, D., A. Hamblin, R. Thériault, J. Beaulieu, and D. Kirkwood (2008), The Upper Ordovician Utica Shales and Lorraine Group flysch in southern Québec: Tectonostratigraphic setting and significance for unconventional gas*Rep.*, Geological Survey of Canada.

Lenton, T. (2011), Early warning of climate tipping points, *Nature Clim. Change*, *1*(4), 201-209.

Lombardi, S., and D. Pinti (1992), Rn-222 behavior at the Latera geothermal field (Northern Latium, Italy), *J. Radioanal. Nucl. Chem.-Artic.*, *161*(2), 365-375.

Lopez, D., and L. Smith (1996), Fluid flow in fault zones: Influence of hydraulic anisotropy and heterogeneity on the fluid flow and heat transfer regime, *Water Resour. Res.*, *32*(10), 3227-3235.

Lunn, R., J. Willson, Z. Shipton, and H. Moir (2008), Simulating brittle fault growth from linkage of preexisting structures, *Journal of Geophysical Research*, *113*.

Machel, H. G. (1999), Effects of groundwater flow on mineral diagenesis , with emphasis on carbonate aquifers, *Hydrogeology Journal*, *7*, 94-107.

Marsily, G. d., F. Delay, J. Gonçalvès, P. Renard, V. Teles, and S. Violette (2005), Dealing with spatial heterogeneity, *Hydrogeology Journal*, *13*, 161-183.

Martini, A., J. Budai, L. Walter, and M. Schoell (1996), Microbial generation of economic accumulations of methane within a shallow organic-rich shale, *Nature*, *383*(6596), 155-158.

Maxwell, S., M. Jones, R. Parker, S. Miong, S. Leaney, D. Dorval, D. D'Amico, J. Logel, E. Anderson, and K. Hammermaster (2009), Fault activation during hydraulic fracturing., in *SEG Technical Program*, edited, pp. 1552-1556.

Mayer, A., W. May, C. Lukkarila, and J. Diehl (2007), Estimation of fault-zone conductance by calibration of a regional groundwater flow model: Desert Hot Springs, California, *Hydrogeology Journal*, *15*.

Montgomery, S., D. Jarvie, K. Bowker, and R. Pollastro (2005), Mississippian Barnett Shale, Fort Worth basin, north-central Texas: Gas-shale play with multiâ€“trillion cubic foot potential, *AAPG Bull.*, *89*(2), 155-175.

Myers, T. (2012), Potential Contaminant Pathways from Hydraulically Fractured Shale to Aquifers, *Ground Water*, no-no.

Nacht, P., M. De Oliveira, D. Roehla, and A. Costa (2012), Investigation of geological fault reactivation and opening, in *Mecánica Computacional* edited, pp. 8687-8697.

Neuzil, C. (1994), How permeable are clays and shales?, *Water Resour. Res.*, *30*, 145–150.

Ngoc, T., E. Konstantinovskaya, R. Lefebvre, and M. Malo (2011), Geotechnical characterization of deep saline aquifers for CO2 geological storage in the Bécancour region, Québec, Canada, in *Geotechnics for Sustainable Development*, edited, Hanoi.

Osborn, S., A. Vengosh, N. Warner, and R. Jackson (2011), Methane contamination of drinking water accompanying gas-well drilling and hydraulic fracturing, *Proceedings of the National Academy of Sciences*, *108*(20), 8172-8176.

Person, M., J. Raffensperger, S. Ge, and G. Garven (1996), Basin-scale hydrogeologic modeling, *Reviews of Geophysics*, *34*(1), 61-87.

Pinti, D., and B. Marty (2000), Noble gases in oil and gas fields: origins and processes, *Fluids and Basin Evolution. Mineral Soc Can Short Course*, *28*, 160-196.

Pollastro, R., D. Jarvie, R. Hill, and C. Adams (2007), Geologic framework of the Mississippian Barnett Shale, Barnett-Paleozoic total petroleum system, Bend archâ€“Fort Worth Basin, Texas, *AAPG Bull.*, *91*(4), 405-436.

Rawling, G., L. Goodwin, and J. Wilson (2001), Internal architecture, permeability and hydrologic significance of contrasting fault-zone types, *Geology*, *29*(1), 43-46.

Revil, A., and L. M. Cathles (1999), Permeability of Shaly Sands, *Water Resour. Res.*, *35*, 651-662.

Rivard, C., J. Molson, D. Soeder, E. Johnson, S. Grasby, B. Wang, and A. Rivera (2012), A review of the November 24-25, 2011 shale gas workshop, Calgary, Alberta – 2. Groundwater resources*Rep.*, Geological Survey of Canada.

Rudnicki, J. (2002), *Alteration of regional stress by reservoirs and other inhomogeneities: Stabilizing or destabilizing?*, 1629-1637 pp.

Saiers, J., and E. Barth (2012), Potential Contaminant Pathways from Hydraulically Fractured Shale Aquifers, *Ground Water*, *50*(6), 826-828.

Sanford, W., L. Plummer, D. McAda, L. Bexfield, and S. Anderholm (2004), Use of environmental tracers to estimate parameters for a predevelopment-ground-water-flow model of the Middle Rio Grande Basin, New Mexico*Rep.*, U. S. Geological Survey Water-Resources Investigations Report 2003-4286, 102p.

Sanford, W. E. (2011), Calibration of models using groundwater age, *Hydrogeology Journal*, *19*(1), 13-16.

Sanford, W. E., L. N. Plummer, D. P. McAda, L. M. Bexfield, and S. K. Anderholm (2004), Hydrochemical tracers in the middle Rio Grande Basin, USA: 2. Calibration of a groundwater-flow model, *Hydrogeology Journal*, *12*, 389-407.

Scanlon, B. R., R. W. Healy, and P. G. Cook (2002), Choosing appropriate techniques for quantifying groundwater recharge, *Hydrogeology Journal*, *V10*, 18-39.

Scholz, C., and C. Anders (1994), The permeability of faults, *Proceedings of Workshop LXIII, The Mechanical Involvement of Fluids in Faulting, U.S. Geol. Surv. Open File Rep. 94-228*, 247-253.

Segall, P. (1989), Earthquakes triggered by fluid extraction, *Geology*(17).

Séjourné, S., X. Malet, R. Lefebvre, and D. Lavoie (2013), Synthèse hydrogéologique du Shale d'Utica et des unités sus-jacentes (Lorraine, Queenston et dépôts meubles), Basses-Terres du Saint-Laurent, Québec*Rep.*, Geological Survey of Canada.

Shipton, Z., J. Evans, D. Kirschner, P. Kolesar, A. Williams, and J. Heath (2004), Analysis of CO2 leakage through 'low-permeability' faults from natural reservoirs in the Colorado Plateau, east-central Utah, *Geological Society, London, Special Publications*, *233*(1), 43-58.

Sibson, R. (1990), Faulting and fluid flow, in *Short Course on Fluids in Tectonically Active Regions of the Continental Crust*, edited by B. E. Nerbitt, pp. 93–132, Mineralogical Association of Canada Handbook.

Smith, L., C. Forster, and J. Evans (1991), Interaction of fault zones, fluid flow, and heat transfer at the basin scale, in *Selected papers: Hydrogeology, Int. Assoc. Hydrogeol.* , edited, Verlag Heinz Heise, Hanover, Germany.

Soeder, D. (1988), Porosity and Permeability of Easter Devonian Gas Shale, edited by S. o. P. Engineers.

Soltanzadeh, H., and C. Hawkes (2008), Semi-analytical models for stress change and fault reactivation induced by reservoir production and injection, *Journal of Petroleum Science and Engineering*, *60*(2), 71-85.

Soltanzadeh, H., and C. Hawkes (2009), Assessing fault reactivation tendency within and surrounding porous reservoirs during fluid production or injection, *International Journal of Rock Mechanics and Mining Sciences*, *46*(1), 1-7.

Sorkhabi, R., and T. Tsuji (2005), *Faults, fluid flow, and petroleum traps*, American Association of Petroleum Geologists.

Streit, E., and R. Hillis (2004), Estimating fault stability and sustainable fluid pressures for underground storage of CO2 in porous rock, *Energy*, *29*(9-10), 1445-1456.

Stute, M., and P. Schlosser (2000), Atmospheric noble gases, in *Cook, P.G., and Herczeg, A.L., Environmental tracers in subsurface hydrology*, edited, pp. p. 349–377, Kluwer Academic Publishers, Boston.

Sumi, L. (2008), Shale Gas: Focus on the Marcellus Shale*Rep.*, The Oil and gas accountability project/Earthworks, Durango, CO.

Thériault, R. (2012), Caractérisation du Shale d'Utica et du Groupe de Lorraine, Basses-Terres du Saint-Laurent - Partie 2 : Interprétation géologique.*Rep.*, Ministère des Ressources naturelles et de la Faune.

Tóth, J. (1962), A theory of groundwater motion in small drainage basins in Central Alberta, Canada, *Journal of Geophysical Research*, *67*(11), 4375-4387.

Tóth, J. (1963), A theoretical analysis of groundwater flow in small drainage basins, *Journal of Geophysical Research*, *68*(16), 4795-4812.

Tóth, J. (1999), Groundwater as a geologic agent: an overview of the causes, processes, and manifestations, *Hydrogeology Journal*, *7*(1), 1-14.

Tran Ngoc, T., R. Lefebvre, M. Malo, and C. Doughty (2012), Feasibility of CO2 injection in the deep aquifers of the Becancour region, in *TOUGH Symposium* edited, Lawrence Berkeley National Laboratorym Berkeley, California.

UNESCO (1978), *World water balance and water resources of the earth*, 663 pp., UNESCO, Paris.

Vogel , J. (1967), Investigation of groundwater flow with radiocarbon, *Isotopes Hydrology*, 355-369.

Voss, C., and A. Provost (2002), SUTRA, A model for saturated-unsaturated variable-density ground-water flow with solute or energy transport, *U.S. Geological Survey Water-Resources Investigations Report*, *02-4231*.

Voss, C. I., and W. W. Wood (1994), Synthesis of geochemical, isotopic and groundwater modelling analysis to explain regional flow in a coastal aquifer of southern Oahu, Hawaii, paper presented at Mathematical models and their applications to isotope studies in groundwater hydrology, International Atomic Energy Agency, Vienna, 1994.

Walvoord, M. A., P. Pegram, F. M. Phillips, M. Person, T. L. Kieft, J. K. Fredrickson, J. P. McKinley, and J. B. Swenson (1999), Groundwater flow and geochemistry in the Southeastern San Juan Basin: Implications for microbial transport and activity, *Water Resour. Res.*, *35*(5), 1409-1424.

Warner, N., R. Jackson, T. Darrah, S. Osborn, A. Down, K. Zhao, A. White, and A. Vengosh Geochemical evidence for possible natural migration of Marcellus Formation brine to shallow aquifers in Pennsylvania, *Proceedings of the National Academy of Sciences*.

Wessels, S., A. De La Peña, M. Kratz, S. Williams-Stroud, and T. Jbeili (2011), Identifying faults and fractures in unconventional reservoirs through microseismic monitoring, *First break*, *29*, 99-104.

Weyhenmeyer, C. E. (2000), Cool glacial temperatures and changes in moisture source recorded in Oman groundwaters, *Science*, *287*(5454), 842-845.

Wiprut, D., and M. Zoback (2000), Fault reactivation and fluid flow along a previously dormant normal fault in the northern North Sea, *Geology*, *28*(7), 595-598.

Yielding, G., B. Freeman, and D. Needham (1997), Quantitative fault seal prediction, *AAPG Bull.*, *81*(6), 897-917.

Yudovich, A., L. Chin, and D. Morgan (1989), Casing deformation in Ekofisk, *J Petrol Tech*.

Zoback (2007), *Reservoir geomechanics*.

Zoback, Kitasei, and Copithorne (2010), Addressing the environmental risks from shale gas development*Rep.*, 365 pp, Worldwatch Institute, U.S. Department of Energy, Washington DC.